PD-TYPE-DEPENDENT SPECTRAL BANDWIDTH IN SOLID POLYMER DIELECTRICS

Cuthbert Nyamupangedengu

A thesis submitted to the Faculty of Engineering and the Built Environment, University of the Witwatersrand, Johannesburg, in fulfilment of the requirements for the degree of Doctor of Philosophy.

Johannesburg, 2011

DECLARATION

I declare that this thesis is my own unaided work. It is being submitted to the degree of Doctor of Philosophy in the University of the Witwatersrand, Johannesburg. It has not been submitted before for any degree or examination to any other university.

Signed this…… day of ……year…….

……..

Cuthbert Nyamupangedengu

Abstract

This thesis is on the study of partial discharge (PD) frequency spectral response to: (a) variations in supply voltage frequency and (b) time of ageing under continuous PD activity. The work extends knowledge on how to interpret frequency domain PD measurements. In addition to fundamental knowledge, the thesis also conceives two novel PD diagnosis tools that are based on spectral analysis. The work contributes to the ongoing efforts by Cigré WG D1.33 on producing an International Electrotechnical Commission (IEC62478) standard in response to the growing interest in unconventional PD diagnosis methods. Unconventional PD diagnosis methods include spectral analysis techniques where information is extracted from selected portions of the PD spectra. Literature shows that there is inadequate knowledge on characterisation of PD mechanisms through spectral analysis, and this can compromise the efficacy of frequency domain PD diagnosis techniques. It is imperative that interpretation of PD spectral measurements be informed by adequate knowledge on the factors that influence PD spectral content. The PD defects studied in this work are those commonly found in solid polymeric insulation such as shielded power cables. The experimental investigations established that firstly, PD spectral content of each defect type responds distinctly to variations in the sinusoidal supply voltage frequency in the range 20 to 400 Hz. Secondly, under long term ageing conditions, PD frequency spectral features of each defect type evolve uniquely. The findings are interpreted in terms of space charge dynamics theory of PD mechanisms. It is concluded that spectral analysis based PD diagnosis should take into account PD spectral dependency on the supply voltage frequency as well as ageing induced evolution.

To my family and friends

"Nature obeys its laws faithfully. It is up to the observer to make correct interpretations".

Jan P. Reynders

AND

"All truth in any sphere is the gift of God and comes to men through the Spirit of God"

William Barclay, 1967

Acknowledgements

My sincere gratitude goes to professors Jan P. Reynders and Ian R. Jandrell for guidance, support (in all respects) and faith in my potential. They ‘set my sail’ into the pinnacles of the academic world and God knows the implications of this in my life. I thank my family, wife (Eunice) and kids (Kuda and Ruva), for their continued patience and support.

Sincere gratitude is also extended to the following institutions for their financial support of research work in the School of Electrical and Information Engineering at the University of the Witwatersrand, Johannesburg:

- Eskom, through the Tertiary Education Support Programme (TESP)
- The National Research Foundation (NRF)
- The South African Government’s Department of Trade and Industry (DTI) through the Technology and Human Resources for Industry Programme (THRIP) funds

A special mention also goes to Tshegofatso Thejane and Willson M. Dube. These are students who were involved in the project as undergraduate vacation work assignments. They enthusiastically assisted in taking measurements during the lengthy ageing tests. Lastly but not least, it was always a pleasure to know that I would get the technical assistance I needed from the Genmin Lab under the good management of Mr. Harry Fellows.

Thanks to the Almighty Father for being the catalyst in making everything possible.

Contents

DECLARATION i

Abstract ii

Acknowledgements iv

List of Figures ix

List of Tables xiii

Acronyms and Abbreviations xiv

1 Introduction 1

1.1 The thesis work motivation 1

1.2 Thesis knowledge contribution 2

1.3 The thesis document structure 3

2 Background 5

2.1 PD technology time-line overview 5

2.2 Conclusion and pointers to the next chapter 9

3 A review of forms of PD energy and the corresponding detection techniques 11

3.1 Introduction 11

3.2 The low frequency (narrowband and wideband) detection methods 15

3.2.1 Calibration 16

3.2.2 Phase–resolved PD analysis (PRPDA) 17

3.3 The ultra-wide-band PD detection and diagnosis systems (unconventional methods) 22

3.3.1 PD pulse shape 22

Pulse rise-time 24

Pulse width 24

Pulse parameters correlation with ageing condition of a PD defect 25

3.3.2 The growing interest in online PD diagnosis 25

3.4 Spectral analysis of PD signals (frequency domain PD diagnosis) 27

3.4.1 The strengths of the frequency domain PD detection techniques 27

3.4.2 The use of a spectrum analyser in detecting PDs in the frequency domain 28

3.4.3 Knowledge deficient areas in UWB PD detection 29

3.5 Summary and pointers to the next chapter 30

4 The experimentation system design and development 31

4.1 Introduction 31
4.2 Determination of the artificial defects dimensions 32
4.2.1 Void defects dimension determination 32
4.3 Design and development of the subdivided electrode test cell 33
4.3.1 Optimisation of the subdivided electrode test cell parameters 34
4.3.2 Construction of the cavity discharge subdivided electrode test cell 41
4.3.3 Construction of the surface discharge subdivided electrode test cell 42
4.3.4 Construction of the point-plane corona discharge subdivided electrode test cell 43
4.4 Design and construction of the capacitive coupler sensor for ultra UWB PD detection in cable test cells 44
4.4.1 Practical tests for coupler sensitivity optimisation 46
4.4.2 Simulations 48
4.4.3 A discussion of the capacitive coupler practical and simulated test results 50
4.4.4 Resultant sensor optimal dimensions 52
4.5 Sensitivity and accuracy optimisation of the spectrum analyser settings for PD detection 54
4.6 Definitions of the PD frequency spectra descriptors used in this thesis 56
4.7 Summary and pointers to the next chapter 57
5 Experimental Work Part I: Investigation into PD spectral response to frequency variations of the supply voltage 58
5.1 Introduction: Why the SVF dependency of PD characteristics is of interest? 58
5.1.1 The need to use frequencies other than the power frequency (50/60 Hz) in PD detection to reduce power rating requirements of the test equipment 59
5.1.2 The need to accelerate insulation aging tests under continuous PD exposure during laboratory based research work 59
5.1.3 The need to understand how PDs are affected by power supply harmonics 59
5.1.4 The need to tune resonant ac test systems for smallest test power capacities 60
5.2 A review of literature on effect of supply voltage frequency on PD characteristics 60
5.2.1 Theory of cavity discharge mechanism 63
5.3 The experimental procedure 67
5.4 Results: Void discharges dependence on supply voltage frequency variation 70
5.4.1 Measurements and observations 70
5.4.2 Cavity PD tests results analysis and discussion 74
5.4.3 Some remarks on practical challenges in cavity PD measurements 76
5.4.4 Key findings on cavity discharges 76

5.5 Results: Surface discharges dependency on supply voltage frequency variation 77
5.5.1 Measurements and observations 77
5.5.2 Surface discharge mechanism analysis 80
5.5.3 Key findings on surface discharges' dependency on SVF 82
5.6 Results: Point-plane corona PD dependency on supply voltage frequency variation 83
5.6.1 Measurements and observations 83
5.6.2 Corona mechanism analysis and test results discussion 86
5.6.3 Key findings on corona discharges dependency on SVF 88
5.7 Summary and pointers to the next chapter 89
6 Experimental Work Part II: Investigation into the time-dependent evolution of PD spectral content 90
6.1 Introduction 90
6.2 The experimental test setup 91
6.3 The testing procedure 94
6.4 Cavity discharge PD spectral evolution test results 95
6.4.1 Measurements and observations 95
6.4.2 Cavity PD mechanisms analysed for interpretation of PD spectra evolution 98
6.4.3 Cavity PD spectral evolution results discussion 101
6.5 Surface discharges PD spectral evolution 105
6.5.1 Experimental measurement results and observations 105
6.5.2 Results analysis and discussion: surface discharge spectral evolution 106
6.6 Point-plane corona in air discharge 'evolution' 109
6.6.1 Experimental results and discussion 109
6.7 Summary and pointers to the next chapter 111
7 Discussion of prospective diagnostic application of the research findings 112
7.1 Prospective diagnostic applications of the knowledge on the supply voltage dependency of frequency spectra 112
7.2 Prospective diagnostic applications of the knowledge on the time evolutionary characteristics of the PD frequency spectra 113
7.3 Summary and pointers to the next chapter 115
8 The thesis conclusion and suggestions for future study 116
8.1 Conclusions on the key findings 116
8.2 Suggestions for future further studies 116
8.2.1 Studying evolution of positive and negative PDs separately 117

8.2.2 Could insulation defects farthest from the high voltage electrode be more harmful than those closest? 117

Appendix A: Sizing cavity PD defects for accelerated ageing tests..... 118

A.1 Introduction 118

A.2 Determination of cavity dimensions 118

Step 1: Determination of the optimum defect radius 119

Step 2: Determination of the optimum cavity height 120

A3. Conclusion 122

Appendix B: Examples of time domain PD pulse shapes responding to changes in the supply voltage characteristics..... 123

References..... 125

List of Figures

Figure 2-1: An illustration of the evolution of the PD diagnosis technology. 6

Figure 2-2: The basic PD detection circuit..... 8

Figure 3-1: An illustration of the various possibilities in detection of PD energy..... 12

Figure 3-2: PD detection systems bandwidth 15

Figure 3-3: Equivalent circuit of the classical PD detection system (Kreuger, 1989)..... 16

Figure 3-4: The prenciple of PRPD analysis. 18

Figure 3-5: An example of phase angle resolved surface discharges signal. 19

Figure 3-6: PD current composition. 23

Figure 3-7: An example of a cavity PD pulse with various pulse shape parameters indicated..... 24

Figure 4-1: The basic layout of the equipment used in the experimentations..... 32

Figure 4-2: The test cell electrode design protocol..... 34

Figure 4-3: Drawings of the electrode systems..... 35

Figure 4-4: Variation of the subdivided electrode stray capacitance ($\mathbf{Cs}$) vs the gap size ($\mathbf{g}$)..... 37

Figure 4-5: Variation of the detected signal amplitude ($\mathbf{V0}$) vs the guard electrode width ($\mathbf{a}$). 39

Figure 4-6: Crossectional view with dimensions of the plane profile electrode disc. 40

Figure 4-7: The frequency response of the subdivided electrode test cell..... 40

Figure 4-8: The artificial cavity defect samples in subdivided electrode test cells..... 42

Figure 4-9: The artificial surface discharge defect samples in subdivided electrode test cells. 42

Figure 4-10: Point-plane corona in air defect incorporated in a subdivided electrode system. 43

Figure 4-11: The main features of a capacitive coupler after Tian et al (2003)..... 45

Figure 4-12: Equivalent circuit of the capacitive coupler..... 46

Figure 4-13: Experimental setup for investigation of the influence of coupler parameters output. 47

Figure 4-14: Sensor response as a function of (a) coupler length and (b) gap size. 48

Figure 4-15: The equivalent circuit for coupler dimension optimisation tests..... 49

Figure 4-16: The variation of the coupler capacitance and gap stray capacitance as a function of the coupler length and gap size respectively. 50

Figure 4-17: A sketch of the fringing electric field in a short capacitive coupler. 51

Figure 4-18: A sketch showing the radial electric field in a long capacitive coupler. 51

Figure 4-19: A plot of the electric fields showing the influence of the semiconducting layer in a capacitor model simulated in Maxwell®. 51

Figure 4-20: The capacitive coupler with experimentally optimised dimensions. 52

Figure 4-21: The measured frequency response of the coupling capacitor. 53

Figure 4-22: Power cable test cells. 53

Figure 4-23: Variation of the detected PD signal content (measured as bandwidth) as a function of the spectrum analyser SWT for various settings of RBW and VBW. 56

Figure 4-24: A typical broadband PD frequency spectrum. 57

Figure 5-1: An illustration of cavity discharge process showing the role of the residual space charge. 63

Figure 5-2: The experimental setup for investigating the influence of supply voltage frequency on partial discharge characteristics. 68

Figure 5-3: Test samples used in the experimental tests on PD dependency on SVF. 68

Figure 5-4: PD spectral bandwidth variation as a function of SVF for HV electrode bounded cavities in polymer insulation. 71

Figure 5-5: PD spectral bandwidth variation as a function of SVF for embedded cavities in polymer insulation. 72

Figure 5-6: PD spectral bandwidth variation as a function of SVF for earth electrode bounded cavities in polymer insulation. 73

Figure 5-7: Scatter plots of cavity PD pulse parameters as a function of the supply voltage frequency (Nyamupangedengu & Jandrell, 2008). 74

Figure 5-8: PD spectral bandwidth variation as a function of SVF for surface discharges occurring along the interface of earth electrode and polymer insulation.. 78

Figure 5-9: PD spectral bandwidth variation as a function of SVF for surface discharges occurring along the interface of HV electrode and polymer insulation.. 79

Figure 5-10: Photographs of surface discharges: at supply voltage frequency of a) 20 Hz and b) 400 Hz 79

Figure 5-11: Scatter plots of surface discharge pulse parameters as a function of the supply voltage frequency (Nyamupangedengu & Jandrell, 2008). 80

Figure 5-12: An illustration of surface discharge mechanisms showing the influence of the slower positive ion cloud. 81

Figure 5-13: PD spectral bandwidth variation as a function of SVF for point-plane corona discharges in air on HV electrode.. 84

Figure 5-14: PD spectral bandwidth variation as a function of SVF for point-plane corona discharges in air on earth electrode.. 85

Figure 5-15: Images of HV electrode corona discharges..... 85

Figure 5-16: Point to plane corona in air pulse parameters as a function of supply voltage frequency. 86

Figure 5-17: Examples of phase-resolved pattern snap shots of point-plane corona. 87

Figure 5-18: An illustration of positive corona mechanism (Maruvada, 2000). 87

Figure 6-1: The accelerated ageing test rig for the PD defects. 92

Figure 6-2: A picture showing the test rig setup for one of the accelerated ageing test episodes.92

Figure 6-3: A schematic illustration of the test procedure. 94

Figure 6-4: Cluster plots of void PD frequency evolution as a function of ageing to total failure.. 96

Figure 6-5: An illustration of the overvoltage that develops in a discharge gap due to the statistical delay of seed electron availability 99

Figure 6-6: A sketch of simplified space charge distribution with a cathode emission condition in a gas-filled insulation cavity during a discharge event initiation process. 100

Figure 6-7: An illustration of the physiochemical changes occurring in a cavity under continuous PD exposure up to total failure (Morshuis, 2005; Temmen, 2000). 101

Figure 6-8: An image of an electrode showing carbonised remnants of solid PD by-products.... 103

Figure 6-9: Prevalence of different PD regimes during the course of defect progression towards total failure..... 104

Figure 6-10: Cluster plots of surface discharges frequency evolution as a function of ageing to total failure. 105

Figure 6-11: Portion of some of the surface discharge samples showing visible signs of cracks and microvoids after long term (400 hours) ageing under PD activity..... 108

Figure 6-12: Examples of completely failed surface discharge test samples..... 109

Figure 6-13: Cluster plots of point-plane in air corona PD spectral bandwidth and magnitude variance over long time ageing. 110

Figure A1: An air filled cavity in a solid dielectric at different possible positions between the two electrodes……..119

Figure A2: A plot of the effective radius (a_{eff}) exposed of cavity to PDs as a function of the actual cavity radius (a)……120

Figure A3: Illustration of air filled cavity in insulation between (a) coaxial and (b) parallel plate electrodes configurations……121

Figure B1: Samples of void defect partial discharge pulses measured in the time domain as a function of supply voltage characteristics ……123

Figure B2: Samples of surface partial discharge pulses measured in the time domain as a function of supply voltage characteristics……124

Figure B3: Samples of point-to-plane corona in air discharge pulses measured in the time domain as a function of supply voltage characteristics ……124

List of Tables

Table 5-1: Summary of highlights in literature on the relationship between the supply voltage frequency and PD characteristics..... 61

Table 6-1: Information about the test cells used in the accelerated ageing tests of the PD defects..... 93

Table 6-2: Characterisation of the time evolution of PD frequency spectra for the void defects. 97

Table 6-3: Characterisation of the 'time evolution' of the surface discharges..... 107

Table 6-4: Characterisation of the 'time evolution' of the point-plane corona in air defects..... 111

Acronyms and Abbreviations

ac	Alternating Current
BNC	Bayonet Neill-Concelman connector
BW	Bandwidth
CBM	Condition Based Maintenance
CIGRÉ	International Council on Large Electric Systems
DAC	Damped Alternating Current
dc	Direct Current
GIS	Gas Insulated Switchgear or Substations
HFCT	High Frequency Current Transformer
HF	High Frequency
HV	High Voltage
IEC	International Electrotechnical Commission
MV	Medium Voltage
pC	pico Coulomb
PD	Partial Discharges
PDIV	Partial Discharge Inception Voltage
PMA	Pulse Magnitude Analysis
PPA	Pulse Phase Analysis
PRPD	Phase Resolved Partial Discharges
PRPDA	Phase Resolved Partial Discharge Analysis
RBW	Resolution Bandwidth of a spectrum analyser
RC	A circuit comprising of resistors and capacitors
RIV	Radio Interference Voltage
RLC	A circuit comprising of resistors, inductors and capacitors
SNR	Signal to Noise ratio

SA	Spectrum Analyser
SVF	Supply Voltage Frequency
SWT	Sweep Time of a spectrum analyser
$\mathbf{t_r}$	Rise Time of a PD pulse
$\mathbf{t_w}$	Width of a PD pulse
$\mathbf{t_f}$	Fall time of a PD pulse
UHF	Ultra High Frequency
UWB	Ultra Wide Band
VBW	Video Bandwidth of a spectrum analyser
VLF	Very Low Frequency
XLPE	Cross-linked Polyethylene

1 Introduction

Insulation is often considered as the weakest part of high voltage (HV) and medium voltage (MV) equipment (Montanari, 2008). Degradation of the insulation is commonly associated with partial discharge activity. Partial discharges (PDs) are 'microsparks' caused by localised stress enhancement at imperfections inside or on the insulation surface (IEEE std 400.3, 2007). Insulation defects can arise from manufacturing and installation flaws or service related ageing. PDs are electric discharge events that generate rapid transient currents whose rise-time, duration and fall-time are in the order of nanoseconds (Kreuger, 1989). In solid dielectrics the discharge processes cause irreversible physiochemical degradation and in most cases progress to total insulation breakdown. PDs are therefore common precursors of electrical insulation failure. The presence of PDs can be considered as an indication of adverse conditions in electrical insulation and PD diagnosis is an assessment of such conditions. Among various methods of electrical insulation diagnosis, PD methods occupy a prominent place (Montanari, 2006; Bartnikas, 2004; Kelen & Danikas, 1995).

1.1 The thesis work motivation

PD detection can be performed either conventionally according to the International Electrotechnical Commission (IEC) 60270 standard or unconventionally according to an IEC62478 standard that is still in preparation (Lemke et al., 2008b). Modern practices in the unconventional PD detection techniques involve analysing the full spectrum or selected high frequency portions of the original full PD power spectrum. This method is also known as the high frequency (HF) or the ultra high frequency (UHF) technique. Furthermore in contemporary unconventional PD detection practice a spectrum analyser is normally used to detect the PDs as it (the spectrum analyser) is tuneable to specific frequency ranges of the available PD spectrum where maximal signal to noise (SNR) ratios can be achieved (Meijer et al., 2006; Lemke et al., 2003). The full PD spectrum is however seldom available as some of the spectral components are usually attenuated due to bandwidth limitations of the detection system. It follows that knowledge of the original PD spectral content together with the frequency response of the PD signal transmission path from origin to point of detection is

imperative as a prerequisite for correct interpretation of the signals particularly those detected only in specific frequency ranges. The requirement becomes even more mandatory considering the stochastic and evolutionary behaviour of PD mechanisms (Morshuis, 1995b). It is essential to understand the variables that influence PD spectral content at origin before distortions in the transmission and detection systems.

A literature study of PD mechanisms shows that among many variables that affect PD mechanisms, the frequency of the supply voltage (test voltage) and time of continuous ageing under PD activity significantly influence PD mechanisms. It is in this context that the work of this thesis was conceived to search for further understanding of the influence of these variables on PD spectral characteristics.

1.2 Thesis knowledge contribution

This thesis contributes and extends knowledge on partial discharge spectral characteristics in the context of frequency domain PD diagnosis of high voltage equipment. A laboratory based experimental setup was designed and developed that enabled measurement of undistorted full PD frequency spectra under various tests conditions. Tests were performed to investigate the correlation between PD spectral features and test voltage frequency for various defects. Similarly the relationship between PD spectral features and time of ageing was investigated. Analyses and interpretation of the findings contribute to extension of the academic knowledge on PD phenomena.

The work reveals two key characteristics of PD frequency spectra. It is found that the spectral bandwidth of partial discharges in solid polymer dielectrics has defect-type-dependent response to (a) supply voltage frequency and (b) time of ageing under continuous PD activity. The knowledge is imperative in ensuring correct interpretation of frequency domain PD diagnosis measurements. It contributes to the ongoing development of the IEC62478 standard on unconventional PD detection methods.

Furthermore the work conceives two novel PD diagnostic tools. Firstly, a defect recognition technique that is based on the defect-type-dependent spectral response to variations in the supply voltage frequency is proposed. Secondly, a criterion for evaluating PD data obtained

from continuous online monitoring techniques is suggested that is based on defect-type-dependent time evolution of PD spectral content.

The work, though covering polymer insulated HV equipment in general, is inclined towards polymer insulated power cables and accessories. In that regard in this document, unless explicitly stated, power cables are implied wherever reference is made or inferred to practical applications.

1.3 The thesis document structure

The thesis document is structured as follows:

Chapter 2: An outline of the PD technology chronological development is presented. It 'calibrates' this work in the context of the general PD diagnosis technology. The complementary and parallel developments of the main two categories of PD detection methods are emphasised. The growing interest in unconventional PD detection methods, particularly those based on spectral analysis, is highlighted.

Chapter 3: An analytical review of the two common categories of PD detection techniques (conventional and unconventional) is presented. There is emphasis on the growing popularity of the unconventional methods. The knowledge gaps, particularly on what can go wrong in interpretation of PD frequency spectra in the unconventional methods, are then highlighted and how these motivated this thesis work.

Chapter 4: The design and development of the experimental investigation system is presented. Various components of the system were custom designed for this work. The formulated design protocols and the final products of the design processes are presented. This chapter has three main parts. The design, development and testing of the subdivided electrode test cells is presented first followed by that of the capacitive couplers that were made on power cable samples. The third section presents tests that were performed to determine the spectrum analyser settings for optimal PD detection.

Chapter 5: The first part of the experimental investigation work is presented. Using the system designed in Chapter 4, tests were conducted to investigate how PD spectral content

responded to variations in the supply voltage frequency. The test results are presented, analysed and discussed.

Chapter 6: The other variable, time of ageing, which affects PD frequency spectra was investigated in this chapter. Accelerated ageing techniques were used. The test rig components were those designed in Chapter 4. The test results are presented, analysed and discussed.

Chapter 7: The prospective diagnostic applications of the knowledge generated in this work are presented in this chapter. New tools for PD defect classification are proposed.

Chapter 8: The thesis work is summarised and concluded. Suggestions for further research work are also presented in this chapter.

Appendix A: Details of the simulations and tests conducted to determine the optimal dimensions of the artificial cavity defects used in the work are presented.

Appendix B: Examples of PD pulse shapes recorded in the time domain as they varied with changes in the supply voltage frequency are given in the appendix.

For logical flow in the thesis document, each chapter begins with highlights of the material covered. At the end of each chapter a summary and pointers to the next chapter are given.

2 Background

A retrospective trace of PD diagnosis technological developments helps in contextualising the research areas of interest in this thesis. This background chapter reviews the past, present and projected future of PD technology. Specific trends in the technology are highlighted particularly the growing popularity of the unconventional methods.

2.1 PD technology time-line overview

The genesis of electrical insulation PD diagnosis technology can be traced back to the beginning of the 20th century as discussed by Kelen (1995). A review of the technological evolution is summarised in the following sections.

An overview of the past, present and possible future of PD diagnosis technologies is illustrated in ***Figure 2-1*** flowchart diagram. This information is synthesised from literature such as by Lemke et al. (2008a), Bartnikas (1987), Bartnikas (2002) and Bolliger & Lemke (2001). Valuable discussions on the evolution of PD diagnosis technology are also found in the following literature: (Schwarz et al., 2008; Sahoo & Salama, 2005; Stone, 2005; Morshuis, 2005; Kelen, 1995; Kelen & Danikas, 1995; Boggs, 1990; Kreuger, 1989; Nattrass, 1993; Wolter et. al., 1978;). The flow chart illustration and accompanying notes on the evolution of the technology are structured in a way that highlights the parallel and complementary development and applications of the two main categories of PD detection methods. The two categories are the conventional and the unconventional techniques. These techniques will be discussed in more detail later but it is noted here that the unconventional PD detection methods initially focused on fundamental research on the understanding of PD mechanisms, but have since evolved into diagnostic applications. Diagnostic applications of the unconventional PD detection methods have given rise to new challenges on the interpretation of PD signals. The work in this thesis is aligned towards contributing to solutions in that regard.

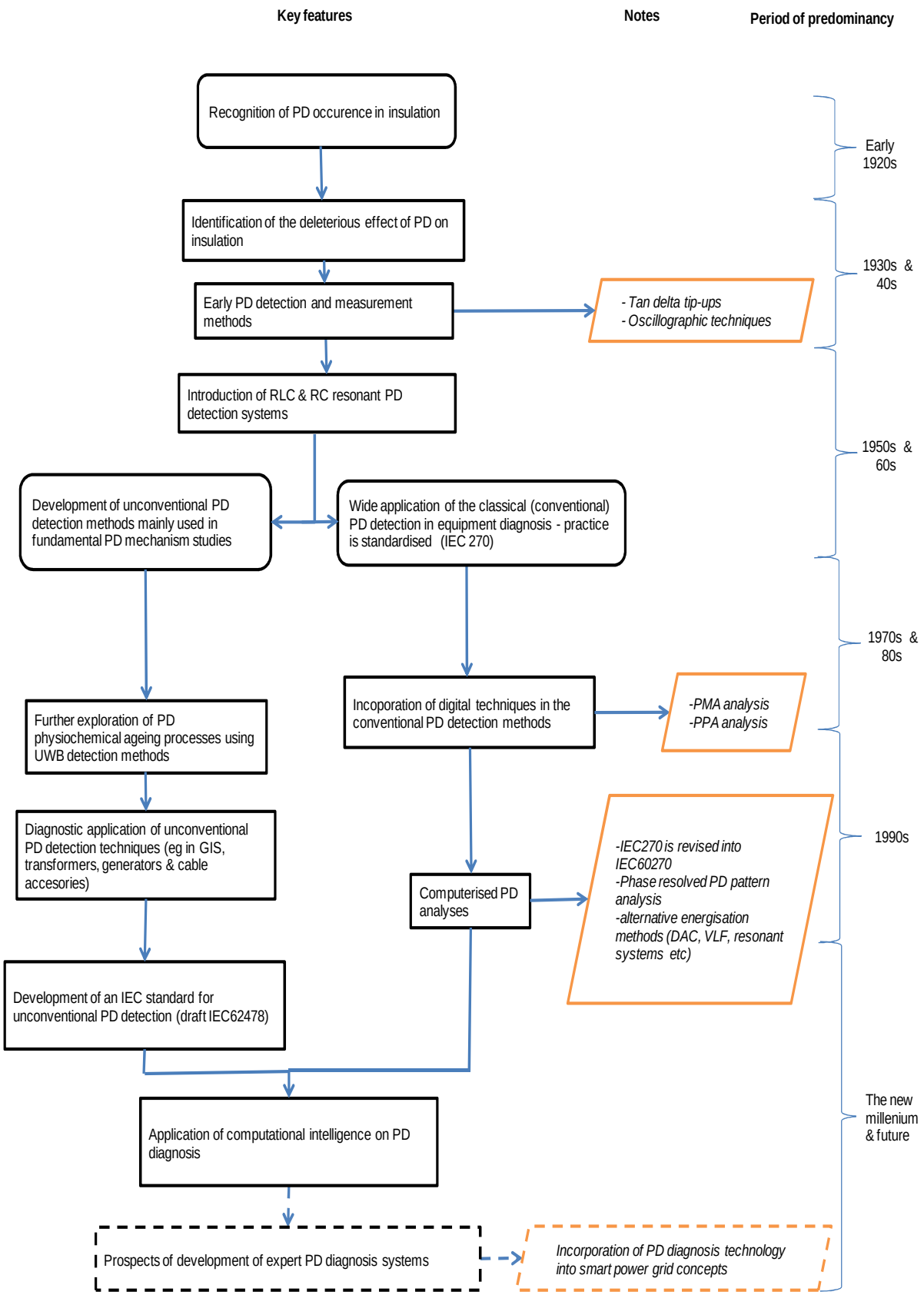

Figure 2-1: ***An illustration of the past, present and projected future of PD diagnosis technologies.***

In one of Bartnikas's review papers on PD technology (Bartnikas, 1987), it was stated that Petersen was among the first engineers to realise that gaseous occlusions in insulating systems under electric stress caused discharges. Tan delta tip-up measurements using the Schering bridge method were among the first PD detection and measurement techniques that were developed in the 1920s. PD inception voltage (PDIV) was determined as the voltage that caused a sudden increase in the tan delta losses (tip-up).

The radio interference character of PDs was recognised and detected as radio interference voltage (RIV) (Bolliger & Lemke, 2001). Oscillographic observation of PDs, a technique that was pioneered by Gemant and von Philippoff among others, subsequently improved PD detection technology. This provided a means of counting PD pulses and determination of PD repetition rates (Bolliger & Lemke, 2001; Bartnikas, 1987).

Initially in PD work, the focus was mainly on detecting the presence of discharges without much knowledge on how the discharges influenced insulation degradation. Interest in understanding PD mechanisms and how they led to total insulation failure became apparent in the 1930s with Mason being among the pioneers in studying PD mechanisms (Kelen, 1995; Bartnikas, 1987). Meanwhile detection methods had improved where RC (circuits comprising of resistors and capacitors) and RLC (circuits comprising of resistors, inductors and capacitors) detection impedances were being used in conjunction with coupling capacitors as PD sensors. PD detection circuits consisting of a coupling capacitor as the PD signal sensor and RC or RLC circuits as detection impedances became standard. This enabled measurement of the PD apparent charge magnitudes. Such techniques, now commonly referred to as the classical or conventional methods, were standardised by various institutions such as the IEC. It was initially documented as IEC270 (published in 1968) and the second edition in 1981. In year 2000 another revised version called the IEC60270 was published that included (among other changes) requirements for digital measuring systems (IEC60270, 2000).

A PD detection circuit setup that uses the sensor option labelled no. 1 in ***Figure 2-2*** is referred to as the classical/conventional PD detection method. Charge transfer that occurs in a discharge event causes a fast current impulse that is detected through a recharge process from the coupling capacitor. The decoupled current pulse flows through a detection impedance connected in series with the coupling capacitor (or alternatively in series with the object under test) and causes a corresponding voltage pulse that is fed into a PD measuring

instrument. Many commercialised PD detection systems are based on this configuration (Schwarz et al., 2008; Boggs, 1990).

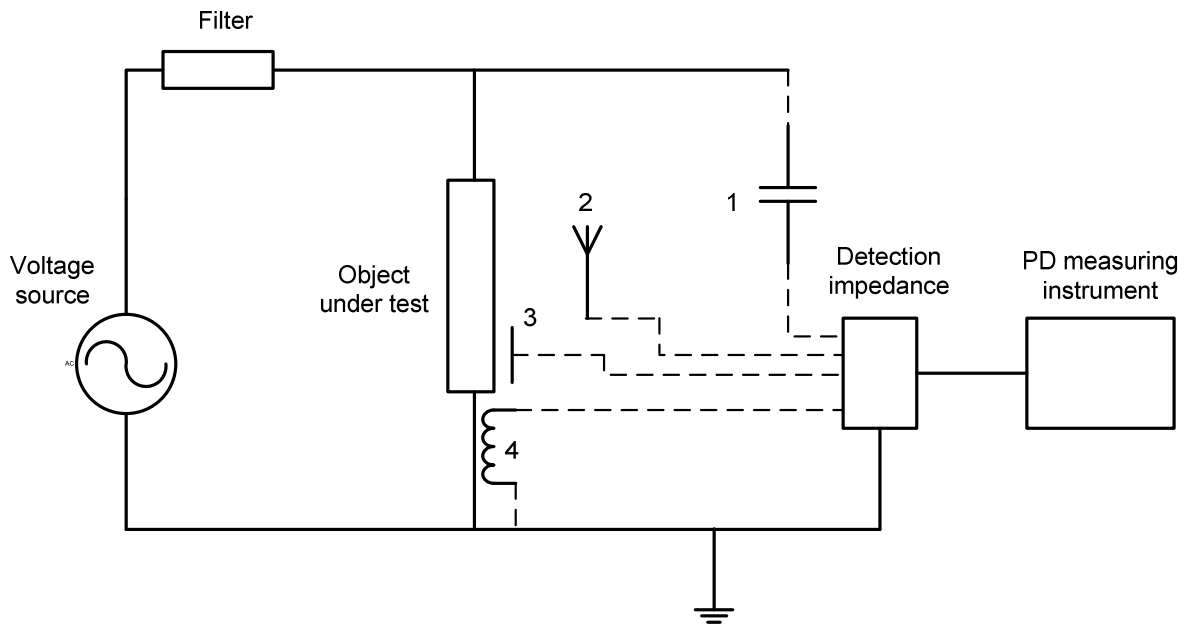

Figure 2-2: ***The basic PD detection circuit. Devices 1, 2, 3 and 4 are PD sensors: coupling capacitor, radiation antenna, capacitive or acoustic probe and inductive probes respectively.***

Although the basic configuration of the classical PD detection setup has not changed since the early years in PD history, the PD signal analysis techniques have evolved significantly over time in response to the developments in signal processing technology (Stone, 2005).

In the 1960s pulse magnitude analysers (PMA) were introduced by researchers such as Bartnikas & Levi (1969). In this technique PD pulse quantities were sorted out as a function of magnitude. In the 1970s techniques to sort PD pulses as a function of phase position on the supply voltage were developed (Stone, 2005) and commonly referred to as pulse phase analysis (PPA). With the advancement of digital signal processing techniques and computer capabilities in the 1990s (Gulski, 1993; Okamoto & Tanaka, 1986) the two techniques were combined into what is now commonly referred to as phase-resolved PD analysis (PRPDA) methods. Currently there is notable interest in the developments and application of artificial intelligence on processing PD phase-resolved (PRPD) patterns aimed at automatic PD classification (Bartnikas, 2002; Sahoo & Salama, 2005).

Up to the mid 1970s the developments of PD detection methods were mainly for quality assurance testing of equipment using the conventional PD test methods. On the other hand the unconventional ultra-wide-band (UWB) techniques were mainly for fundamental research in PD mechanisms. The principle of unconventional PD detection involves decoupling (using sensors such as 2, 3 and 4 in ***Figure 2-2***) and interpretation of the electromagnetic signals emitted by the discharge process.

In the early history, PD researchers already realised that there was need for a sound understanding of the PD phenomena in order to improve effectiveness in PD diagnosis. UWB PD detection techniques were pursued in that regard. Consequently researchers such as Mason (1995), Devins (1984), Bartnikas (1987) in the 1960s, played leading roles in delving into fundamental aspects of PD mechanisms and this involved the use of UWB PD detection methods.

Subsequent to the mid 70s, the main focus in PD research and development work has been application in equipment condition diagnostic testing (Stone, 2005). Furthermore, in response to the increasing demand of online and continuous condition monitoring techniques (Ahmed & Srinivas, 1998) UWB methods that had previuosly been predominantly reserved for fundamental PD mechanism research have been transformed into diagnostic applications (Lemke et al., 2008a). Consequently the unconventional PD detection methods using UWB sensors such as high frequency current transformer (HFCT) (Ahmed & Srinivas, 1998), RF antennas (Raja et al., 2002a; Wong, 2004), capacitive couplers (Lemke & Schmiegel, 1991; Tian et al., 2003) and acoustic sensors (Lundgaard, 1992) have become widely used. UWB PD diagnosis is now commonly applied in gas-insulated switchgear (GIS), power cable accessories, power transformers and rotating machines (Pearson et al., 1995; Bolliger & Lemke, 2001). As a result of such developments an IEC standard (IEC 62478) is being prepared for the unconventional PD detection methods (Lemke et al., 2008b) and this opens up new knowledge areas for research.

2.2 Conclusion and pointers to the next chapter

It is evident that there have been sustained research and development efforts in PD diagnosis technology since the early 20th century. As technology in general continuously improves, new

challenges in PD diagnosis arise in response to new expectations in the industry. Currently there is emphasis on developing diagnostic applications in unconventional PD detection methods and this has created new challenges. In order to unveil these challenges, the next chapter reviews the most common PD detection methods. The review narrows down to electrical methods which are then analysed in more detail. The pitfalls or challenges in the technology are identified and transformed into the objectives of this thesis work: exploration of the spectral characteristics of PDs.

3 A review of forms of PD energy and the corresponding detection techniques

Various forms of energy that are emitted by partial discharge activity are discussed in this chapter. Detection of electromagnetic emissions, being the most common PD detection technique, is then analysed in more detail. The emerging popularity of the UWB techniques under the umbrella of unconventional PD detection methods is presented and how the work reported in this thesis seeks to address the knowledge gaps.

3.1 Introduction

This thesis is concerned with the key variables that influence PD spectral content and have implications on the interpretations of PD signals detected and analysed in the frequency domain. Frequency domain PD diagnosis is an alternative to other techniques such as acoustic, optical, time domain and phase-resolved methods. This chapter reviews the common PD detection and analysis techniques and how in some cases the frequency domain techniques are of higher preference.

Partial discharges emit various forms of energy such as light, acoustic and electromagnetic waves. PD detection involves sensing and analysing the emitted energy (IEEE std 400.3, 2007; Schwarz et al., 2008; Bodega et al., 2004; Stone, 2005; Kuffel et al., 1984; Kreuger, 1989;). The various forms of PD energy and the corresponding detection methods are indicated in ***Figure 3-1***. In this chapter acoustic and optical PD signals are briefly discussed while PD chemical energy is only mentioned. Focus is then directed towards PD electromagnetic emissions and the corresponding detection methods because these are the detection techniques of interest in this thesis work.

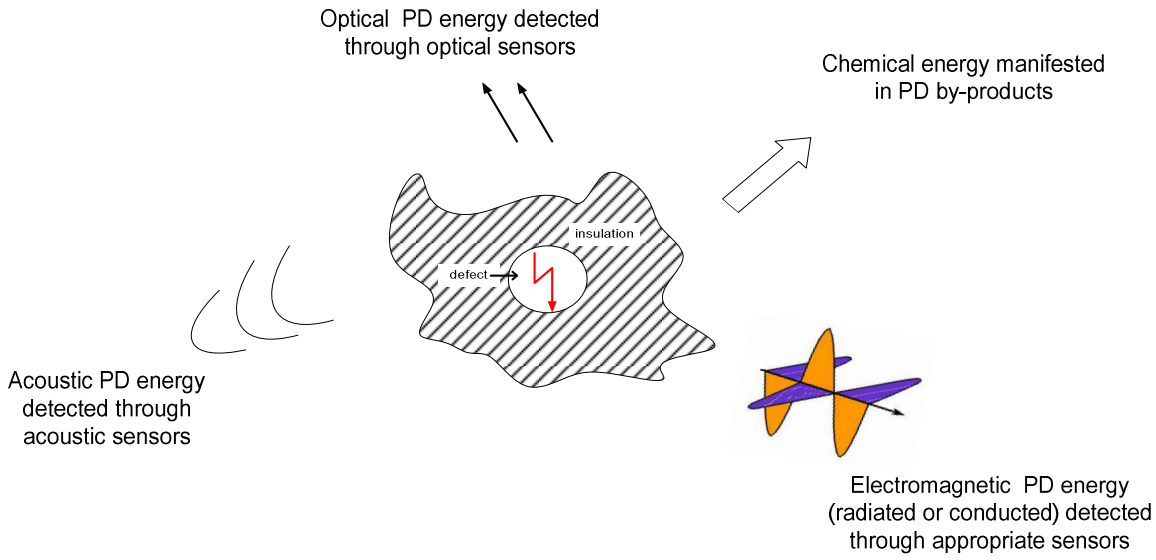

Figure 3-1: An illustration of the various forms of PD energy.

PD acoustic energy: The micro 'explosions' in the form of electrical discharge cause sudden air pressure variations in the discharge area. The pressure wave then propagates by means of molecular vibrations throughout the rest of the insulation system. The short duration of the discharge events result in compression waves of frequency that range from and exceeding the audible levels: 10 Hz to 300 kHz (Schwarz et al., 2008; Stone et al., 2005; Kemp, 1995; Lundgaard, 1992). The detected PD acoustic signal is a function of the nature of the PD mechanisms at the origin, the acoustic signal transmission properties of the insulation system and the sensor response characteristics.

A major strength of the acoustic PD detection method is the relatively high immunity to electrical interference. Furthermore acoustic PD detection has better sensitivity in large capacitive equipment where electrical methods have limited sensitivities; the sensitivity of acoustic methods is not a function of capacitance of the test object as in electrical methods. Another advantage of the acoustic PD detection over other methods is easier source location in complex systems such as power transformers (Markalous et al., 2008; Lundgaard, 1992). Limitations in the acoustic methods are mainly in the relatively high attenuation of acoustic signals in most materials that make up electrical systems (Kemp, 1995).

PD optical energy: The charge avalanches in a discharge process are characterised by various ionisation, excitation and recombination processes that produce light among other

forms of energy. The resultant optical spectrum ranges from ultraviolet to infrared. The light burst rate and duration correspond to that of the discharge events. Fast cameras such as those with photomultipliers are used to capture the emitted PD light. Optical PD detection methods therefore provide direct information on PD processes at source and this is an advantage over other methods that depend on secondary information (Kemp, 1995; Kelen & Danikas, 1995). Optical PD detection systems are safer and more immune to interferences as they are galvanically isolated from the electrical system under measurement (Schwarz et al., 2008). A disadvantage however is the requirement that the insulation has to be translucent in order to be able to observe and detect the light and this becomes a major limitation in practical applications in the field. Applications of optical PD detection methods have consequently been generally limited to laboratory experimental work where special provisions are devised to enable observation of the optical signals (Okubo et al., 2002; Holboll et al., 1995; Morshuis 1993).

PD electromagnetic emissions: Like optical emissions, electromagnetic energy is also emitted from the excitation, ionisation and recombination processes in a discharge event. The energy is transmitted through radiation and conduction from the point of discharge to the rest of the environment. The PD signal frequency content at the origin, depending on the nature and condition of the defect, ranges from a few kHz to GHz. That of the signal acquired by the detection system depends on the frequency response of the detection instruments as well as of the path from source to the point of detection. It is important to note that detection of PDs through electromagnetic emissions is an indirect method. Interpretation of the signals should therefore take into account the effect of the media that the signals travel through from source to point of detection (Kelen & Danikas, 1995).

Most researchers often detect PDs simultaneously using different methods in order to take advantage of the complementary strengths of the different methods. As an example a synchronised combination of optical and electromagnetic detection of PD has been successfully used by Morshuis (1993), Holboll et al, (1995) and Okubo et al, (2002) resulting in revelations of important aspects of PD phenomena. The advancement of signal processing techniques has enabled development of effective electrical methods of PD detection and these have become, by far, the most common methods of PD diagnosis (Stone, 2005). The basic building blocks of an electromagnetic PD energy detection system comprises of a test voltage

source, the device under test, a sensor and a signal processing system as illustrated earlier in ***Figure 2-2***.

The sensor can be a combination of a coupling capacitor and a detection impedance, an inductive or capacitive probe in the case of conducted electromagnetic emissions or an antenna for radiated PD electromagnetic energy.

In the conventional method the sensor is the coupling capacitor and senses the signals by providing an easier path to earth for the high frequency PD current while blocking the 50/60 Hz power frequency. The coupling capacitor should be suitably insulated to withstand the test voltage stress. A detection impedance is connected in the path of PD current pulse and the resultant voltage is fed into a suitable measuring instrument such as an oscilloscope. The frequency response of the detection impedance and that of the measuring instrument determines the portion of the original PD energy that is available for measurement.

PD pulse energy content is a decreasing function of frequency. The frequency ranges from few Hz to orders of GHz (IEEE std 400.3, 2007). The PD detection methods can also be categorised in terms of frequency bandwidth capabilities. In that regard the detection frequency options are as listed below (IEC 60270, 2000).

- Narrow band: bandwidth of 9 kHz to 30 kHz with midband frequency between 50 kHz and 1000 kHz.
- Wide-band: signal frequency range bounded by lower limit of between 30 kHz and 100 kHz, upper limit of 500 kHz and detection bandwidth of between 100 kHz and 400 kHz.
- Ultrawideband: frequency range from 100 kHz up to and beyond 1 GHz.

Figure 3-2 shows an illustration of the frequency band options in the detection of PDs relative to the full spectrum of the original signal. The choice of frequency range for PD detection depends on the signal parameters of interest.

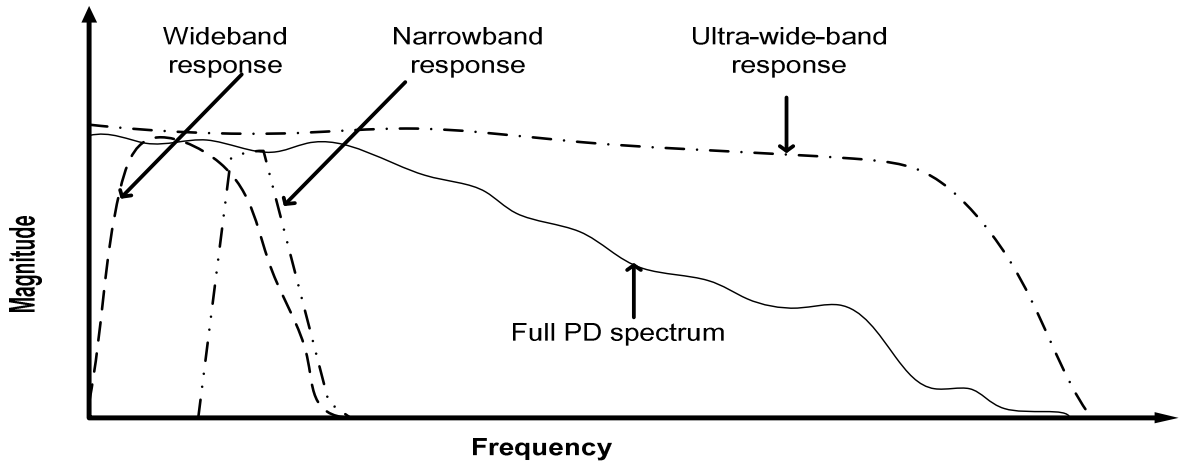

Figure 3-2: ***A sketch illustration of narrowband, wideband and ultrawideband frequency responses of PD detection systems in comparison with the full PD spectrum.***

3.2 The low frequency (narrowband and wideband) detection methods

In the initial development of PD detection technologies, focus was mainly on the determination of the discharge apparent magnitude. It was generally agreed (then) that the PD magnitude correlated with insulation degradation severity, but this is no longer true in some cases (Stone et al., 1992). The low frequency method has detection impedances comprising of resistive, inductive and capacitive components that integrate the pulses to give the apparent charge. In order to determine accurate apparent charge magnitude, the detection frequency range should be sufficiently low and this is a requirement of the IEC60270 conventional PD detection standard.

The conventional PD detection method is widely used for design and quality control tests in the manufacturing industry, maintenance tests in power utilities and research work in universities and test laboratories (Stone, 2005). It is essentially a limited bandwidth low frequency scheme that enables measurement of a wide range of PD parameters such as apparent charge, repetition rate, energy and pulse phase distributions. Some of the key strengths of the detection method include: calibration for PD magnitude measurement and use of customised test voltages under offline conditions. Some important aspects, such as calibration and phase-resolved analysis, of the conventional PD detection method are reviewed in the following subsections.

3.2.1 Calibration

The basic PD detection method, also known as the classical or conventional, allows for calibration and measurement of the apparent charge magnitude in pico-Coulombs (pC). Calibration of the whole test setup is achieved by injecting a pulse of known charge magnitude and taking note of the response. The measured PD magnitude is only a fraction of the actual charge that is transferred at the discharge origin and is termed apparent charge. It is a function of the dimensions and electrical parameters of the test object. The same charge transfer (discharge event) occurring in different types of objects gives different values of apparent charge. The influence of test object dimensions on the PD detection sensitivity can be explained in terms of the relationship between the capacitance value of the coupling capacitor and that of the test object. With reference to ***Figure 3-3***, the sensitivity of the conventional detection system is optimal when the capacitance of the coupling capacitor is of the same order of magnitude as that of the device under test in accordance with the relationship expressed in Equation 3.1 (Kreuger, 1989).

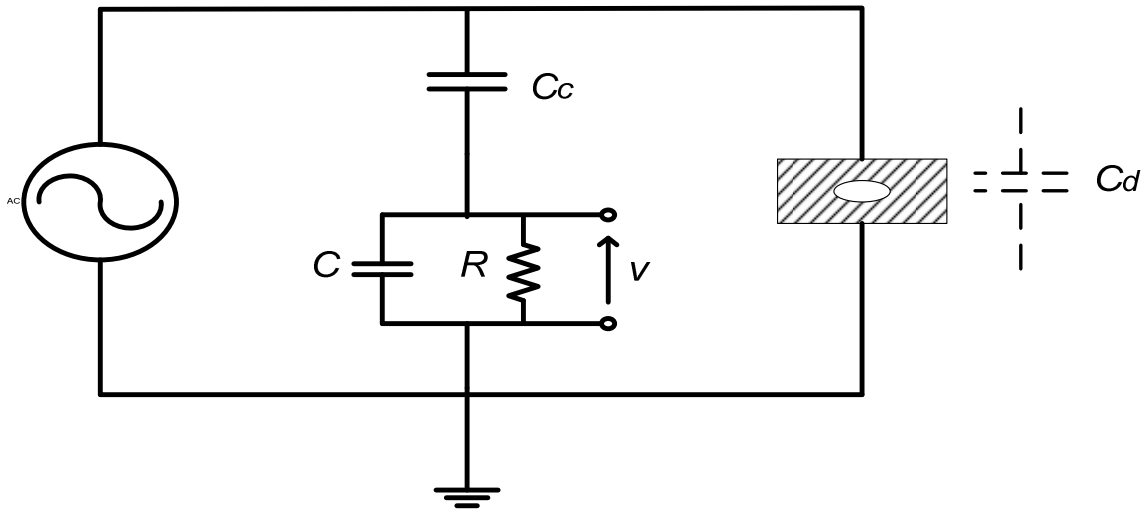

Figure 3-3: ***Equivalent circuit of the classical PD detection system (Kreuger, 1989).***

$$\boldsymbol{v} = \frac{\boldsymbol{q}\boldsymbol{e}^{-\left(\boldsymbol{t}/\boldsymbol{R}\boldsymbol{C}_{\boldsymbol{T}}\right)}}{\boldsymbol{C}_{\boldsymbol{d}}+\boldsymbol{C}\left(\boldsymbol{1}+{\boldsymbol{C}_{\boldsymbol{d}}}/{\boldsymbol{C}_{\boldsymbol{c}}}\right)} \tag{3.1}$$

Where:

v is the magnitude of the detected signal in volts [V]

$C_T = \frac{C_d C_c}{C_d + C_c} + C$ is the total capacitance in the circuit [F]

q is the PD charge magnitude in Coulombs [C]

$C_d, C\ and\ C_c$ are the capacitances of test object, detection impedance and coupling capacitor respectively [F]

R is the resistance in the detection impedance [Ω]

PD detection sensitivity therefore diminishes with the increase in physical size of the object being tested. This relationship has unfavourable implications in the field application of PD diagnosis tests. This is because generally the higher the voltage rating, the bigger the equipment, the less sensitive the PD tests and yet ironically the more important it is to know the PD status. In that regard it means that the same defect in test objects of different voltage insulation ratings gives different values of PD magnitude. This often becomes a major shortfall in the classical PD detection techniques (Boggs & Stone, 1982).

Calibration is an important characteristic of the conventional PD diagnosis methods. Another important strength of conventional PD diagnosis is the use of phase-resolved analysis techniques as discussed in the following section.

3.2.2 Phase–resolved PD analysis (PRPDA)

The presentation of PD pulses on a time base that coincides with the sine wave of the test voltage has always been the traditional and preferred method of displaying PD signals (Kreuger, 1989). Alternatively the two halves of the sine wave can be joined into an elliptical time base. The manner in which the PD pulses cluster on the elliptical base correlates with the type of the discharges. In 1969 the International Council on Large Electric Systems (CIGRÉ) published a brochure indicating typical PD defects and their corresponding patterns on elliptical time base (Cigré WG 21.03, 1969). This could be regarded as comprehensive knowledge that formed the foundation on which most of the subsequent work on phase-resolved PD analysis was based.

PD analysis methods then evolved into quantitative statistical procedures over the years. This was enabled by the advent of digital and computerised signal analysis capabilities. Pioneers

in this technology include Okamoto & Tanaka (1986). Subsequent fundamental developments in digital analysis of PDs (Hikita et al., 1994; Gulski, 1993; Hikita et al., 1990) resulted in a concept now commonly referred PRPD analysis techniques. The concept of statistical PRPD analysis entails dividing the power frequency voltage wave into phase windows as shown in ***Figure 3-4*** (Gulski, 1995; Kreuger et al., 1993).

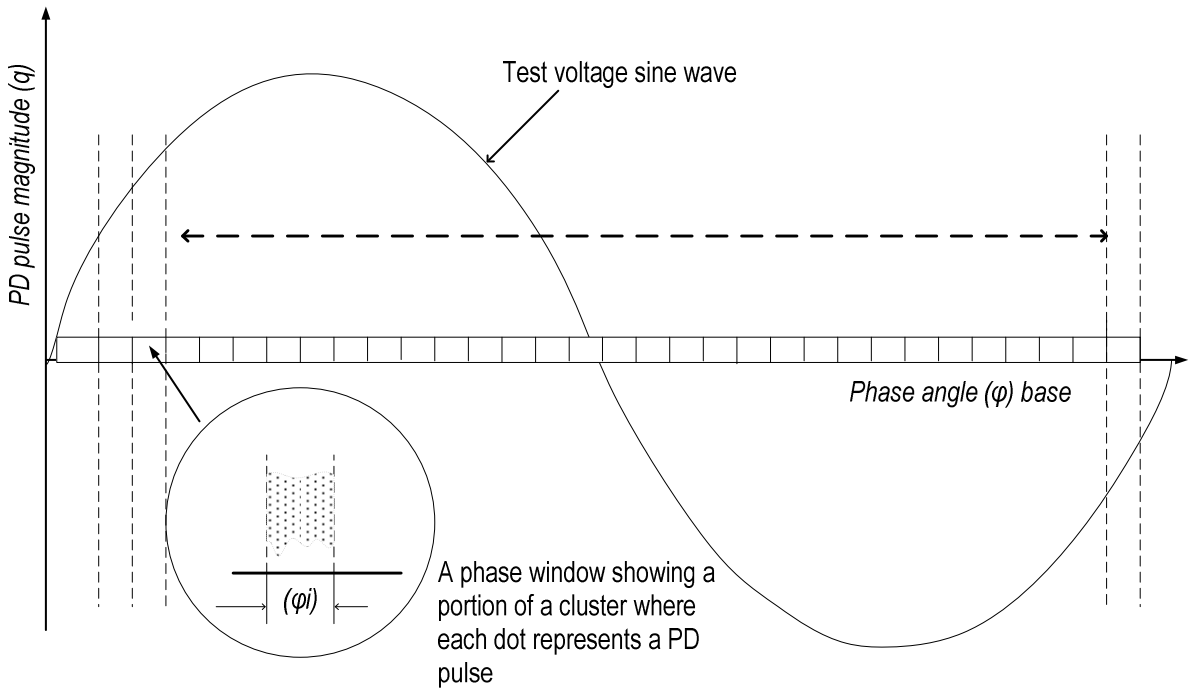

Figure 3-4: ***An illustration of the concept of dividing the power frequency wave into phase windows and registration of each PD pulse magnitude in each window: the principle of PRPD analysis.***

In each phase window the magnitude of each discharge is recorded during a suitable time such as 2 or 5 minutes. From the recorded data and for each phase window, parameters such as the maximum PD magnitude (H_{qmax}), average discharge magnitude (H_{qn}), number of discharges (H_n), and the discharge instantaneous inception voltage (V_i) can be determined. A sequential cascade of the phase windows on the abscissa with the corresponding H_{qmax} , H_{qn} , H_n or V_i on the ordinate gives cluster plots of the PD parameters known as PRPD patterns. ***Figure 3-5*** shows a screen shot of PRPD pattern recorded using a commercial PD test instrument.

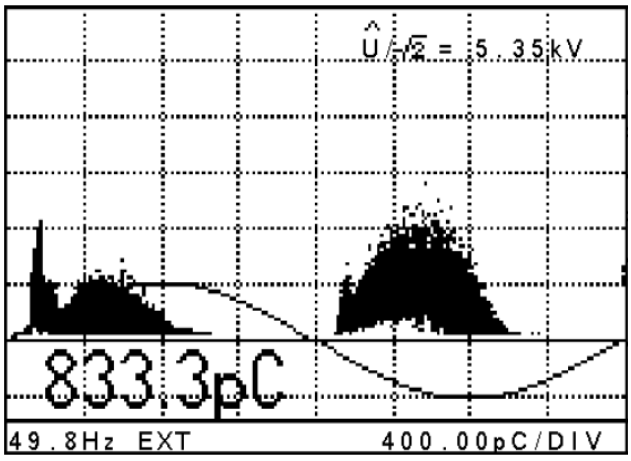

Figure 3-5: ***An example of phase angle resolved surface discharges (recorded using a Power Diagnostics ICM Compact® PD detection system). The cluster patterns in the two half cycles are distinctly different.***

PD recognition using PRPD patterns can be performed either through visual evaluation of the cluster plots or quantitative statistical analyses or image processing.

Typical PD defects and corresponding PRPD patterns that were published by Cigré WG 21.03 (1969) facilitate quick or preliminary recognition of defects through visual evaluation. It has also since been known that the PRPD patterns change with time of voltage application, and in some cases the visual impressions are very distinct thereby enabling accurate inference on the evolutionary behaviour of the PD mechanisms. As an example, some researchers (Kim et al., 2004; Hikita et al., 1994; Hikita et al., 1990) independently made similar observations where PRPD patterns changed in shape from ‘turtle like’ to ‘fat rabbit like’ and then finally to ‘slim rabbit’ shape as cavity defects in polymer insulation changed from virgin to aged and severely aged respectively. Visual evaluation of PRPD patterns however has limitations in that some differences in features may not be conspicuous and therefore not easy to describe qualitatively (Gulski and Kreuger, 1992). Moreover the sets of patterns to be compared can be numerous and difficult to process visually. In that regard quantitative statistical analysis techniques become convenient in further processing the data.

In quantitative statistical analysis of PD patterns, statistical distributions of the phase-angle quantities such as H_{qmax} , H_{qn} and H_n are analysed by means of statistical operators (Lapp & Kranz, 2000). Skewness (S_k), Kurtosis (K_u), and Cross-correlation factor (CC), among other possibilities, are the commonly used operators (Gulski and Kreuger, 1992). Skew (a measure of the asymmetry of the distribution) is an indication of how the statistical distribution leans

to the left or right relative to the standard distribution. Kurtosis is a measure of how sharp the distribution is relative to the standard statistical distribution. Cross-correlation factor is a measure of similarity between two distributions and in this case the distribution in the positive half cycle and that in the negative half cycle. The data in each half cycle is treated separately as it has been deduced that the statistical distributions in the two half cycles may be different depending on the nature of the defect. In essence, the statistical operators quantitatively describe the shapes of the distributions in each half of the power cycle.

Each type of defect has unique combinations of S_k, K_u and CC operators of the statistical distributions H_{qmax}, H_{qn} and H_n; these are often referred to as PD fingerprints. Furthermore each statistical operator value changes following specific trends as the PDs evolve with time. In that regard many workers have identified key characteristic features of PD patterns using statistical operators for some typical defects (Kim et al., 2004; Gulski & Krivda, 1995; Tanaka, 1995; Kelen & Danikas, 1995; Gulski, 1995; Hikita et al., 1994; Kreuger, et al., 1993; Gulski, 1993; Gulski & Kreuger, 1992; Okamoto & Tanaka, 1986; Hikita et al., 1990). Examples of such characteristics are listed below:

- The skewness of H_{qn} is a function of the cavity defect shape. Flat cavities give positive and higher values of skew that decrease and become negative as the cavity elongates in the direction of the electric field.
- Electrode-bounded cavities as well as multiple cavities have positive skew of H_{qn} while surface discharges and electrical trees are characterised by zero or negative skew. The change of skew values from positive to zero or negative is a likely indication of progression of PD insulation defects to total failure since the last phases of PD induced insulation failures are characterised by initiation of electrical trees.
- The kurtosis of H_n distribution is positive for multiple discharges and treeing PDs while single discharges give negative values.

The above listed characteristics can be used in the recognition of unknown defects.

There are many combinations and trends of the statistical operators that characterise PD defect types as well as the ageing stages. Computational intelligence, among other data processing techniques, is a favourable candidate tool for improving the effectiveness in data processing and enables automatic PD classification. Consequently this has attracted considerable research attention (Sahoo & Salama, 2005). Success in this technology however

has been and is still debatable (Krivda, 1995) and as a result experts have cautioned over-reliance on computational intelligence as a tool in PD diagnosis (Bartnikas, 2002).

It is imperative to note that PRPD analyses have predominantly been applied on PD signals that are acquired through the conventional PD detection technique where the detection bandwidth is limited to a maximum of 500 kHz (Lemke et al., 2008a&b). Although this technique is widely used in commercial as well as research work there are limitations regarding revelations of the complex discharge mechanism details (Schwarz et al., 2008; Stone et al., 1992). Complete reliance on PRPD technology without sound understanding of the underlying discharge physical mechanisms may lead to false interpretation of diagnosis test results. Effective interpretation of the observed correlations between the PRPD patterns and the nature and ageing of the source therefore requires an understanding of the underlying physical mechanisms of the PD. In that regard ultra-wide-band (UWB) PD detection methods are used where the entire PD signal bandwidth is acquired.

In addition to the aforementioned limitation of the conventional PD detection methods field application feasibility limitations with the conventional PD detection are encountered when testing highly capacitive or complex equipment. Capacitive equipment include power cables, capacitor banks and GIS. Equipment with complex structures include power generators and transformers (Boggs & Stone, 1982). Reasonable detection sensitivities in such equipment can be more easily achieved through use of inductive or capacitive coupling sensors (probes) that capture far much more PD bandwidth than that in the conventional method (Lemke et al., 2008b). PRPD analysis tools can also be applied to unconventionally detected PD signals (Meijer et al., 2006). It should however be quickly pointed out that there is still a big debate on the feasibility of calibrating the measurement system for PD magnitude determination under the unconventional methods. Hopefully the IEC 62478, currently being drafted, will address this problem in future.

The growing interest in UWB PD detection methods could also be attributed to the relative ease with which the unconventional inductive, capacitive and acoustic PD couplers can be applied on equipment for online continuous condition monitoring schemes. Online condition monitoring (reviewed in more detail later in section 3.3.2) is now an important tool in contemporary maintenance management practice (Veen, 2005; Ahmed & Srinivas, 1998; Orton, 2003).

The shortfalls in conventional PD detection can be addressed through use of UWB techniques. The following section reviews various aspects of the UWB PD detection methods with emphasis on PD spectral analysis. The latter however also has limitations and the work of this thesis deals with some of such limitations. The following section reviews the UWB PD detection method highlighting the strengths and weaknesses.

3.3 The ultra-wide-band PD detection and diagnosis systems (unconventional methods)

Ultra-wide-band PD detection methods (also often referred to as unconventional detection methods) are commonly employed to study and understand the primary mechanisms in discharge processes. Furthermore, unlike the classical method, unconventional PD detection methods can be easily incorporated into online PD diagnosis systems. These characteristics are major advantages of the unconventional techniques over the classical method, and are reviewed in this section.

3.3.1 PD pulse shape

Since development of adequately fast response instrumentation in the 1990s (Stone, 2005), research in UWB PD detection has been developing in parallel to the classical methods and producing valuable complementary knowledge. UWB PD detection methods enable acquisition of PD pulses with shapes that represent the motion of electrons and positive ions generated during the discharge process. The measured PD pulse is the resultant envelope of overlapping electronic, negative and positive ionic currents as illustrated in ***Figure 3-6*** (Van Brunt, 1994; Devins, 1984; Verhaart & van der Laan, 1982). Changes in the pulse height, rise-time, width and fall-times are therefore manifestations of how the dynamics of electrons and ions respond to the various factors influencing the PD process.

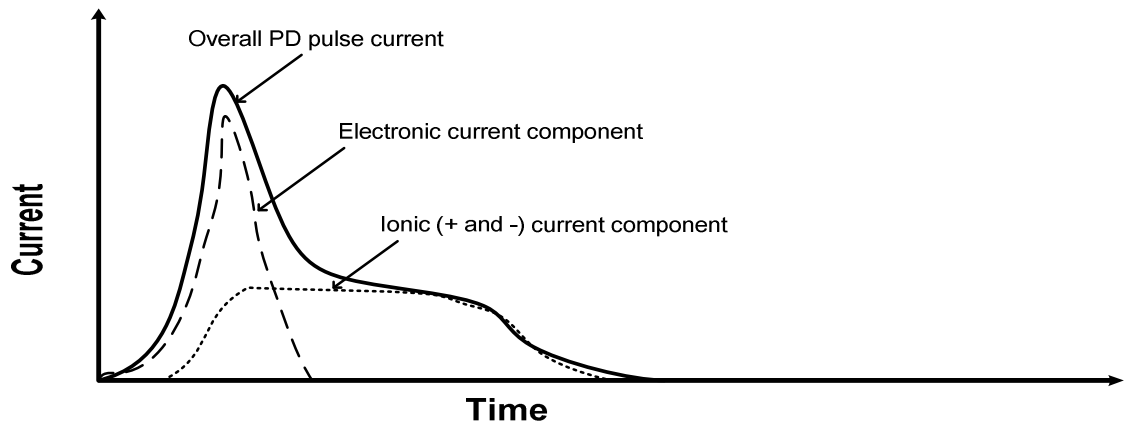

Figure 3-6: ***An illustration of the composition of a PD pulse (after Devins (1984); Verhaart et al (1982) and Van Brunt (1994)).***

In order to use the PD pulse shape as a source of information about the PD mechanisms, the pulse should be free from distortions such as those introduced by bandwidth limitations of the signal path from the origin to point of detection. The time constant of the detection system should therefore be at most equal to the duration of the fastest PD pulse (Brosche et al., 1999; Morshuis 1995c; Kurrat & Peier, 1991). Such a condition dictates that UWB PD detection systems should be physically compact and the bandwidth of the detection instrumentation be in the order of GHz. Among various alternatives, the subdivided (also known as guard electrode system) is commonly used in laboratory based PD detection work (Morshuis, 1995c; Wetzer et al., 1991; Verhaart & van der Laan, 1982).

Various researchers like Devins (1984); Morshuis (1993); Wetzer et al (1991), Alshelkhly & Kranz (1991), using UWB based PD studies, poduced significant knowledge on the understanding of the fundamental mechanisms of partial discharges. The PD pulse shape parameters as depicted in ***Figure 3-7*** and the corresponding information contained therein are dicussed in the following sections.

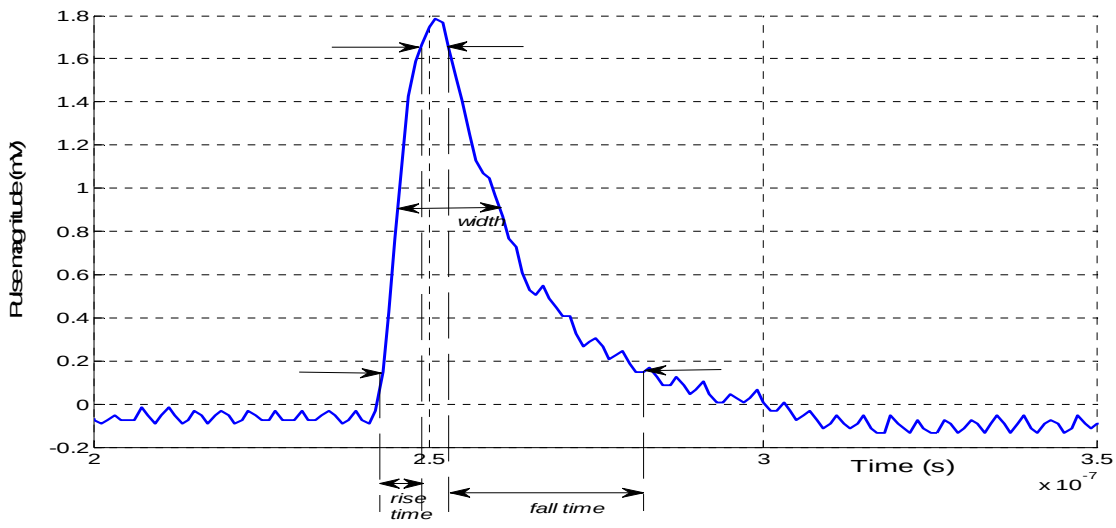

Figure 3-7: ***An example of a cavity PD pulse with various pulse shape parameters indicated.***

Pulse rise-time

PD pulse rise time corresponds to the progression speed of the discharge avalanches extension into the discharge area. Conditions such as the stress magnitude and the seed electron availability influence the nature of the discharge avalanches and affect the pulse rise-time. Furthermore the changes in the PD pulse rise-time can be symptoms of changing conditions in the discharge area. As an example, the time dependent change in the PD pulse rise-time can be an indication of a defect ageing progress.

Pulse width

The PD pulse width as indicated in ***Figure 3-7*** is understood to be a function of the discharge gap size (Brosche et al., 1999; Devins, 1984). It corresponds to the positive ion transit time across the gap and is independent of the gap overvoltage where the latter is defined as the difference in voltage across the discharge gap between the actual and theoretical PD inception (Devins, 1984). It follows that in principle the discharge gap size can be deduced from the PD pulse width, but only in cases of low gap overvoltage that produces Townsend, glow or pseudo-glow PDs. In the case of spark pulse type, the significantly high gap overvoltage causes intensified space charge conditions that produce avalanches that are characterised by larger and faster electron motion. This results in the PD electronic current component dwarfing the ionic counterpart. The resultant pulse is therefore predominantly defined by the electronic current and has both fast rise and fall times (Bartnikas & Novak, 1995).

Pulse parameters correlation with ageing condition of a PD defect

Partial discharges can be categorised into classes that are characterised by specific pulse shapes and correlated with the extent of defect ageing. Depending on the gap overvoltage magnitude, PDs can either be of the Townsend, glow, pseudo-glow or spark type (Okubo et al., 2002; Morshuis 1995b; Bartnikas & Novak, 1992; Morshuis & Kreuger, 1990;). It has been suggested that small cavity discharges are cathode emission sustained processes (Bartnikas, 2004). The space charges that appear near the cathode cause the cathode emission phenomenon. The intensity of the space charge, which in turn depends on the gap overvoltage magnitude, determines the speed and number of avalanches in the discharge process, and ultimately defines the pulse shape. In solid polymer dielectrics PD mechanisms cause physiochemical changes in the discharge area resulting in the gap overvoltage increasing or decreasing thereby altering the pulse shape (Morshuis, 1993; Bartnikas, 2008). The transitions from one PD type to another under continuous alternating supply voltage are now known to be symptoms of ageing as the PD defect progresses to total failure (Morshuis, 2005).

Extraction of diagnostic information from pulse shapes is a characteristic strength of UWB PD detection methods. In addition UWB PD detection can easily be incorporated into online PD diagnosis systems. The latter is desired in contemporary asset management practice. The following section reviews the growing interest in online PD diagnosis technology.

3.3.2 The growing interest in online PD diagnosis

PD tests can be conducted online (while the equipment is in operation) or offline (where the equipment under test is isolated from the rest of the circuit). The classical PD detection method is more suitable for offline tests. Advantages of offline tests include minimisation of external interferences achieved by decoupling the equipment being tested from the rest of the plant. Furthermore, discharge-free, variable and sometimes customised test voltage sources can be used. This enables PD tests at elevated electrical stresses that simulate overvoltage situations or re-ignition of those PDs that would have extinguished under normal operational voltage and yet still causing insulation degradation. In addition various test voltage types such as oscillating wave, very low frequency such as 0.1 Hz (for high capacitive equipment)

and high frequency (for high inductive equipment) can be used. Very useful PD information is obtained this way (Bodega et al., 2004).

Conventional PD detection methods under online conditions, however, are difficult to implement. This becomes a major shortfall considering the increasing relevance of online condition assessment of high voltage insulation where equipment disconnection for tests is undesirable due to operational, financial, economic and/or safety constraints (Ahmed & Srinivas, 1998; Veen, 2005). In such cases non-intrusive PD detection systems are employed. PD signals are decoupled from the equipment using PD probes such as coupling capacitor sensors, HFCT and antennas. There are cases where sensors are conveniently incorporated into the equipment during manufacture or installation (Cigré WG 21.16, 2001).

The strength of online PD detection is in the possibility of taking PD measurements without interrupting the operational status of the equipment. Furthermore continuous data logging enables trending and continuous monitoring of insulation condition. These techniques have gained popularity and with the advent of smart grid concepts (Jiang et al., 2009), more emphasis of online condition monitoring of equipment is anticipated.

A major challenge associated with online PD diagnosis is the vulnerability to external interferences. The presence of the power frequency voltage on the equipment that forms part of sometimes large power grids is often associated with nuisance electrical quantities such as harmonics, corona and other spurious PDs that interfere with the PD signals of interest. In that regard the subject of PD noise mitigation under online conditions has been attracting considerable research interests and yielding useful results (Renforth et al., 2008; Veen, 2005). Significant progress has been made to the extent that online PD monitoring systems are now common in the industry (Denissov et al., 2007a; Ladde et al., 2007; Srinivas & Bernstein, 2007; Gulski et al., 2005; Golubev et al. 2001).

A challenge in online PD diagnosis methods is how some PDs can become illusive to detection at normal operational voltage. Some PDs diminish in magnitude and repetition rate under normal operational voltage due to physiochemical processes in the discharge area and yet they would be progressively deleterious. Unless in continuous monitoring these PDs are detected and noted as they decrease in magnitude to the point of no detection, the absence of such PDs at the instant of observation can be erroneously classified as a healthy condition. Such cases are not as problematic in offline tests because the PDs re-ignite when the voltage

is raised above the normal operational level sometimes up to twice the normal operational voltage such as specified in the IEEE std 400.3 (2007). Proper interpretation of PD trending data acquired through online diagnosis systems entails good understanding of the evolutionary behaviour of PD signals throughout the entire period from initial inception to total breakdown. Such knowledge should include the possible defect-type-dependent variations in the signal evolution trends and leads to part of this thesis's objective in which evolution trends of PD spectra of different defects are studied.

Whether online or offline, in unconventional PD detection techniques, PD signals are commonly viewed as frequency spectra. The following sections review the concept of spectral analysis of partial discharges.

3.4 Spectral analysis of PD signals (frequency domain PD diagnosis)

There are various ways of detecting PDs and the common being acoustic, phase-resolved, time-resolved and frequency domain methods. Frequency domain PD detection entails displaying discharge signals as spectra of frequency components.

The technique of spectral analysis of partial discharges has been studied in laboratories as well as field conditions by various workers such as: Boggs (2003), Thayoob et al (2003), Ahmed & Srinivas (1998), Cheng et al (1998), Morshuis (1995a) and Hudon et al (1994).

3.4.1 The strengths of the frequency domain PD detection techniques

Some of the features of frequency domain PD diagnosis that make it preferable over other techniques under certain circumstances include:

i. In the frequency domain it is possible to view the entire bandwidth of the PD together with any other interferences. Suitable portions of the spectrum that are free from external interferences can then be selected and used while the rest of the spectra is discarded, thereby improving detection sensitivity. It is for this reason that PDs are detected in the HF or UHF portions of the PD frequency spectra in high voltage equipment such as GIS,

generators, power transformers and cable accessories; these equipment impose minimum frequency dependent distortions in the HF and UHF ranges (Bartnikas, 2002). The lower frequency portion of the spectrum can be discarded as it is usually polluted by harmonics from machines, drives and communication gadgets.

In power cables the significantly high frequency dependent attenuation characteristics of the cables prevents most high frequency interferences from propagating along the cable. When detecting PDs in a cable accessory with the sensor being close to the accessory, the rest of the power cable filters out any high frequency signal travelling towards the accessory. The accessory is therefore shielded from high frequency interferences. High detection sensitivities can be achieved within the HF and UHF ranges by taking advantage of the intrinsic high frequency filtering properties of the cable (Dennisov et al, 2007b).

ii. In some cases PD defect recognition is easier in the frequency domain than in other methods. PD frequency spectra can exhibit more PD type dependent distinctive features than the corresponding time domain signals (Cigre WG 15.06, 2002; Cheng et al., 1998; Morshuis, 1995b). An example of success in this regard is that reported by Thayoob et al (2003). They used PD frequency domain signals to successfully recognise various soil conditions in which the power cables with PDs were buried.

iii. PDs in a cable with water trees can be distinguished from those without water trees by using the frequency domain techniques as reported by Ahmed and Srinivas (1998). A PD pulse travelling through a cable portion that has water trees encounters partial reflections and diffractions caused by the water trees. The phenomenon manifests as increased white noise background on the PD frequency spectrum.

Generally there are two ways of detecting PDs in the frequency domain. A common method is detecting the time-resolved pulses and then transforming into equivalent frequency spectra through mathematical tools such as Fourier transforms. Alternatively PDs can be detected and displayed directly as frequency spectra using a spectrum analyser.

3.4.2 The use of a spectrum analyser in detecting PDs in the frequency domain

A spectrum analyser enables viewing of the PD signal together with the accompanying interfering signals such that the instrument can be tuned to selected portions of the signal that give the best signal to noise (SNR) ratio. This technique has also been referred to as tuned PD

measurements (Bartnikas, 2002). In the zero-span mode and tuned to a specific frequency, the spectrum analyser also displays phase-resolved partial discharge pulses; this flexibility makes the instrument quite attractive. More details pertaining to the detection of PDs using a spectrum analyser are discussed later in Section 4.5.

3.4.3 Knowledge deficient areas in UWB PD detection

The use of PD pulse shape as source of information on PD mechanism, online applications and convenience of PD spectral analysis are characteristics that give UWB PD detection techniques an edge over other detection methods. There are, however, some knowledge deficient areas in UWB PD detection methods especially in spectral analysis, and the intention of this thesis work is to explore and generate new knowledge in these deficient areas.

A critical analysis of literature on UWB PD studies and corresponding technologies indicates existence of some 'grey areas' that attract further research attention. There is an imbalance between the PD knowledge that is derived from conventional PD detection methods and that generated through the UWB methods. Characterisation of PD sources through spectral analysis is not as well understood as that through phase resolved analysis as discussed below:

i. In literature, PRPD studies have been based on conventional PD detection methods and in most cases have been conducted using a wide range of typical PD defect models such as cavity, surface, corona and electrical trees (Krivda, 1995; Gulski, 1993). The same however cannot be said about UWB PD studies where there has been a tendency towards focusing mainly on cavity discharges. As an example work by Bartnikas & Novak (1992), Bartnikas & Novak (1995), Devins (1984), Morshuis (1993), Tanaka & Ikeda (1971), Crichton et al (1989) and Niemeyer (1995) that have significantly contributed to the knowledge on PD mechanisms, were all based on cavity discharges. Questions therefore arise concerning how this knowledge is transferable to other types of discharges such as surface and corona that are also of concern in the PD diagnosis technology. In this thesis work therefore the frequency domain UWB PD studies included other defect types (surface and corona discharge defects) in addition to cavities.

ii. In HF or UHF PD detection (techniques common in the diagnosis of gas insulated equipment, power transformers and power cable accessories) a spectrum analyser is used as it can be tuned to detect PDs in the higher frequency portions of the PD spectrum. This technique was already identified as far back as early 70s (Harrold, 1971). Given that in such cases the detected signal is only a portion of the entire PD frequency spectrum, information contained in the original signal is truncated. Correct interpretation of PD frequency domain PD tests results is compromised if there is no adequate knowledge of the original full spectrum and its relationship with the detected portion. In literature the knowledge on characterising PD sources through spectral analysis especially by use of spectrum analyser is limited.

Correct characterisation of PD sources using spectral analysis focuses on solutions to the above listed shortfalls. This requires an understanding of the factors that influence PD spectral characteritics at the origin. Such factors include: (a) variations in the supply voltage frequency and (b) time of defect ageing under continuous exposure to PD. An experimental investigation was therefore conceived to explore the influences of the supply voltage frequency and time of ageing of PD spectral content. In order for the investigation work to align into the identified knowledge gaps, different PD defect types, in addition to the commonly studied cavities, were used. Furthermore the studies covered the full bandwidth of the PD signal.

3.5 Summary and pointers to the next chapter

Both the PRPD and UWB techniques have been reviewed and shortfalls in the technologies identified. The need to understand the PD spectral characteristics at origin has been discussed in the context of improving HF and UHF techniques. The following chapter presents the design and development of the experimental system used to explore characterisation of PD sources using spectral analysis. Two characteristics of PD spectra were studied; the dependency on supply voltage frequency and dependency on time of continuous exposure to PD.

4 The experimentation system design and development

In the previous chapter pitfalls in the interpretation of PD frequency spectra have been discussed. Solutions to these challenges are in the understanding of the factors that influence PD frequency spectra. This work focuses on the supply voltage frequency and time of ageing as key factors that influence PD spectral content. In order to perform the studies, a distortion free PD detection system had to be designed, developed and tested. This chapter presents the design protocols that were formulated to create subdivided electrode test cells and power cable capacitive couplers that gave adequate sensitivities and bandwidth needed in the UWB PD measurements. Since a spectrum analyser would be used as the measuring instrument, the procedure for optimising the instrument settings is also presented in the chapter.

4.1 Introduction

In order to experimentally study the influence of supply voltage frequency (SVF) and time of ageing on PD spectra, it is essential that the detected signal is free from distortions. The experimental setup was carefully designed and developed to give adequate frequency response and sensitivity.

The basic layout of the experimental setup used in all the tests conducted in this study is delineated in ***Figure 4-1***. Various test cells with different insulation defects were used in the experiments. Since the experimental investigations were of a comparative nature, the components of the test setup were carefully designed, selected and instruments set that enabled control and exposure of all the samples to the same conditions. This chapter explains how the test cells were designed and developed as well as how the spectrum analyser settings were determined. Typical full cycle design procedures were followed in the design of the various components of the test rig.

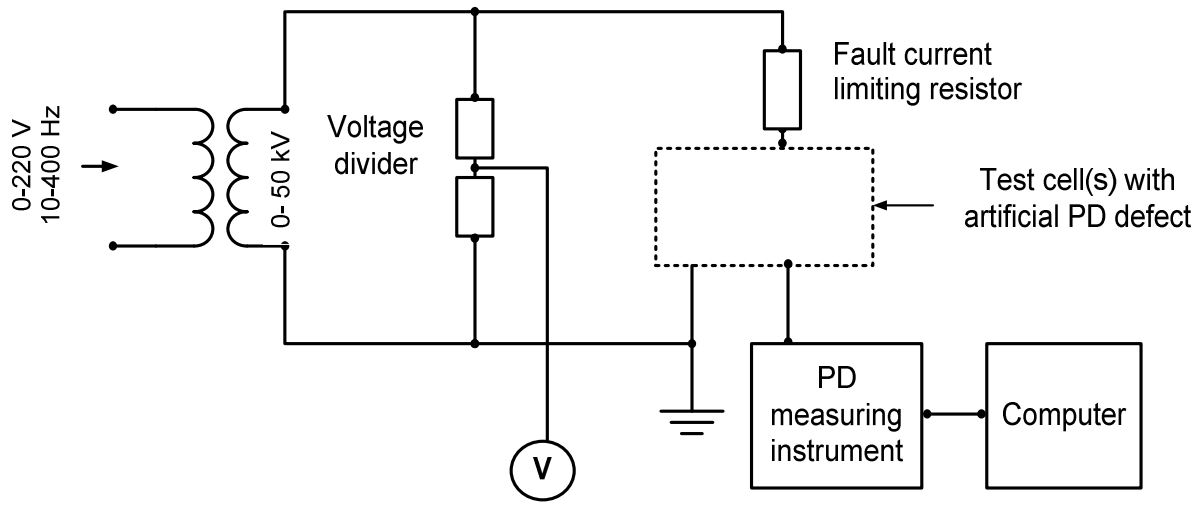

Figure 4-1: The basic layout of the equipment used in the experimentations.

4.2 Determination of the artificial defects dimensions

Partial discharge defect dimensions influence PD signal characteristics. In this work it was necessary that all the test cells gave the same initial PD inception voltage and reasonable initial PD signal magnitude that would not require pre-amplification. The artificial void defects dimensions were theoretically predicted and then verified through practical experiments. Those of surface and corona discharges were determined through practical iterative tests only.

4.2.1 Void defects dimension determination

Though partial discharge phenomenon is characterised by complex processes, various researchers have managed to formulate theoretical models (both deterministic and probabilistic) that can reasonably simulate PD mechanisms (Niemeyer, 1995; Heitz, 1999; Crichton et al., 1989). In that regard, the dimensions of an air cavity defect that initiates PDs at a chosen voltage can be theoretically predetermined. The dimensions of the disc shaped cavities that were used in this thesis work were determined to be 2 mm wide by 1 mm deep. The procedure followed in determining the cavity dimensions is presented in more detail in Appendix A.

Since most of the work in this thesis revolved around analysis of PD power frequency spectra, it meant that the frequency behaviour of the key components in the experimental system (the test cells and the measuring instrument) had to be established. The following sections explain in detail how the two types of test cells used in the work: the subdivided electrode system and the coupling capacitor on power cable samples, were designed and also how the settings of the PD detection instrument (the spectrum analyser) were determined.

4.3 Design and development of the subdivided electrode test cell

In order to detect a PD signal such that its frequency content is similar to that at the point of origin, the bandwidth of the detection system (including the PD path from point of origin to the detection instrument) should be equal to or bigger than that of the original PD. Physical compactness of the system is therefore a prerequisite (Wetzer et al., 1991).

An electrode setup was needed as a PD test cell that would be characterised by UWB frequency response, reasonable PD detection sensitivity and flexibility enabling easy creation of various types of typical PD defects models in solid dielectrics. A literature search for a suitable generic design meeting such specifications narrowed down to a setup comprising of two parallel plane profile electrodes with one of the electrodes subdivided into a measuring disc and an earthed guard ring. Such PD test cell designs have been used before by various researchers to study fast discharge mechanisms (Morshuis, 1995c; Wetzer et al., 1991; Verhaart & van der Laan, 1982; Trinh, 1980; Pearson & Harrison, 1969).

The subdivided parallel plane profile electrode system was adopted for use in this work. In order to customise the dimensions of the electrodes to meet the desired performance, a design procedure was devised and implemented. ***Figure 4-2*** shows a flowchart depiction of the design protocol.

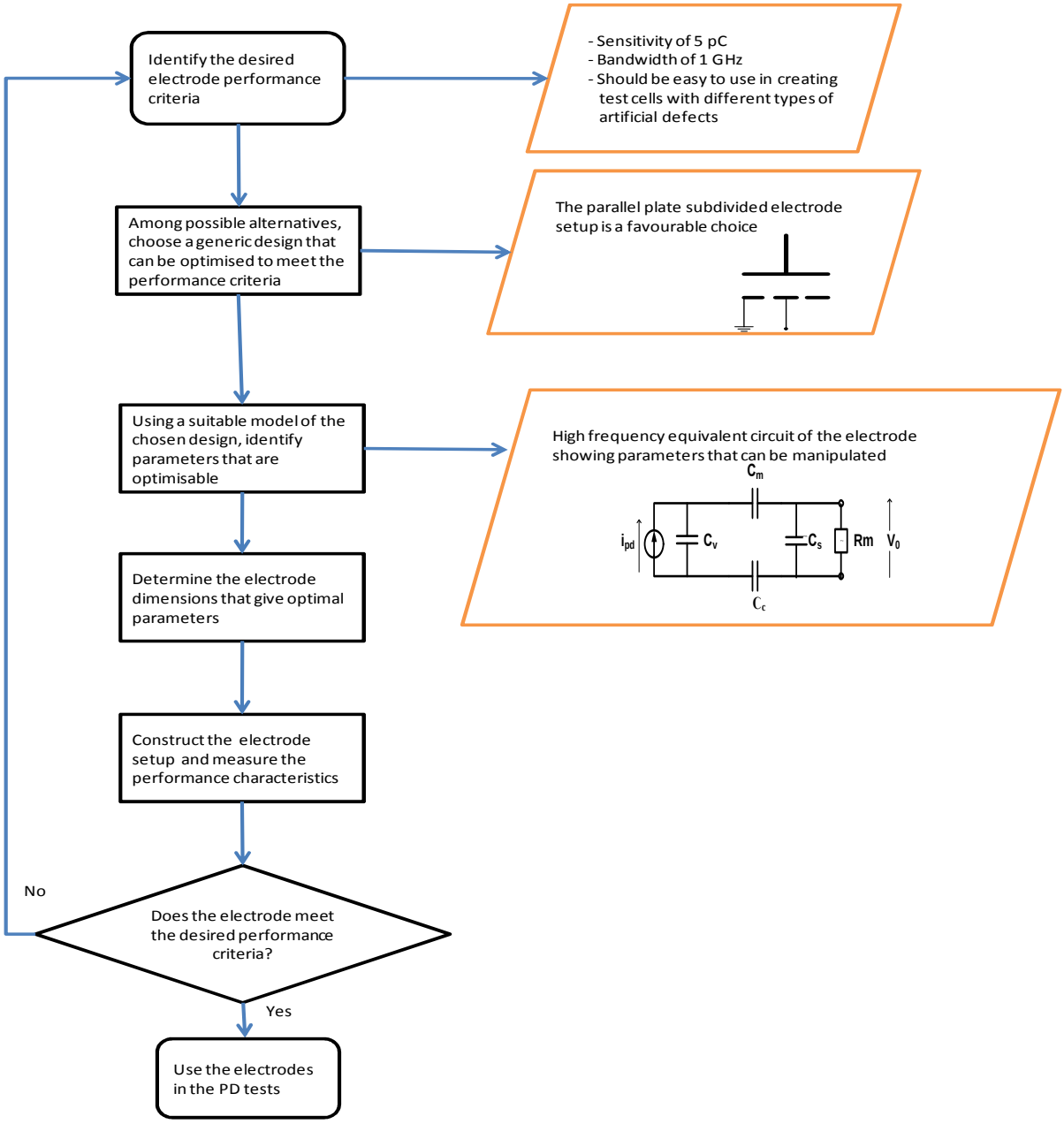

Figure 4-2: ***An illustration of the logical procedure formulated to optimise the test cell electrode parameters.***

4.3.1 Optimisation of the subdivided electrode test cell parameters

With reference to the electrode system drawings in ***Figure 4-3(a)*** and ***(c)*** and the equivalent circuit model in ***Figure 4-3(b)***, the key electrical parameters that determine the high frequency performance of the electrode setup are: the void defect capacitance (C_v), measuring capacitance (C_m), coupling capacitance (C_c), the stray capacitance (C_s) and the measuring impedance (R_m).

C_v is determined from the cavity defect dimensions as explained in detail in Appendix A. The detection resistance (R_m) is chosen as a 50 Ω resistor that matches the characteristic impedance of the signal cable terminating into the measuring electrode. The resistor is of low inductance in order to limit resonance effect that adversely affects the electrode system frequency response. The parameters C_m, C_c, and C_s are interrelated and depend on the physical dimensions of the electrodes. The electrode dimensions were therefore carefully determined as presented in the following subsection.

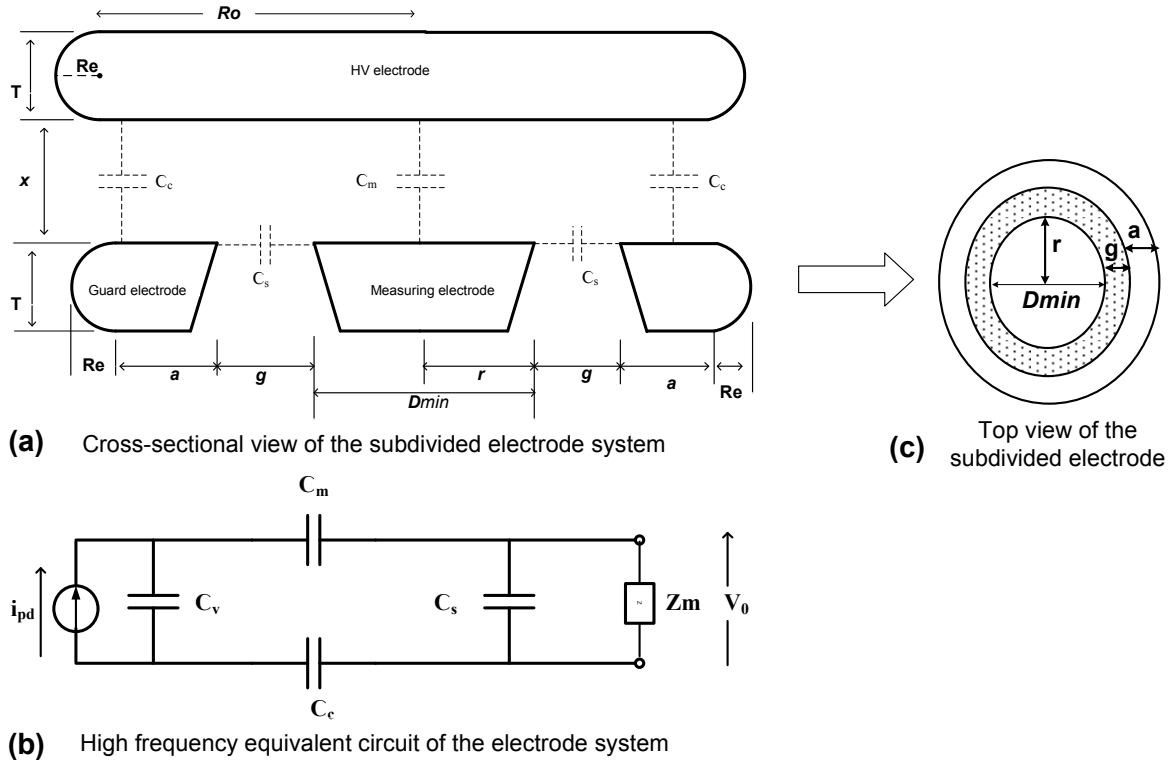

Figure 4-3: ***Drawings of the electrode systems showing the equivalent electrical variables and the physical dimensions.***

4.3.1.1 Determination of the electrode dimensions

The geometrical parameters of the subdivided electrode that influence sensitivity and frequency response are the measuring disc diameter (D_{min}), thickness (T), radius of curvature (R_e), gap length (g) and guard electrode width (a) as shown in ***Figure 4-3(a)***.

Each of these parameters had to be carefully determined for optimal performance of the electrode in PD detection. The following subsections explain the procedures followed in the determination of each parameter.

The measuring electrode diameter (D_{min})

The measuring electrode diameter (D_{min}) is a key dimension as it affects the electrical parameters C_m, C_c, and C_s. Its magnitude should be such that it is not too big as it results in large C_s that in turn reduces the detection sensitivity. On the other hand (and of equal importance) is that the D_{min} must not be too small as this results in induction of charge on the guard electrode in accordance with the Ramo-Shockely theorem (Shockley, 1938). According to Wetzer & van der Laan (1989) and Wetzer et al (1991) the measuring electrode diameter (D_{min}) is related to the separation distance (x) between the HV electrode and measuring electrode and void diameter (d_v) through Equation 4.1 given below.

$$x \leq \frac{D_{min} - d_v}{4} \tag{4.1}$$

For a void diameter d_v = 3 mm and electrode separation x = 3 mm (corresponding to typical insulation thickness of MV power cables), the optimal diameter D_{min} of the measuring electrode is calculated as **≥ 15 mm**.

Electrode thickness (T)

According to the work by Trinh (1980), for the field along the end sections of the electrode to be less than in the gap and in order to avoid excessive local field enhancement along the end sections, the electrode thickness (T) should satisfy the condition $T \geq 2x$; where x is the separation between the HV electrode and the earthed electrode. T is the electrode thickness. In the case of $x = 3$, then T is at least **6 mm**.

Radius of curvature (R_e) of the electrode end-section

A plane profile electrode (as shown in ***Figure 4-3***) has a linear section of radius R_0 and terminated by a semicircular section of radius R_e. The thickness $T = 2R_e$ and for $T \geq 6$ mm, $R_e \geq$ **3 mm.**

The subdivided electrode gap length (g)

High frequency signal losses occur through the subdivided electrode gap between the measuring disc and the guard ring. The losses are proportional to the magnitude of the stray capacitance (C_s) which in turn is a function of the gap size g. The losses can therefore be minimised by ensuring that g is optimally big. With reference to the electrode drawings in ***Figure 4-3,*** the stray capacitance (C_s) can be expressed in terms of electrode thickness (T), measuring electrode radius (r) and gap size (g) as given in Equation 4.2.

$$C_s = \frac{2\pi\varepsilon_0\varepsilon_r T}{In(\frac{r+g}{r})} \tag{4.2}$$

ε_0 and ε_r are the permittivities of free space and the relative permittivity of the dielectric in the gap respectively. The subdivided electrode was cast into epoxy resin ($\varepsilon_r = 4$) to prevent unwanted surface discharges. Substituting the values of $r, T,$ ε_0 and ε_r reduces the equation to one with g as the only unknown variable. The value of g that corresponds to the knee-point of the plot of C_s as a function of g, as shown in ***Figure 4-4***, is considered as the gap size that gives optimally low stray capacitance. Such a gap in this case is **10 mm** wide**.**

In order to further improve the sensitivity of the electrode the stray capacitance losses were further minimised by bevelling (at 45^0) the walls of the gap between the measuring electrode and the guard ring; this technique was also used by Morshuis, (1993).

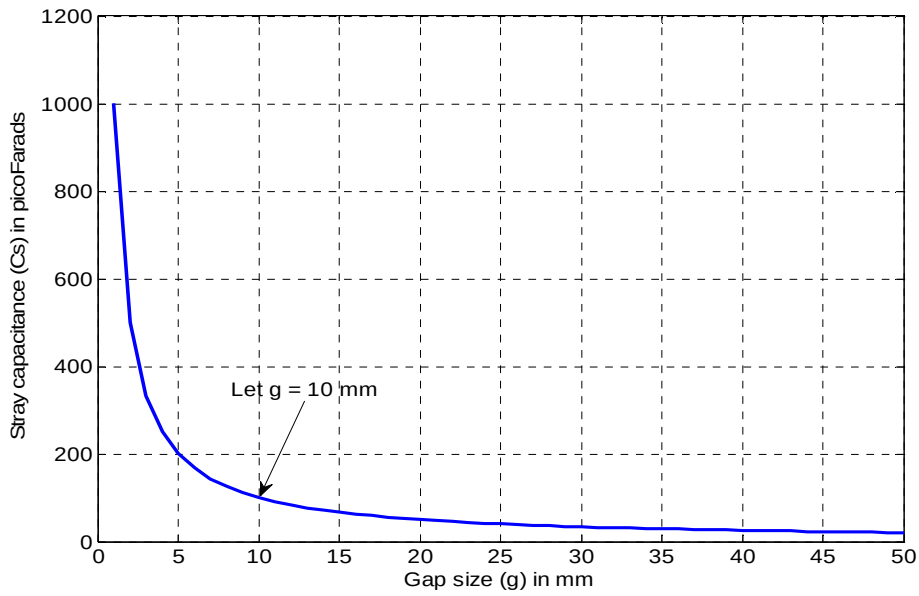

Figure 4-4: ***A plot of the variation of the subdivided electrode stray capacitance (C_s) as a function of the gap size (g).***

The guard electrode width (a)

The guard electrode forms a coupling capacitance (C_c) with respect to the adjacent the HV electrode disc. With reference to the high frequency equivalent circuit of the electrode setup (***Figure 4-3*** **(b)**), the voltage V_0 across the measuring impedance Z_m due to the discharge current i_{pd} can be expressed as given in Equation 4.3 (Verhaart & van der Laan, 1982) where C_m is the capacitance between the measuring electrode and the HV electrode.

$$V_0 = Z_m i_{pd}\left(1 - \frac{C_m}{C_c + C_m}\right) - Z_m \frac{dV_0}{dt}\left(\frac{C_c C_m}{C_c + C_m}\right) \tag{4.3}$$

The compactness of the subdivided electrode system minimises signal reflections and inductively induced resonances. This condition results in minimal subtractive components in the expression of V_0 that are represented by the second term in Equation 4.3. Moreover if $C_c \gg C_m$, the second term in the equation becomes negligible. The detected signal (V_0) becomes inversely proportional to the coupling capacitance C_c. Expressing C_c in terms of the dimensions of the electrode setup and then substituting this into Equation 4.3 gives an expression for V_0 in terms of the dimensional parameters of the subdivided electrode setup as given in Equation 4.4.

$$V_0 = Z_m i_g \left\{1 - \frac{C_m}{\left(\frac{\varepsilon_0 \pi[(r+g+a)^2 - (r+g)^2]}{x} + C_m\right)}\right\} \tag{4.4}$$

A plot of V_0 as a function of the guard electrode width (a) as shown in ***Figure 4-5*** enables choice of an optimal value of a which in this case is **15 mm**.

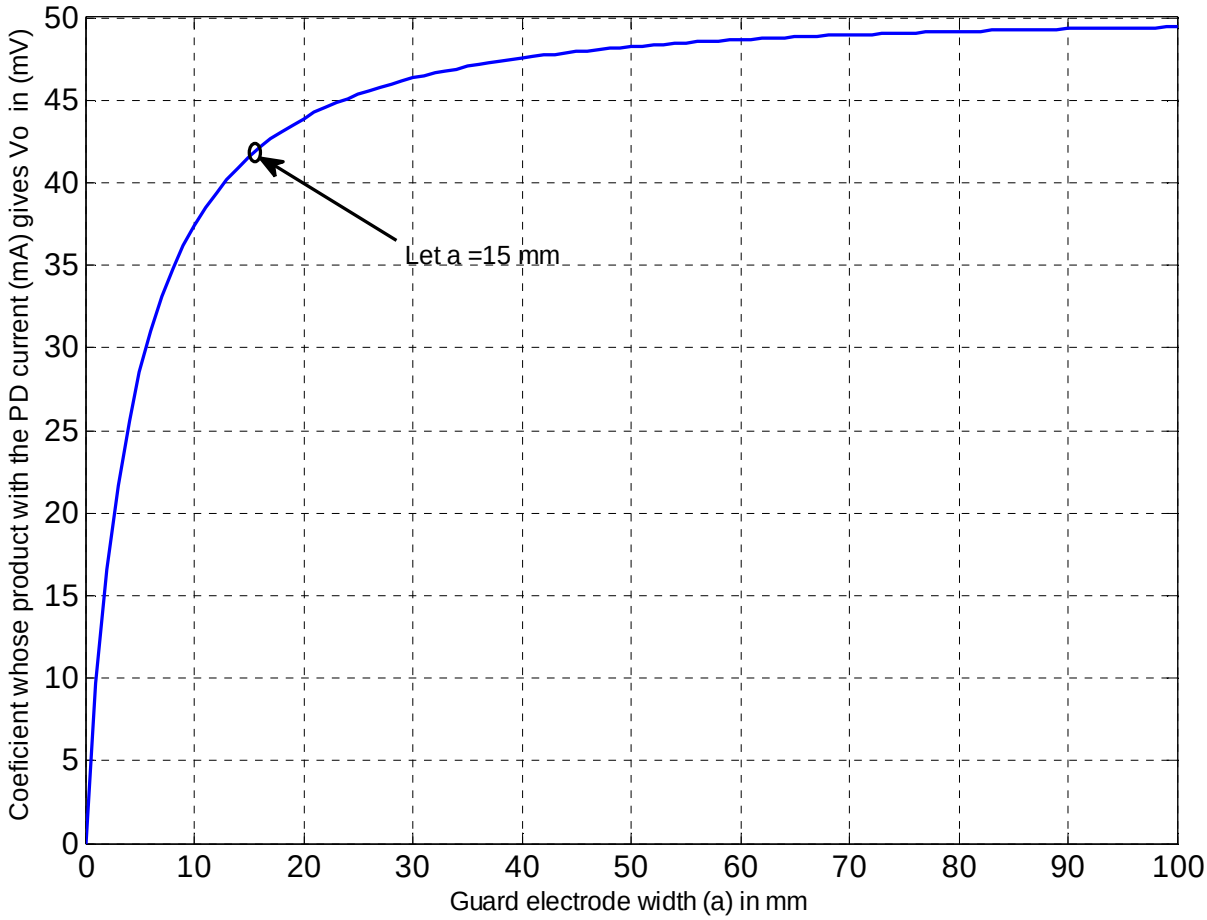

Figure 4-5: ***Variation of the detected signal amplitude (V_0) as a function of the guard electrode width (a).***

4.3.1.2 The resultant design

The resultant optimal dimensions of the subdivided electrode are shown in the electrode drawings of ***Figure 4-6***. An S_{21} frequency response of the electrode measured using an Anritsu® network analyser is shown in ***Figure 4-7***. The response is of a band-pass type with upper cut-off frequency at about 1.3 GHz. Such a response is adequate for this thesis work where frequency components of up to 1 GHz were anticipated.

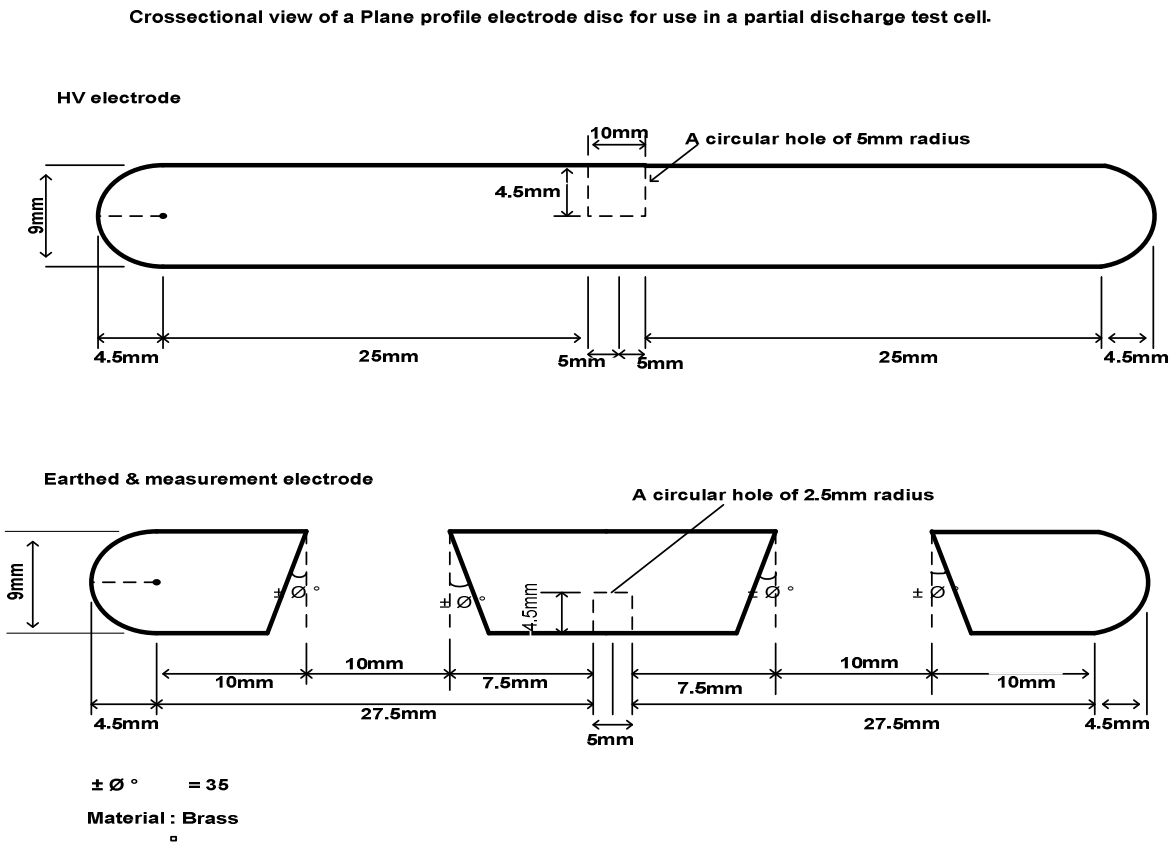

Figure 4-6: Crossectional view with dimensions of the plane profile electrode disc designed and developed for use in UWB PD test cells.

Figure 4-7: The frequency response of the subdivided electrode measured using an Anritsu Network Analyser®.

The subdivided electrode components were then used to construct various test cells with artificial defects in polymer insulation (cavity, surface and point-plane corona) as explained in the following sections.

4.3.2 Construction of the cavity discharge subdivided electrode test cell

Cavity defects in solid dielectric insulation are air bubbles trapped either during manufacturing processes or assembling as in power cable accessories (Kreuger, 1989). Cavities can also occur in equipment insulation as cracks or insulation delamination induced by operational stresses in service ageing. It is important to note that in power cables the manufacturing technologies have advanced to the extent that incidences of accidental trapping of gas bubbles in insulation are rare. Cavity defects however can be found in cable accessories such as terminations and joints. These are normally accidentally introduced through poor workmanship during assembling work (Petzold et al., 2008).

Except for cases where actual power cable samples were used (see Section 4.4) the artificial void defect test cells in the rest of the experiments in this study comprised of the subdivided plane electrodes sandwiching polymer sheets. A disc cavity was created by punching a hole through some of the insulation sheets that were then appropriately stacked together with unpunched sheets to create a cavity at desired positions as either high voltage electrode bound, insulation bound or earth electrode bound as shown in ***Figure 4-8***. The whole test cell assembly was cast in epoxy resin to prevent unwanted surface discharges. Care was taken to prevent accidental trapping of gas bubbles in the epoxy. Furthermore, transparent epoxy was used so that each test cell could be visually checked for unwanted defects.

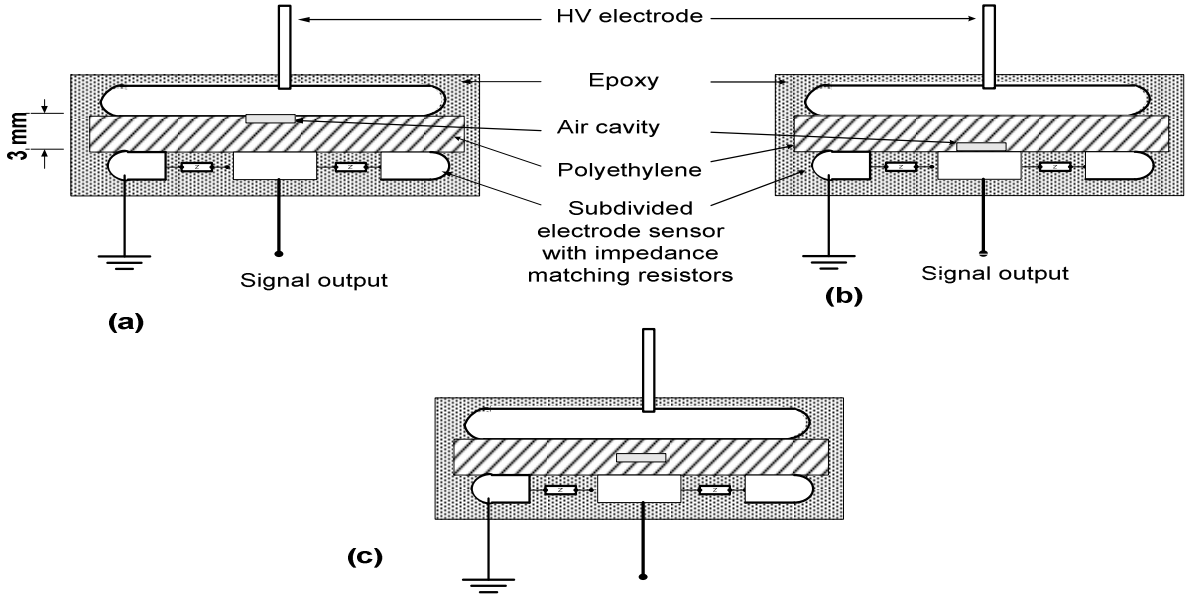

Figure 4-8: ***The artificial cavity defect samples in subdivided electrode test cells: (a) is cavity bounded by HV electrode and insulation (b) is cavity bounded by earth electrode and insulation and (c) cavity embedded in insulation.***

4.3.3 Construction of the surface discharge subdivided electrode test cell

Surface discharge defects occur in construction flows that create conditions of intensified tangential electric field along metal electrode interface with insulation or along boundaries of different insulation types (Kreuger, 1989). In this work surface discharges were simulated either in actual shielded power cables as explained later in Section 4.4 or by sandwiching defect free polymer sheets between electrodes as shown in ***Figure 4-9***.

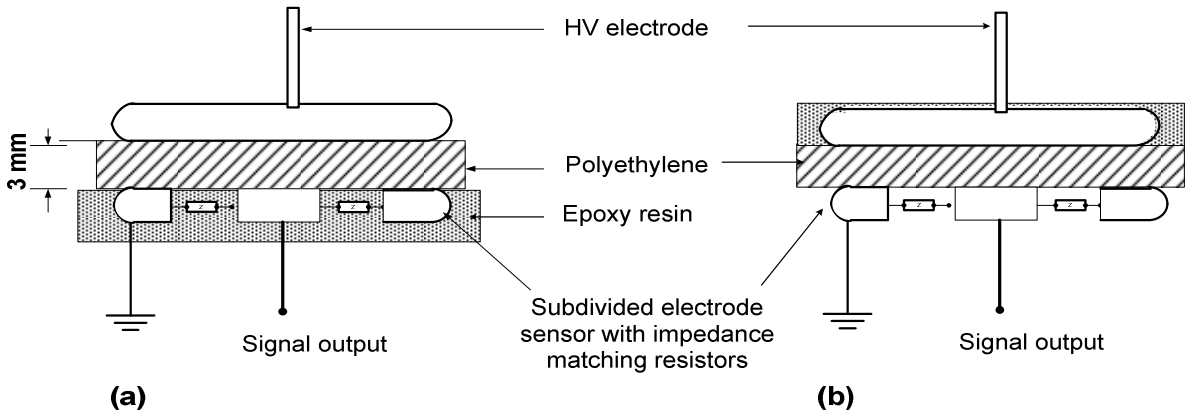

Figure 4-9: ***The artificial surface discharge defect samples in subdivided electrode test cells. (a) surface discharges along the interface between the HV electrode and insulation and (b) surface discharges between the earth electrode and insulation.***

One of the metallic electrodes was completely insulated leaving the other uninsulated so that discharges occurred along the interface with the polymer either along the HV electrode in the case of ***Figure 4-9(a)*** or along the earth electrode in the case of ***Figure 4-9(b)***. The two common cases of surface discharges found in HV equipment were therefore simulated this way.

4.3.4 Construction of the point-plane corona discharge subdivided electrode test cell

Corona discharges in air occur on sharp stress enhancement points in the presence of strong electric field. The sharp points can be either on the HV or earth potential. Such defects in high voltage equipment occur due to construction errors that create sharp metallic points adjacent to other metallic parts in the presence of high electric field. The enhanced electric field on these sharp points initiates corona discharges in air.

Corona discharge defects in this work were simulated as long copper needles attached to either the HV electrode or earth electrode as shown in ***Figure 4-10***. In both cases of artificial corona the electrode edges were insulated by casting in epoxy to avoid any spurious corona discharges.

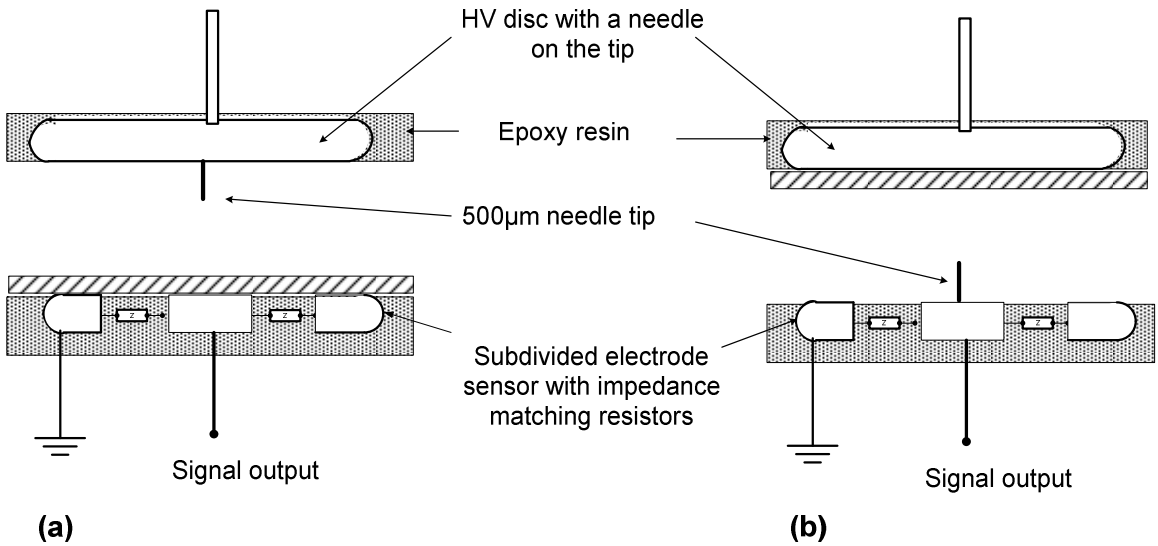

Figure 4-10: ***Point-plane corona in air defect incorporated in a subdivided electrode system. (a) is point to plane corona on the HV electrode while (b) is corona on the earth electrode.***

4.4 Design and construction of the capacitive coupler sensor for ultra UWB PD detection in cable test cells

In order to use test cells that were similar to actual high voltage constructions, samples of 11 kV single core extruded power cables were included in the array of test cells in the work. This concept of simulating and testing defects in actual HV equipment has proven useful in other related work such as Krivda (1995). Common defects found in cable accessories were artificially introduced in the cable test samples. PDs had to be detected from these cable test samples with sensitivity and frequency responses that were similar to those of the parallel plane electrode setup. A search in literature showed that coupling capacitor sensors made on power cables give the desired performances (Tian et al., 2003; Cigre WG 21.16, 2001).

A coupling capacitor on a power cable is a sensor that is made by appropriately interrupting the outer metallic shield of the cable to create an opening on which a metallic foil is wrapped around leaving suitable gaps on either side as shown in ***Figure 4-11*** (Tian et al., 2003; Cigre WG 21.16, 2001). Its advantages over other sensors include better sensitivity, wider bandwidth, higher signal to noise ratio and easier to install and calibrate. In PD diagnosis of power cables the interest in coupling capacitors in general has been motivated by their suitability for online monitoring of PD signals and diagnosis of specific portions/accessories of a power cable (Tian et al, 2003).

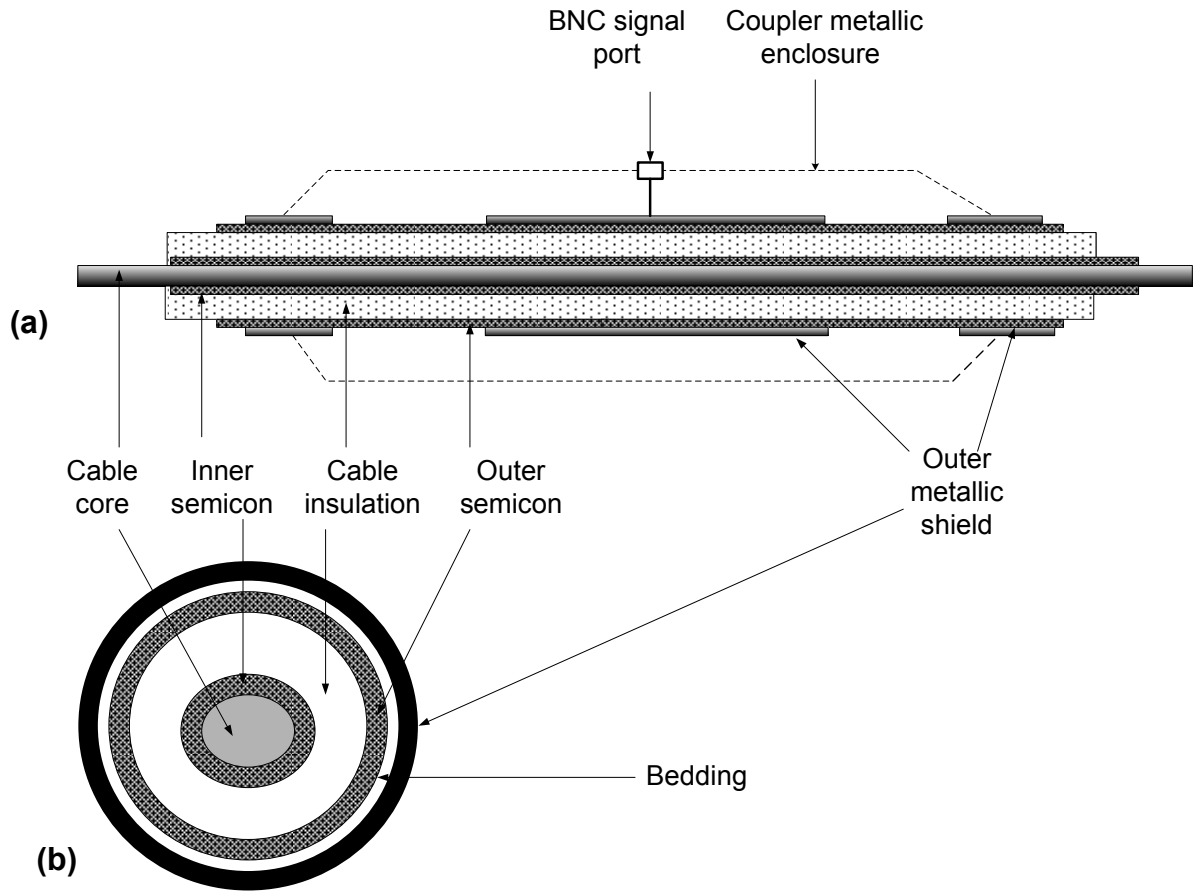

Figure 4-11: The main features of a capacitive coupler after Tian et al (2003).

The cable samples used in this work were cut off a commercial type 11 kV single core cross-linked polyethylene (XLPE) cable with copper tape as outer metallic sheath. The cross section profile of the cable is shown in ***Figure 4-11***. The desired sensitivity and frequency response of the coupling capacitor sensors were 5 pC and at least 1 GHz respectively; these had to be similar to those of the subdivided electrode. In order to achieve these specifications, the coupling capacitor dimensions were carefully and experimentally determined. In literature there is no evidence of procedures that can be followed in the determination of coupling capacitor optimal dimensions. A procedure to optimise the sensitivity and bandwidth of the coupling capacitor was therefore devised, implemented and published (Nyamupangedengu et al., 2007). It entailed identifying the sensor's electrical parameters that influenced the sensitivity and bandwidth and how these parameters in turn depended on the sensor dimensions. The equivalent circuit of the coupling capacitor is as shown in ***Figure 4-12*** (Wang et al., 2005; Zhong et al., 2004; Tian et al., 2003).

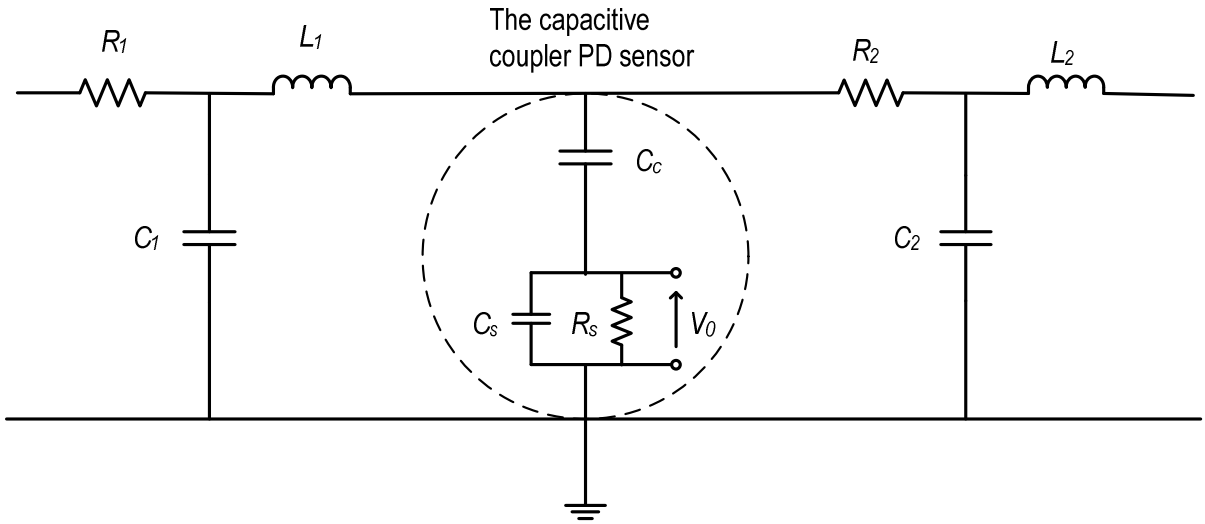

Figure 4-12: Equivalent circuit of the capacitive coupler.

In ***Figure 4-12*** the parameters R_1, L_1, C_1 and R_2, L_2, C_2 are the lumped or distributed parameters of the cable sections on either side of the coupling capacitor. C_c is the capacitance between the metallic strip and the cable core and, C_s and R_s are the capacitance and resistance respectively across the interrupted outer metallic sheath.

4.4.1 Practical tests for coupler sensitivity optimisation

For optimum sensitivity and bandwidth, the coupling capacitance C_c and leakage resistance R_s should be as big as possible while the stray capacitance C_s should be as small as possible. With reference to ***Figure 4-13***, for a given cable size, C_c depends on the length (L) of the coupler metallic strip while C_s is a function of the gap size (g) . A procedure was formulated to experimentally determine the optimal values of L and g for the 70 mm^2 XLPE cable used in this work.

An experiment to investigate the parameters that affect capacitive coupler sensitivity was set up as shown in ***Figure 4-13***. In order to use the same sample for tests involving variation of the coupler length while maintaining the same gap size and cable length, a sliding metallic sleeve was incorporated into the test sample. The sleeve was introduced to move longitudinally and compensate for any change in the gap size caused by alteration of the coupler length. The technique also enabled use of the same sample for measurements involving variations of the

gap while maintaining fixed coupler and cable lengths. A metal foil was placed over the sliding sleeve to bridge it with the far-end cable section. This maintained the cable's coaxial structure that could otherwise have been disturbed by the introduction of the sliding sleeve.

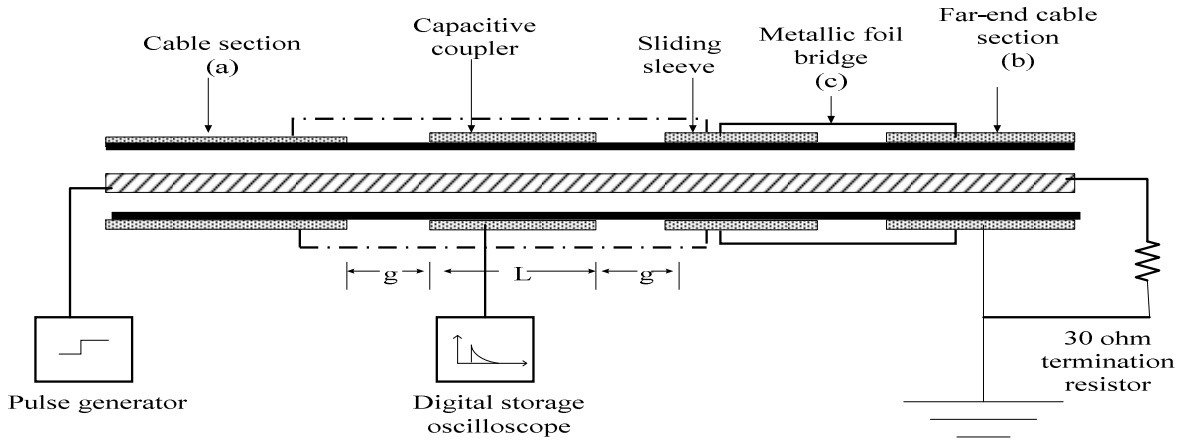

Figure 4-13: Experimental setup for investigation of the influence of coupler parameters on the output.

A step-wave, from a Hewlett Packard® pulse generator, with 5 V amplitude and rise-time of 1.0 ns, was injected into the cable core. The output signal from the coupler was fed into the 50 Ω input of a Tektronix® 500 MHz digital oscilloscope connected to the coupler through a 50 Ω signal cable. The power cable was terminated in its characteristic impedance to minimise reflections.

The investigation of the coupler response to gap size variations involved recording the sensor output while varying the gap size as the coupler length was kept constant. A plot of the coupler gain as a function of the gap size is shown in ***Figure 4-14(a)***. The sensor output increased with the increase in gap but only to a value beyond which it became constant.

To investigate the influence of coupler length on the output, while maintaining a constant gap, the coupler length was varied from 17 mm to 200 mm and each time the corresponding magnitude of the output signal was noted. A plot of the coupler gain as a function of the coupler length is shown in ***Figure 4-14(b)***. It was observed that the sensor output increased with increase in the coupler length but only to a point, beyond which it plateaued.

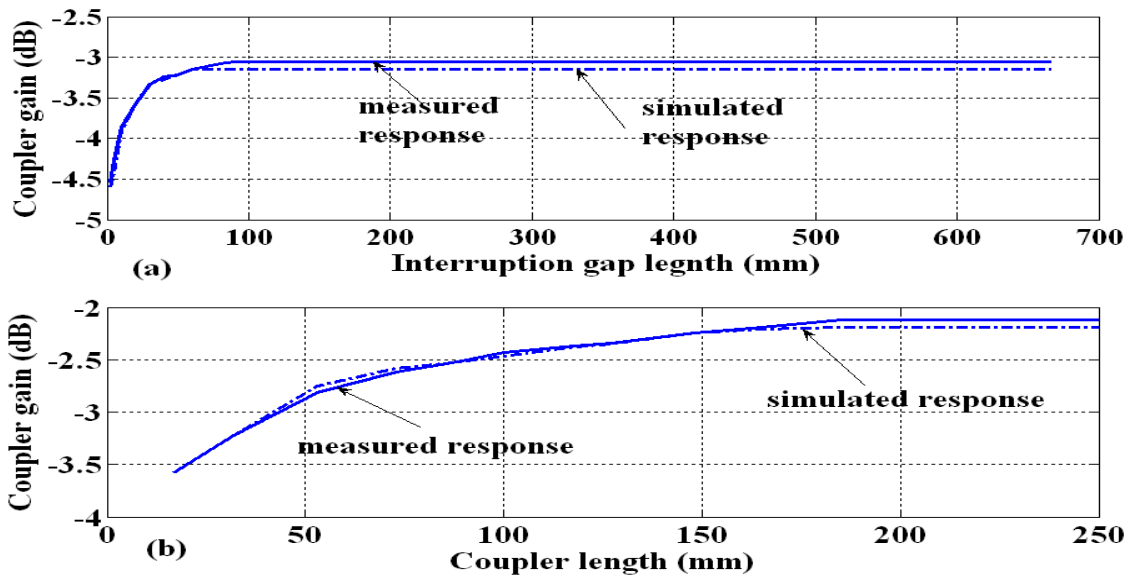

Figure 4-14: ***Sensor response as a function of (a) gap size and (b) coupler length.***

In literature it is acknowledged that it is difficult to quantify C_c and C_s due to the influence of the cable's outer semiconducting layer that has frequency dependent characteristics. Instead of attempting to numerically determine the values of C_c and C_s and how they vary with variations of L and g respectively, a simulation combined with a curve fitting procedure was implemented as explained in the next section.

4.4.2 Simulations

The practical tests setup shown in ***Figure 4-13*** was simulated in the Simulink tool box of MATLAB® using the equivalent model shown in ***Figure 4-15***. The parameters of the cable were those of the actual sample used in the practical tests. The cable had XLPE insulation, outer and inner diameters of 25 mm and 19 mm respectively and was about one meter long. The input pulse used in the measurements was recorded and used as input in the model. The power cable was terminated into its characteristic impedance of 30 Ω. The gap stray resistance was chosen as 1 MΩ after Tian et al (2003). The detection impedance was the 50 Ω input impedance of the oscilloscope.

While maintaining a constant gap (to make the stray capacitance constant), for each measured value of sensor output, the coupling capacitance was adjusted until the output in the model was as close as possible to that measured in the actual physical tests. A curve fitting plot of the simulated coupler response on the same axis as that of the measured values is shown in ***Figure 4-14(b)***. The same procedure was followed for the gap while maintaining the coupler length constant and the results were as shown in ***Figure 4-14 (a)***.

It was deduced that as the coupler length increased, the corresponding coupler capacitance (C_c) increased but non-linearly. Similarly the increase in the interruption gap caused a non-linear increase in the corresponding stray capacitance (C_s). The observed trends are graphically depicted in ***Figure 4-16***. These results confirm the non-linear influence of the semiconducting screen on the coupler capacitance and gap stray capacitance; the relationship is difficult to predict analytically.

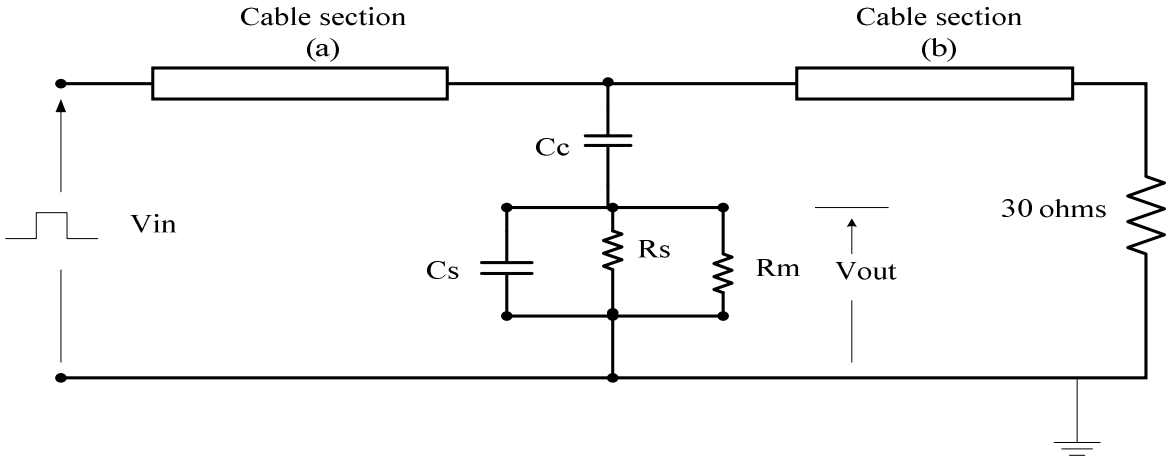

Figure 4-15: ***The equivalent circuit for coupler dimension optimisation tests. (a) and (b) are the near and far-end cable sections, modelled with distributed parameters. C_c is the coupler capacitance, C_s is the gap stray capacitance, R_s is the gap stray resistance and R_m is the oscilloscope input impedance.***

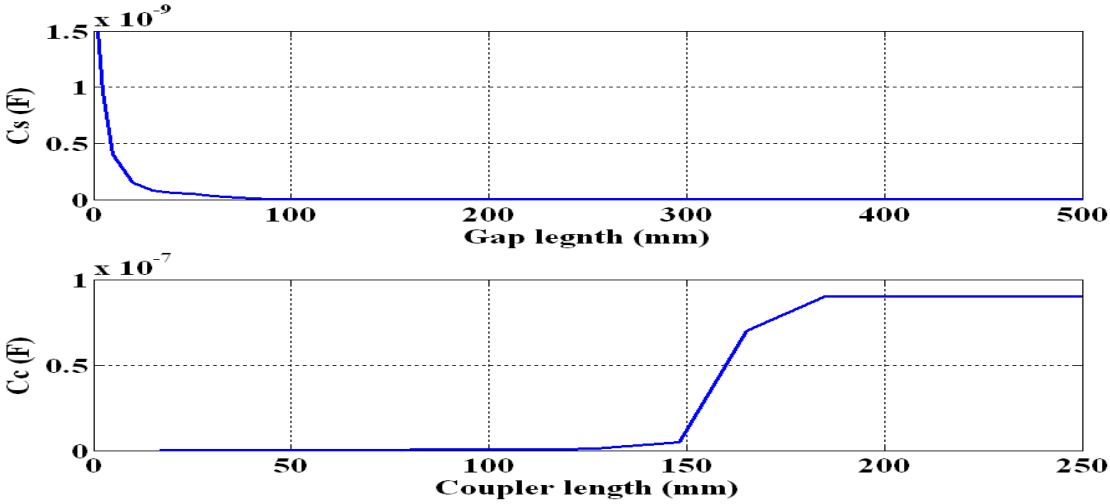

Figure 4-16: ***The variation of the coupler capacitance and gap stray capacitance as a function of the coupler length and gap size respectively.***

4.4.3 A discussion of the capacitive coupler practical and simulated test results

The variations of the coupler capacitance as a function of the coupler length and the influence of the semiconducting screen may be explained in terms of how the fringing and radial electric fields vary with change in the coupler length.

For small coupler lengths there is a minimum radial field; the fringing field dominates as illustrated in ***Figure 4-17***. The corresponding coupling capacitance is therefore small. As the coupler length increases, the fringing field extends further into the insulation until some of the field gets to the core and becomes the radial field as illustrated in ***Figure 4-18***. The coupling capacitance consequently increases. The increase in the coupling capacitance continues until, with reference to the equivalent circuit in ***Figure 4-15***, the corresponding capacitive impedance is so small relative to the detection impedance that any incremental change results in insignificant change of the detected signal. The presence of the semiconducting screen and its dielectric properties at high frequency (Boggs, 2001) distorts the fringing field in a manner that enhances the coupler capacitance.

A field plot of the capacitive coupler simulated in Maxwell® (an electric field simulation package) shows an equipotential region in the semiconducting layer that extends into the gap from the edges of the coupler electrode as shown in ***Figure 4-19***. The length of the extension is a function of frequency (Boggs, 2001). In the simulation, the frequency was assumed to be

10 MHz and the corresponding semiconducting layer parameters (permittivity of 32 and conductivity of 6 x 10^{-8} S/m) were deduced from Jager & Lindbom (2005).

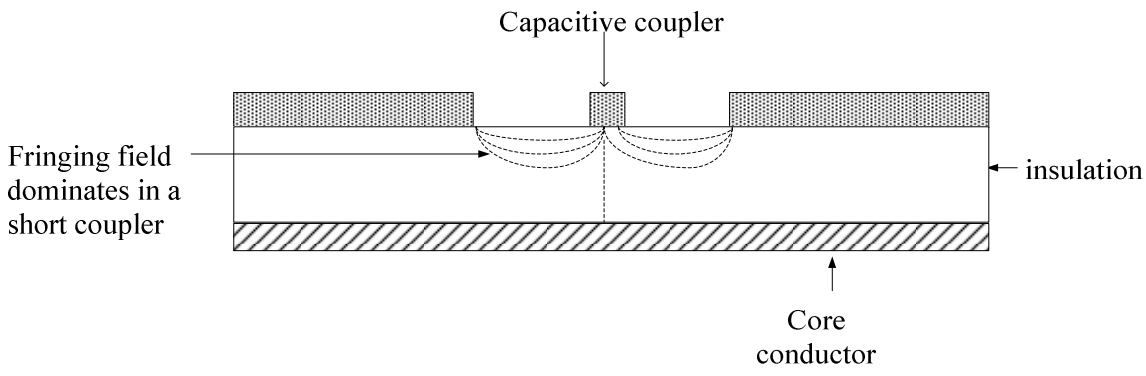

Figure 4-17: ***A sketch of the fringing electric field in a short capacitive coupler.***

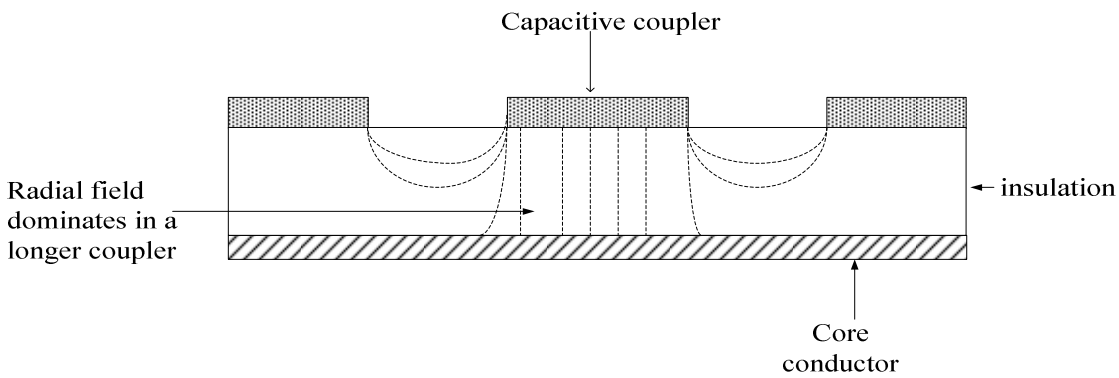

Figure 4-18: ***A sketch showing the radial electric field in a long capacitive coupler.***

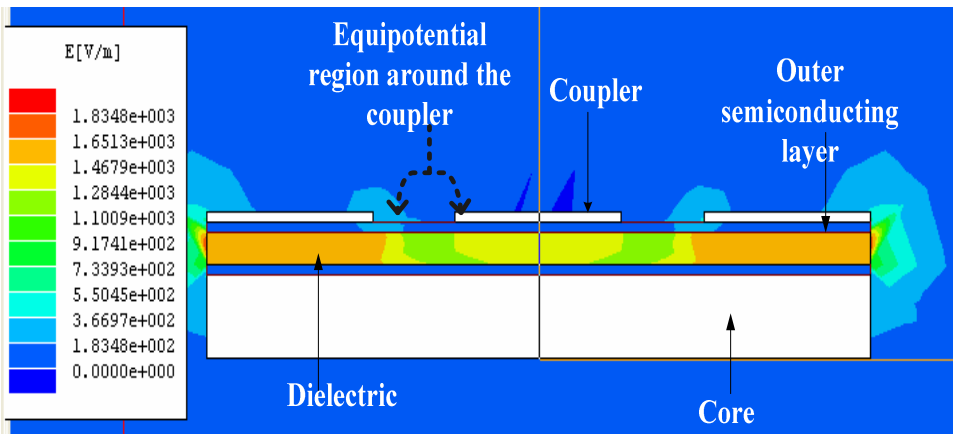

Figure 4-19: ***A plot of the electric fields showing the influence of the semiconducting layer in a capacitor model simulated in Maxwell®.***

4.4.4 Resultant sensor optimal dimensions

The coupler sensor designed using the aforementioned procedure and used in the UWB PD tests in this work is shown in ***Figure 4-20***. The measured frequency response of the prototype coupler is shown in ***Figure 4-21***. The response shows resonance features and compares favourably with those of similar work reported by Tian (2003). Furthermore the response was adequate for this thesis work where frequency components up to 1 GHz were anticipated. ***Figure 4-22*** shows three test samples made out of such coupling capacitors in which artificial PD defects were introduced: (a) an artificial cavity created between insulation and outer metallic shield (b) surface discharge defect simulated as unterminated cable-end and (c) surface discharges on an exposed insulation patch.

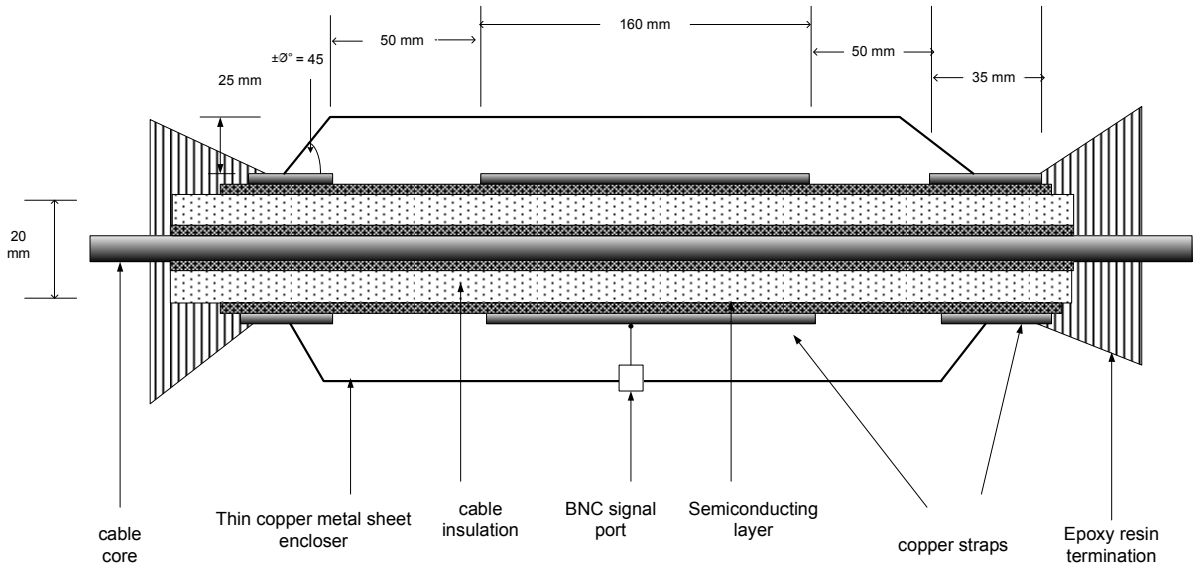

Figure 4-20: The capacitive coupler with optimised dimensions that were determined experimentally.

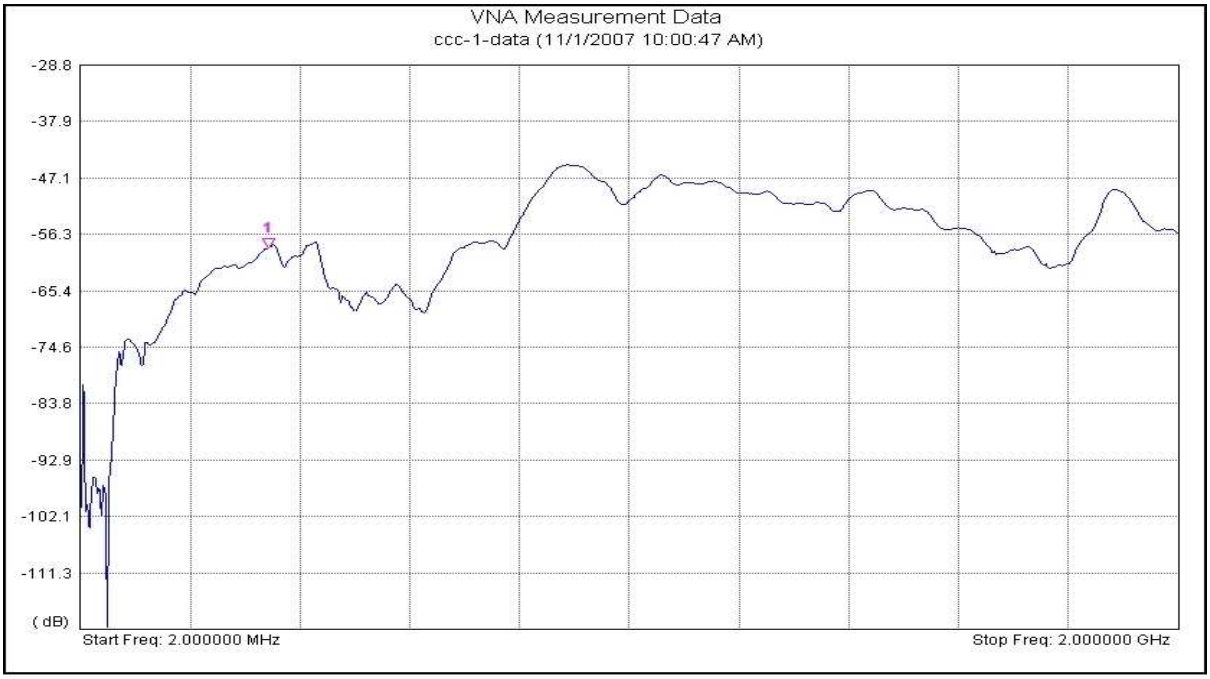

Figure 4-21: ***The frequency response of the coupling capacitor measured using an Anritsu® network analyser.***

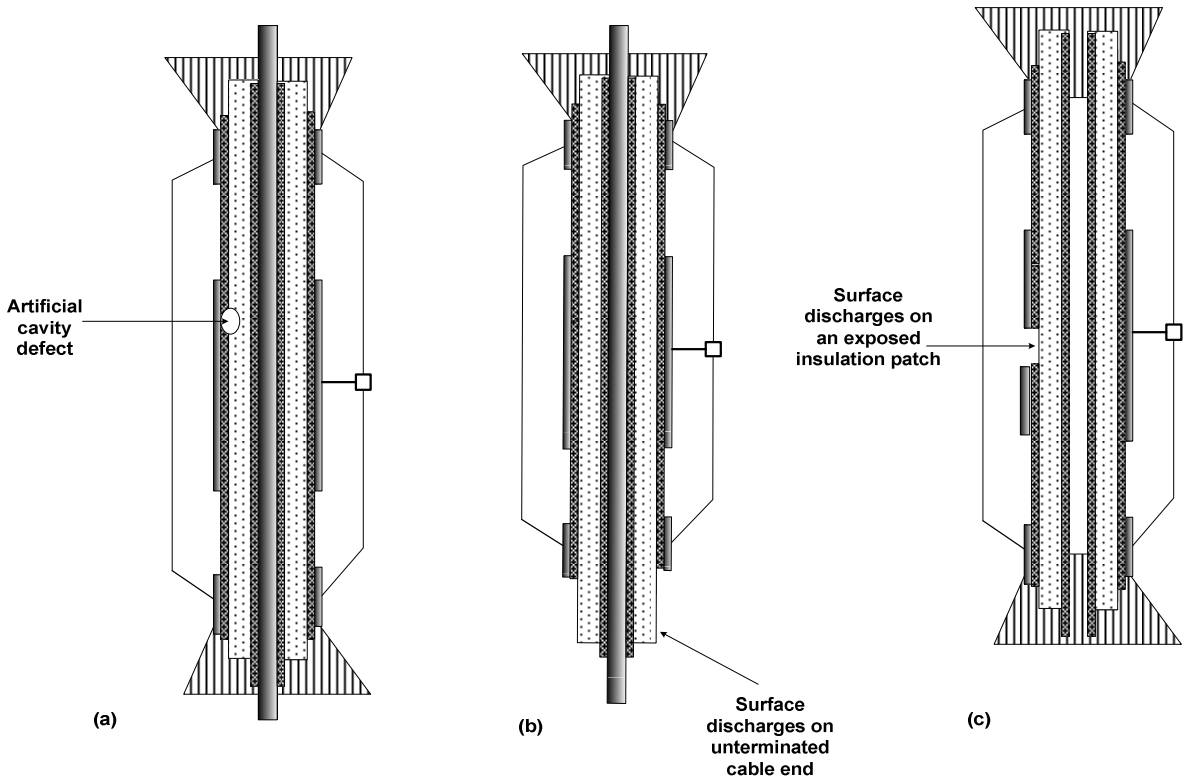

Figure 4-22: ***Power cable test cells with (a) an artificial cavity created between insulation and outer metallic shield (b) surface discharge defect simulated as unterminated cable end and (c) surface discharge on a patch of exposed insulation.***

In order to match the UWB characteristics of the PD sensors (subdivided electrode and coupling capacitor sensors), the PD detection instrument had to be appropriately tuned. The instrument used in this case was a spectrum analyser. The following section explains how the spectrum analyser settings were optimised.

4.5 Sensitivity and accuracy optimisation of the spectrum analyser settings for PD detection

This section begins with a literature review of similar work involving spectrum analyser-based PD detection and how issues of the instrument settings are important in the accuracy of measurements. The section ends with an explanation of the criteria followed in the determination of the spectrum analyser optimal settings used in the work.

Partial discharges are stochastic in nature. They occur in random bursts. Compared to detection of continuous signals, detection of PDs using a spectrum analyser requires more careful selection of the settings for best accuracy. A literature survey on PD detection using spectrum analysers shows that the instrument settings used in the tests varied from one case to another. As an example in Ahmed and Srinivas' work (1998), two sets of spectrum analyser settings were used. In the first case, for a span of 0 to 100 MHz the settings were: sweep time (SWT) of 750 ms, resolution bandwidth (RBW) of 3 MHz and video bandwidth (VBW) of 300 kHz. In another case by the same researchers however, for spans of 0 to 50 MHz and 0 to 30 MHz the settings were: SWT of 20 ms, RBW of 300 kHz and 100 kHz VBW. It is presumed that the SWT in the stated cases were chosen to give the best response for each frequency span. There were however no discussions in the said literature concerning the criteria used in choosing the spectrum analyser settings. Similarly Raja et al (2002) used a SWT of 3 seconds for a span of 0.2 to 1.5 GHz but did not substantiate their choice of settings. In another publication (Raja & Floribert, 2002), however, the same authors indicated (but without further elaboration) that the spectrum analyser's SWT influenced the detection settings.

Meijer and co-researchers published work on acquisition of PDs in SF_6 insulation using a spectrum analyser (Zoetmulder et al., 2003; Meijer et al., 1999; Meijer et al., 1996). Presumably after having noted the importance of spectrum analyser settings on PD detection

accuracy, they conducted experimental tests to investigate the instrument's settings for optimal sensitivity and accuracy in detecting in PD signals. Their generalised conclusion was that the accuracy of spectrum analyser PD measurements increased with increase in SWT up to a value (5 seconds in their case) beyond which there were no any further improvements.

In the present work, tests were also conducted to investigate the optimal settings of a heterodyne sweep tuned spectrum analyser (Rohde & Schwarts®) for the PD detection experiments. Using an artificial corona discharge source in air to give fairly consistently repetitive PDs, the spectrum analyser SWT was varied from lowest to highest possible values for various permutations and combinations of the RBW and VBW. In all the cases a frequency span of 0 to 1 GHz (the range that would be used in the main investigation tests) was used. Comparative plots of the detected PD frequency content variations, measured as spectral bandwidth, are shown in ***Figure 4-23***. It can be seen that the best spectrum analyser response was obtained when the SWT, RBW and VBW were at highest possible settings. As also deduced by Meijer et al (1996), though the PD signal content improved with increase in SWT, it was only up to a specific value beyond which no further improvements could be observed.

From literature as well as similar investigations conducted in this work, it can be deduced that the sensitivity and accuracy of spectrum analysers in PD detection depends on the combination of SWT, RBW and VBW settings. Each spectrum analyser however, depending on type and manufacturer, has unique combination of such settings that give optimal PD detection sensitivity. Generally the SWT, RBW and VBW should be as high as possible. It means that prior to using a spectrum analyser in PD measurements optimal settings of the instrument have to be established and should be part of the overall sensitivity benchmarking process.

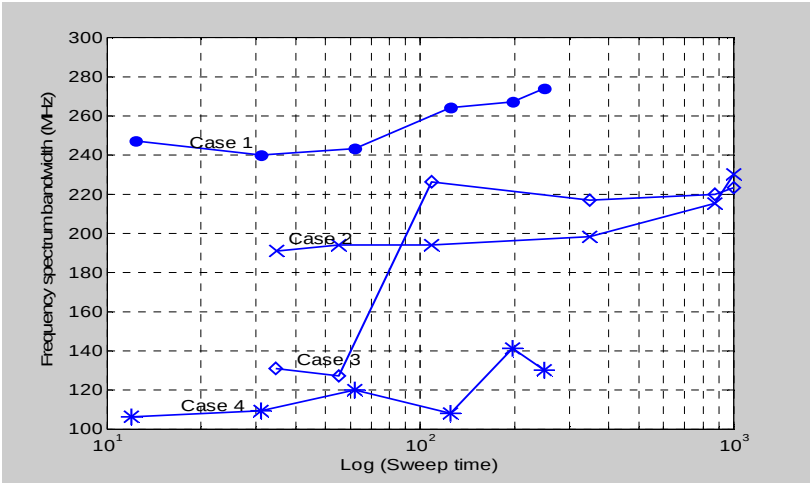

Figure 4-23: ***Variation of the detected PD signal content (measured as bandwidth) as a function of the spectrum analyser SWT for various settings of RBW and VBW.***

Case 1: *RBW and VBW are held at maximum values of 1 MHz while the SWT is varied from 12 ms to 250 ms*

Case 2: *RBW is held at minimum of 300 kHz while VBW is at maximum of 1 MHz and the SWT is varied from 35 ms to 1s*

Case 3: *RBW is at maximum of 1 MHz and VBW is held at minimum of 20 kHz while the SWT is varied from 12 ms to 250 ms*

Case 4: *Both RBW and VBW are held at minimum of 300 kHz and 20 kHz respectively while the SWT is varied from 34.5 ms to 1s*

Based on spectrum analyser optimisation findings, all measurements in this thesis work were conducted with the spectrum analyser SWT set at maximum possible value of 250 ms for a span of 9 kHz to 1 GHz. The RBW and VBW were also both set at maximum possible values of 1 MHz.

4.6 Definitions of the PD frequency spectra descriptors used in this thesis

Among possible features or descriptors that characterise a frequency spectrum, the frequency bandwidth and magnitude variance exhibited distinct trends for each defect type as a function of long term ageing. The bandwidth of the spectrum was defined in this work as the highest frequency component visually discernable above the background noise level as indicated in ***Figure 4-24***.

Magnitude variance in the context of this work was a measure of how the magnitude of the frequency components spread on both sides of the mean and calculated using the formula given in Equation 4.5.

$$\text{Variance (dBm}^2) = \frac{\sum(q-q_{wmean})^2 f}{\sum f} \tag{4.5}$$

Where:

q = is the spectrum component magnitude [dBm].

f = is the component frequency [MHz].

q_{wmean} = is the weighted mean magnitude given by $\frac{\sum(fq)}{\sum f}$ [dBm].

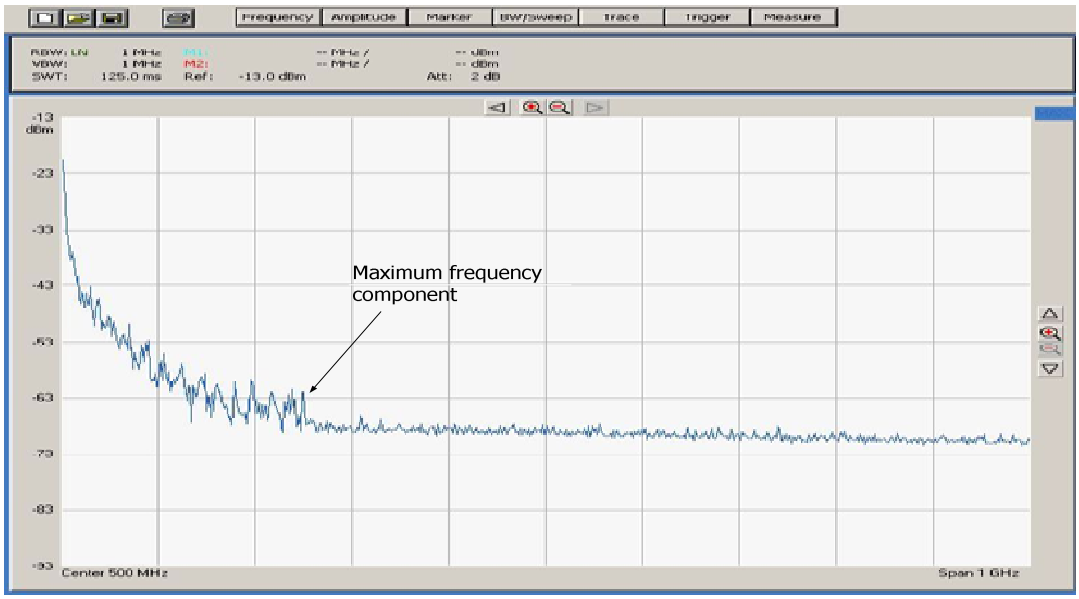

Figure 4-24: ***A typical broadband PD frequency spectrum showing how the maximum frequency (bandwidth) descriptor is read.***

4.7 Summary and pointers to the next chapter

In this chapter the methods used in designing various components of the experimental system have been presented. The method for determining optimal instrument settings for PD spectral detection has also been presented. The definition of the bandwidth measurement used in this thesis has been explained. The experimental system was then established and used to study the PD frequency spectral behaviour under specific controlled conditions as presented in the subsequent chapters. Part I of the investigation is presented in the next chapter and is on how PD spectral content of different types of insulation defects respond to variations in the supply voltage frequency.

5 Experimental Work Part I: Investigation into PD spectral response to frequency variations of the supply voltage

This chapter presents the investigation work on how PD spectral bandwidth depends on the supply voltage frequency. In Chapter 3, where the knowledge gaps that this work sought to address were explained, supply voltage frequency was identified as one of the key variables whose influence on PD spectra needed to be understood. This chapter begins with a literature review on PD characteristics dependency on supply voltage frequency. The literature survey further confirms the limitations in this knowledge domain. The experimental investigation is then presented, results analysed and discussed. The key findings for each type of defect are presented.

5.1 Introduction: Why the SVF dependency of PD characteristics is of interest?

The first of the two key variables whose influence on PD frequency spectra were investigated is the supply voltage frequency (SVF). The reason why this variable is of interest is that many researchers have shown similar interest albeit focusing on other PD characteristics other than the PD signal frequency content. Literature shows that there has been sustained interest in research into how PD characteristics depend on the SVF. Some of the reasons for such interests include the need to perform PD tests at different SVF, the need to accelerate PD ageing tests and the need to understand the influence of harmonics pollution on PD characteristics. These motivators for research in PD characteristics dependency on SVF are briefly reviewed in the following sections.

5.1.1 The need to use frequencies other than the power frequency (50/60 Hz) in PD detection to reduce power rating requirements of the test equipment.

A test voltage frequency of 50/60 Hz may not be technically and economically viable for testing largely capacitive equipment such as power cables. In such cases lower frequencies are desirable. Similarly, higher frequencies are more suitable for inductive equipment such as transformers (IEEE C57.113, 1991) and generators. Consequently, technologies such as 0.1 Hz and dumped ac voltage (DAC) have been developed and commercialised (Wester et al., 2007). The latter can have ringing frequencies that range from a few hundred to thousands of Hz depending on the length of the cable being tested. The flexibility in the choice of frequency of PD test voltage raises a question on the comparability or trending of PD results that are obtained using test voltages of different frequencies (Wester et al., 2007; Cavallini & Montanari, 2006; Bodega et al., 2004).

5.1.2 The need to accelerate insulation aging tests under continuous PD exposure during laboratory based research work

In laboratory based research, higher voltages and frequencies are usually used as accelerating agents in PD aging tests (Radu et al., 2003; Morshuis, 1993; Reynders, 1978). This is done in order to increase the rate of PD induced degradation. The rate of insulation degradation in service at the power frequency can then be inferred. The technique of accelerated aging of PD defects through increasing the test voltage frequency is based on the assumption that the change in the frequency only alters the rate of aging mechanisms and not the nature of the mechanisms (Reynders, 1978). Evidence in literature that supports this assumption is scarce.

5.1.3 The need to understand how PDs are affected by power supply harmonics

Discharges can occur in insulation of equipment that is exposed to power supply distorted by harmonics. Whether and how the harmonics aggravate the PD induced insulation degradation is a question that is yet to be fully explored (Brengtsson, et al., 2009).

5.1.4 The need to tune resonant ac test systems for smallest test power capacities

In resonant ac power cable test systems an inductor is connected in circuit with the voltage source and the cable under test to create a resonance condition that results in reduced power demand for the test setup. Limitations in the variations of inductor's reactance to match the corresponding capacitance of the cable for a resonance condition may entail varying the test voltage frequency in order to achieve the required resonance. The cable in such cases is tested at frequencies different from 50/60 Hz.

5.2 A review of literature on effect of supply voltage frequency on PD characteristics

Various researchers have published findings pertaining to the dependency of PDs on the supply voltage shapes and frequencies. The ranges of supply voltage frequency (SVF) considered generally varied significantly from case to case. A summary of some of the important aspects of the literature on PD dependency on SVF is presented in ***Table 5-1.***

Other literature on the effect of SVF on insulation includes that by Mason (1992) who investigated the influence of SVF on partial discharge inception voltage (PDIV) and short time breakdown voltage of insulation. Mason concluded that in frequency ranges up to a few kHz, the effect on PDIV was too small to explain the observed reduction of short time breakdown voltage of insulation. He suggested that localised heating due to repetitive PDs could be the main cause of the reduction of short time break down voltage of insulation. Gockenbach & Hauschild (2000) also reported results on work involving investigation of SVF effect on the insulation withstand voltage where they concluded that in the frequency range 20 Hz to 300 Hz, insulation experienced the same electric stress effects.

Table 5-1: ***Summary of highlights in literature on the relationship between the supply voltage frequency and PD characteristics.***

Researchers	Frequency range considered	Type of defects	PD characteristics studied	Key findings
(Miller & Black, 1977)	0.1 to 50 Hz	*2-8 mm diameter cavities* in epoxy as well as polyethylene insulation (also surface discharges in cable and stator samples)	PD inception voltage (PDIV) and PD magnitude	- PD characteristics in the stated frequency range were generally independent of the supply voltage frequency. - Experimentation with polyethylene was more difficult than with epoxy because of more induced insulation condition changes. - Surface PDs increased with increase in frequency of supply voltage!
(Radu et al., 2003)	1 to 30 kHz	*0.5 mm gap between dielectric* in Helium at atmospheric pressure	- Glow and pseudo – glow pulse height, repetition rate, width and rise time	- Pulse height remained quasi constant. - Repetition rate reduced with increase in supply voltage frequency. - Pulse width and rise-time reduced with increase in the supply voltage frequency.
(Wester et al., 2007; Bodega et al., 2002)	50 Hz; 0.1 Hz; DAC (260, 520 and 930 Hz)	*2-3 mm diameter cavities* in cast polyester resin	- PD inception delay - PD magnitude and phase patterns	- At frequencies below 50 Hz there were equal chances that the PD characteristics could either be similar or different to those at 50 Hz. - Above 200 Hz PD maximal magnitude decreased with increase in supply voltage frequency. - Overall shape of the phase resolved patterns were generally independent of the supply voltage frequency variations.
(Cavallini & Montanari, 2006; Hauschild, 2006)	0.1; 20; 50 & 300 Hz	*2 mm diameter spherical cavities* in polyethylene, surface and corona discharges	- PD maximal magnitude - PDIV - PD repetition rate - PRPD patterns	- Maximal magnitude decreased with frequency. - PDIV increased with increase in supply voltage frequency. - PRPD patterns changed.
(Forssen & Edin, 2008)	0.01 to 100 Hz	1.5 – 10 mm diameter disc shaped cavities in polycarbonate insulation	- PD maximum and minimum magnitude, - PD repetition rate and PDIV	- PDIV increased with voltage - Average & maximal PD magnitude depended on cavity diameter such that no change occurred for 1.5 mm cavity but for bigger cavities decreased with increase in supply voltage frequency. - No change in minimal PD magnitude - Maximum PD magnitude decreased with increase in supply voltage frequency - PRPD patterns changed.

It is notable that there has been a considerable mix of agreements and controversies in the conclusions on the various research results. An example is that generally most of the researchers, except for Miller & Black (1977), agree that the minimal PD magnitude is independent of the SVF while the maximal magnitude decreases with frequency. A remarkable clarification on the magnitude question was presented by Forssen & Edin (2008) who found out that the dependency of PD magnitude on supply voltage frequency was dependent on the cavity size. They concluded that in small cavities (diameters equal to or less than 1.5 mm) both maximal and minimal PD magnitudes were independent of the SVF. In

larger cavities however the PD magnitudes decreased with increase in the SVF. This was attributed to the possibilities of influence of multiple and simultaneous occurrences of PDs in larger cavities. Another common agreement among researchers is on how the PD inception voltage increases and repetition rate decreases with increase in SVF for cavity PDs.

An example of an area of controversy or disagreement is on the extent of the influence of SVF on PD phase-resolved patterns. As an example, while conclusions from Bodega et al (2004) point towards minimal influence, that by Cavallini et al (2006) as well as Forssen & Edin (2008) reported significant changes, confirming that more work is still needed in this regard.

A scrutiny of most PD parameters studied as summarised in the fourth column of ***Table 5-1*** shows that most of the researchers have focused mainly on conventional PD characteristics such as PDIV and PD extinction voltage (PDEV), apparent magnitude and PRPD patterns. These parameters are conventionally used to characterise partial discharge signals as guided by popular standards such as IEC60270. Of late, however, there has been growing interest in the unconventional characterisation of PDs such as in the HF and UHF techniques (Stone, 2005). In such cases interest is in the information contained in PD pulse shape (in the time domain) or corresponding spectral characteristics (in the frequency domain). The current knowledge on PD characteristics dependency on supply voltage type should be extended to PD pulse shape and frequency content. It is in this context that the work in this part of the thesis focuses on PD spectral characteristics.

Furthermore from the third column (titled '*Type of PD Defects'*) in ***Table 5-1*** it is evident that most of the studies on the influence of SVF on PD characteristics have been performed using cavity defects. This trend could be attributed to an assumption that cavities are among the most common defects found in solid insulation as stated by Gutfleisch & Niemeyer (1995) and Cavallini & Montanari (2006). It is however known that surface discharges and corona also occur in insulation systems. An extension of knowledge on the relationship between SVF and PDs to other types of discharges such as surface discharges and corona is valuable in enriching the effectiveness of PD diagnosis technology. In this work therefore equal attention was given to cavity, surface and corona discharges.

Another interesting observation in the literature is that most of the workers studied cavity discharges and used (in general terms) the same PD mechanism model for simulations and

interpretations of experimental observations (albeit often with some variations). The model is based on Niemeyer (1995), Niemeyer et al. (1991), Fruth & Niemeyer (1992) and other related literature such as (Devins, 1984; Van Brunt, 1994; Heitz, 1999; Crichton et al., 1989; Boggs, 1990; Chan et al., 1991). The model considers partial discharges as being phenomena characterised by a combination of deterministic and probabilistic processes. The following section presents a synthesis of the theory. This is the theory that is used later in Section 5.4 to interpret tests results on cavity PD spectral response to SVF variations.

5.2.1 Theory of cavity discharge mechanism

Cavity PD events sequence are illustrated in ***Figure 5-1*** as derived from Niemeyer's generalised PD model (Niemeyer, 1995).

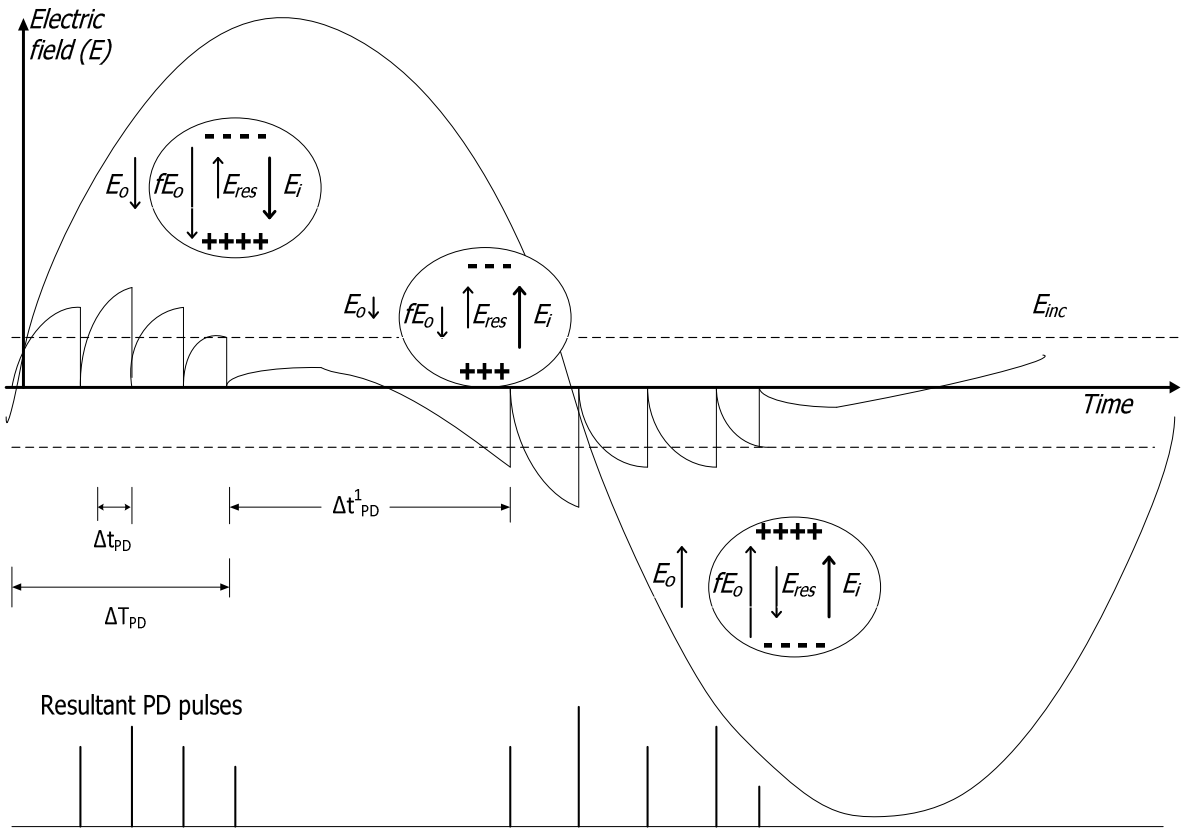

Figure 5-1: ***An illustration of cavity discharge processes showing the role of the residual space charge.***

The discharge process begins with establishment of the resultant electric field E_i that is responsible for initiation of a discharge in the cavity and is given by Equation 5.1.

$$E_i = fE_0 + E_{res} \tag{5.1}$$

Where:

E_0 = electric field in the insulation due to the externally applied voltage [V/m].

f = the stress enhancement factor which is a function of the cavity dimensions. In spherical cavities $f = \frac{3\varepsilon_r}{2\varepsilon_r + 1}$ (Chang et al., 1986), ε_r is the dielectric constant of the insulation [F/m].

E_{res} = the field created by the space charge that is deployed on the cavity walls after a discharge event [V/m].

The stress in the cavity increases until stress conditions become conducive to PD inception, that is, the resultant stress becomes at least equal to the streamer initiation threshold. In an air filled spherical cavity the threshold stress (E_{str}) is given by Equation 5.2.

$$E_{str} = p\left(E_i/p\right)_{cr}\left[1 + B/\sqrt{2rp}\right] \tag{5.2}$$

Where for air in the cavity:

$(E_i/p)_{cr}$ = 25 [V/Pa.m]

B = 8.6 [Pa.m]

p = gas pressure in the cavity [Pa].

r = cavity radius [m].

In the presence of the electric stress that is sufficiently strong for streamer discharge initiation a discharge only occurs when an initiatory or seed electron becomes available in the cavity at strategic positions such as near the anode. The source of such an electron can be either volume or surface emission processes. Volume generation of the seed electron involves

release of free electrons by gas molecules or negative ions due to ionisation from cosmic/radioactive radiation. The surface emission process involves de-trapping of electrons from residual charge (q_{res}) that would have been deployed on the cavity surfaces by the previous discharge events. In small cavities not exposed to radioactive radiation and where the cavity surfaces have high work function, the dominant seed electron source can be assumed to be surface emission process (Cavallini & Montanari, 2006). Some of the residual charge is lost through conduction across the cavity walls and this process is governed by a decay time constant (λ_{cond}) derived from the RC model of the cavity and is given by Equation 5.3.

$$\lambda_{cond} = \frac{\varepsilon_r D_{cavity}}{4\sigma_s} \tag{5.3}$$

Where:

ε_r = the insulation dielectric constant [F/m].

D_{cavity} = the cavity diameter [m].

σ_s = the cavity surface conductivity and this parameter increases with ageing of the cavity under continuous exposure to PDs [S].

The remaining electrons, that would have survived loss through conduction, further diminish in quantity as some migrate deep into the insulation. This loss is accounted for through a decay term as given in Equation 5.4.

$$\text{Migration loss factor} = e^{(-\frac{t}{\lambda_{tr}})} \tag{5.4}$$

Where:

λ_{tr} = is the time constant of loss through the migration [s].

t = is the time elapsed since the last PD event [s].

The rate of de-trapping electrons from the cavity walls ($\dot{N}_e$) is given by Equation 5.5.

$$(\dot{N}_e) = N_e v_0 \exp\left(-\frac{\Phi - \sqrt{eE_i/(4\pi\varepsilon_0)}}{kT}\right) \tag{5.5}$$

Where:

$(\Phi - \sqrt{eE_i/(4\pi\varepsilon_0)})$ = the effective trap depth [eV].

v_0 = fundamental phonon frequency for the insulation [s^{-1}].

e = elementary charge [C].

Φ = effective detrapping work function [eV].

ε_0 = permittivity of vacuum [F/m].

k = the Boltzmann constant [Jk^{-1}].

T = temperature [K].

(N_e) = total number of electrons available for detrapping

At instances when the cavity surfaces are negatively charged, the total number of electrons available for detrapping is scaled down by a factor (ξ) that accounts for the more difficult process of detrapping electrons from negatively charged insulation surfaces (Gutfleisch & Niemeyer, 1995).

At any given instant the production of an initiatory electron from the cavity surface is a stochastic process that can be expressed as a probability function and denoted by Equation 5.6.

$$P(dt) = 1 - e^{-(N_e dt)} \tag{5.6}$$

When initiated the discharge event causes the field in the cavity to change from E_i to a residual value E_{res}. The difference in the electric field is associated with a charge transfer given by Equation 5.7.

$$\Delta q(t) = \varepsilon_0 \pi r^2 (E_i(t) - E_{res}) \tag{5.7}$$

Where:

r = the cavity radius [m].

$E_i(t)$ = the resultant field in the cavity [V/m].

E_{res} = the field remaining in the cavity after a discharge event [V/m].

The resultant field in the cavity consequently varies with time as a function of the sinusoidal external stress. At each point on the voltage wave the magnitude of the charge generated in the cavity can be determined.

The above outlined model of cavity discharge mechanisms is widely used by researchers in PD phenomena. Likewise the model is the basis of interpreting the tests results obtained in this thesis experiments performed to investigate how cavity PD spectra respond to variations in the supply voltage frequency. The next section presents the experimental investigation work.

5.3 The experimental procedure

While various aspects of PD characteristics dependency on SVF have been investigated, those on PD spectra have not been afforded similar attention. An experiment was conceived to investigate how the SVF influenced PD spectral content for various defects as presented in this section.

The experimental setup for the investigation of PD spectral content dependency on supply voltage frequency is depicted in ***Figure 5-2***. The test cells showing the type and dimensions (not drawn to scale) of the artificial PD defects are schematically depicted in ***Figure 5-3***. The defect dimensions were chosen such that in all cases the PDIV was the same: 6 kV at 50 Hz. All test samples were preconditioned by continuous stressing at 7 kV for an hour to avoid taking measurements in the first hour of voltage application where PD behaviour, particularly in voids, could be more influenced by rapid physiochemical changes in the defect than the controlled variables (Morshuis, 1993). Each cell was then tested separately at 7 kV.

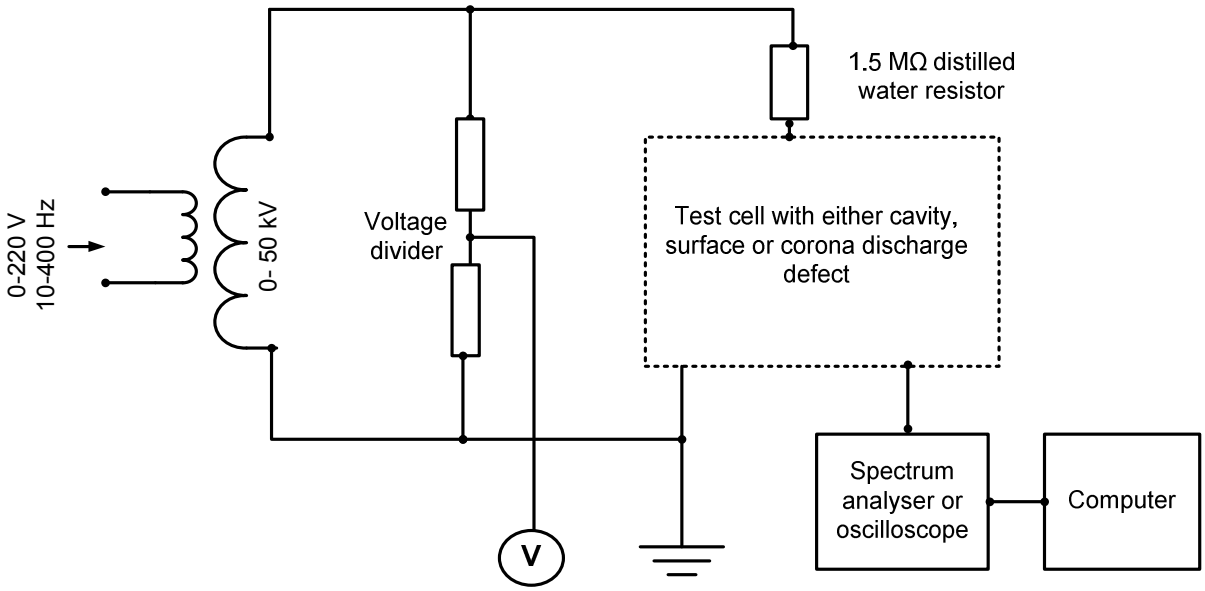

Figure 5-2: ***The experimental setup for investigating the influence of supply voltage frequency on partial discharge characteristics.***

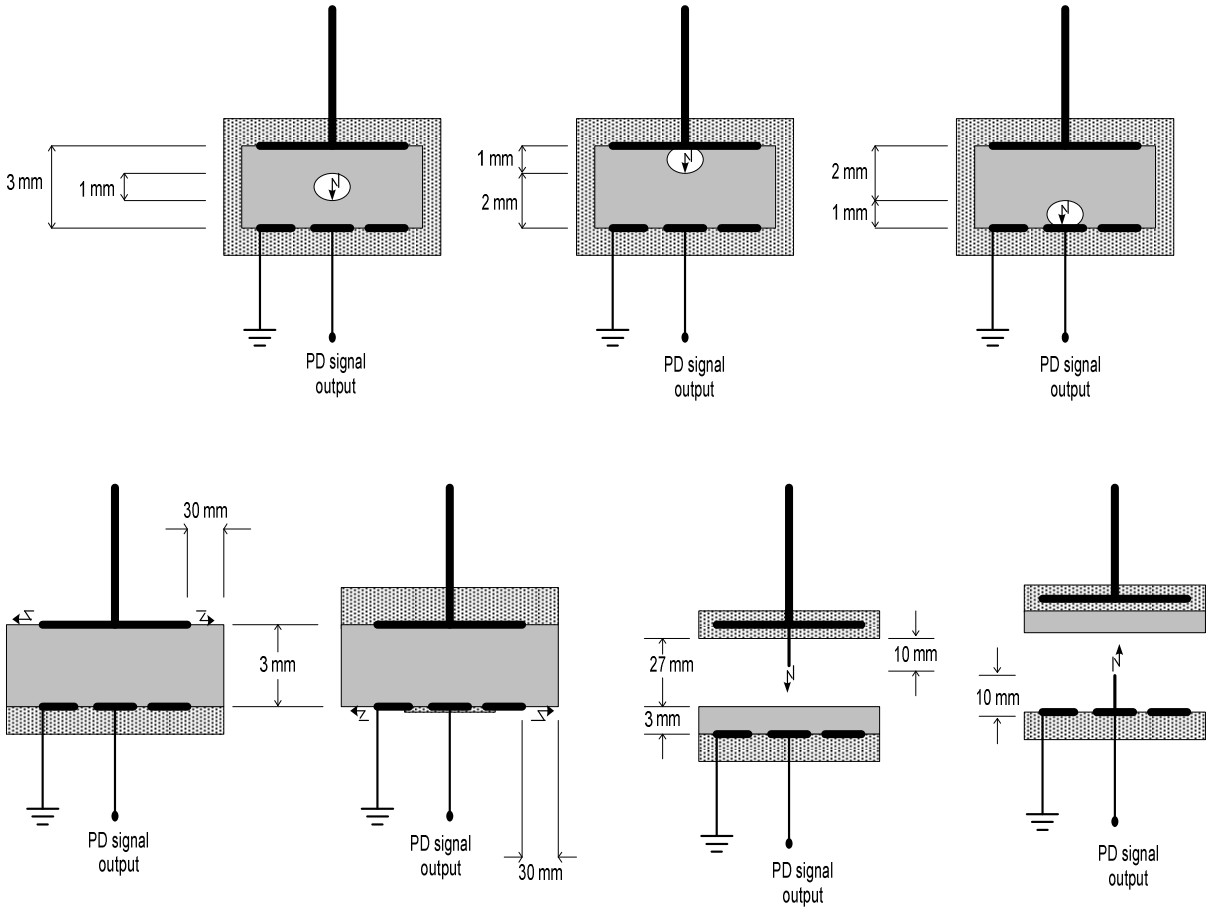

Figure 5-3: ***Test samples showing type of PD defect models and dimensions used in the experimental investigation of PD dependency on supply voltage frequency. The tip radius of the corona discharging copper needle was about 50 µm.***

The PD signals were captured as frequency spectra using a 3 GHz sweep tuned spectrum analyser. The cumulative frequency spectra acquired by the spectrum analyser set in full span and maximum amplitude hold mode was stored for each supply voltage frequency. The spectrum analyser settings were kept at constant optimal values throughout all the tests. The procedure followed in the determination of these optimal settings was explained earlier in Section 4.5. The optimal settings of the spectrum analyser were: SWT – 250 ms, RBW – 1 MHz and VBW – 1 MHz. Each spectral record at every SVF was a maximum hold trace registered at each spectral frequency component over a period of 2 minutes of continuous repetitive sweeps. The SVF was varied from 20 to 400 Hz and incremented in steps of 20 Hz. Five independent measurements were taken at every step. The 2-minute test duration and number of measurements per every test step for each sample were optimally minimal in order to limit PD induced ageing effects that would otherwise adversely influence the test results. In order to check results repeatability, a number of independent but similar tests were conducted.

The experimental tests were conducted in a screened laboratory environment at ambient atmospheric conditions of 20°C to 25°C and 50% humidity. Each set of measurements did not take more than 3 hours including the preconditioning time.

Related tests, but in the time domain, were conducted on similar test samples. The same experimental setup and procedures were used but with a digital oscilloscope as the detection instrument instead of the spectrum analyser. The 500 MHz oscilloscope adequately reproduced the original PD pulse shapes (when the PDs were detected using a 3 GHz spectrum analyser, after preconditioning for an hour, the PD spectral bandwidth of all the defects did not exceeded 500 MHz). In order to record the true shape of the PD pulses at every SVF, the time base of the oscilloscope was set to values that enabled measurement of the rise-time, fall-time, width and amplitude of the pulses using the inbuilt functions of the oscilloscope. Unlike in the frequency domain where the spectrum analyser combined the frequency components of both negative and positive discharges, in the time domain it was easier to separate the positive and negative pulses. At each measurement step five positive and five negative PD pulses were captured and stored for analysis.

The results of the experimental tests categorised per test sample type are presented and analysed in the next sections.

5.4 Results: Void discharges dependence on supply voltage frequency variation

This section presents the experimental observations, discussion of the results and comments on the practical challenges encountered in the experimental measurements of cavity discharges. The measurement results are presented first followed by a discussion of the results using cavity PD mechanism theory.

5.4.1 Measurements and observations

The spectral bandwidth of cavity PD were generally not responsive to changes in the SVF from 20 to 400 Hz irrespective of the cavity position between the electrodes where the cases investigated were: HV electrode bound, earth electrode bound and fully embedded cavity in insulation. The scatter plots of the spectral bandwidths as a function of the SVF are presented in ***Figure 5-4***, ***Figure 5-5*** and ***Figure 5-6***. It is notable that the degree of stochastic scatter as indicated by confidence range at each measuring point in the plots was more pronounced than in surface discharge and corona. A closer look at the scatter plots also suggests some quasi-modulation in the trends.

Similar measurements were conducted in the time domain where the pulse shapes of positive and negative cavity PDs were measured as a function of the SVF. Except for negative PD pulse height that decreased with increase in SVF, all the other PD pulse parameters were not responsive to the changes in the SVF in range 20 to 400 Hz as shown in ***Figure 5-7*** (Nyamupangedengu & Jandrell, 2008). Examples of the recorded pulses are shown in Appendix B.

PD defect type	Spectral bandwidth as a function of the supply voltage frequency
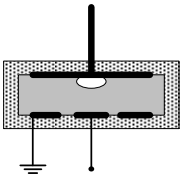 HV electrode bounded cavity	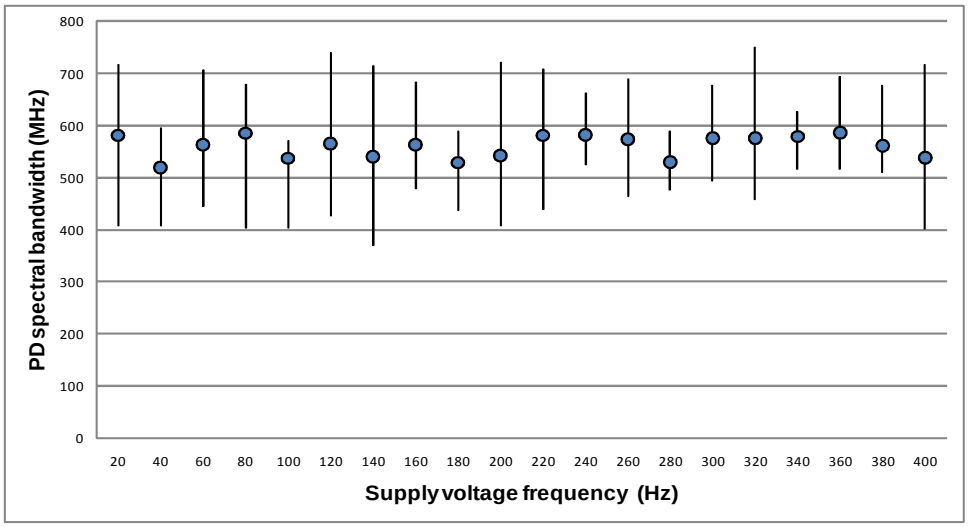
	Typical spectra at lowest and highest frequency of the supply voltage
	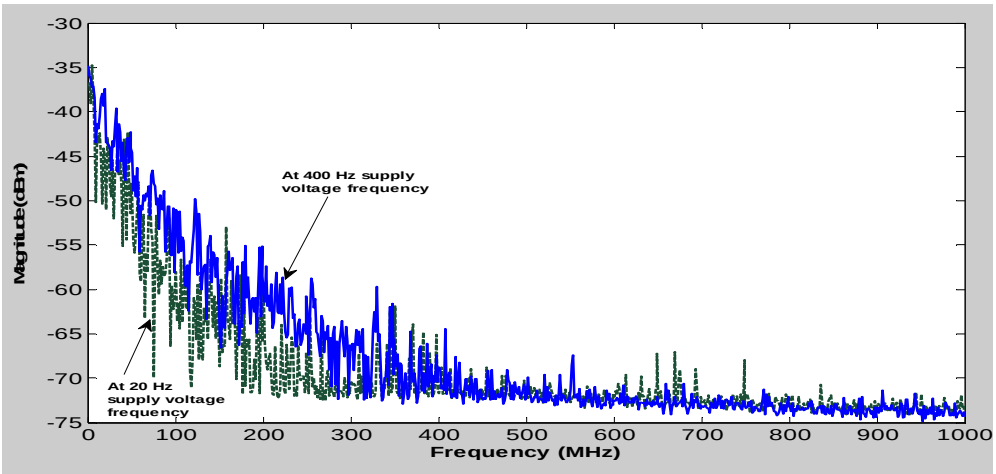

Figure 5-4: PD spectral bandwidth variation as a function of SVF for HV electrode bounded cavities in polymer insulation.

PD defect type	Spectral bandwidth as a function of the supply voltage frequency
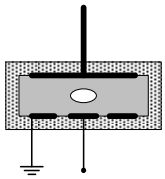 Insulation bounded cavity	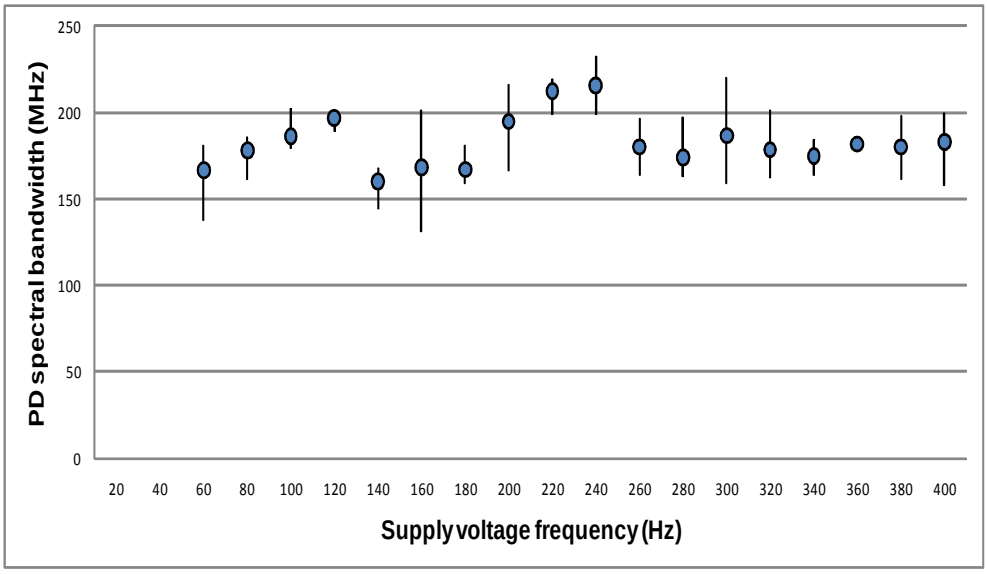
	Typical spectra at lowest and highest frequency of the supply voltage
	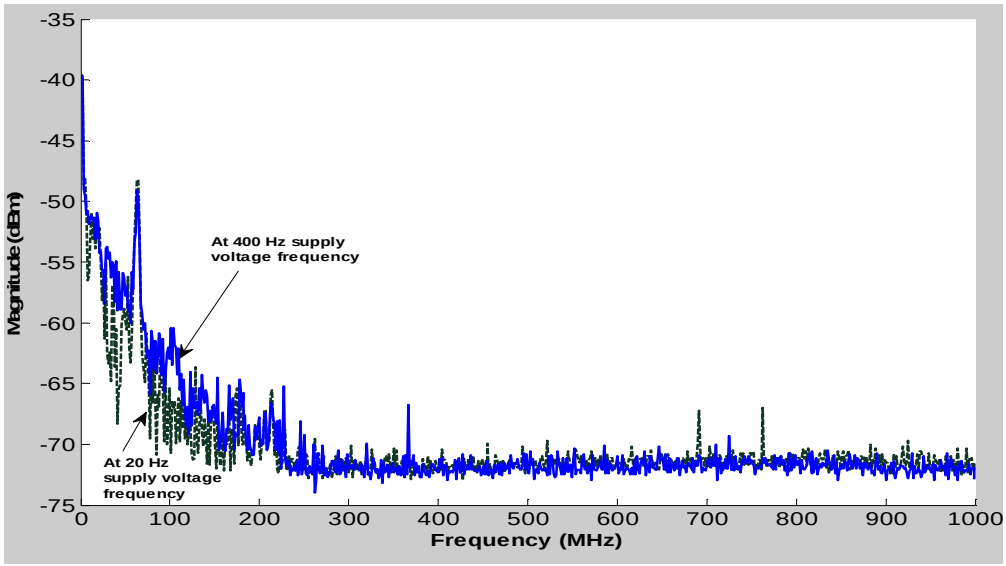

Figure 5-5: PD spectral bandwidth variation as a function of SVF for embedded cavities in polymer insulation.

PD defect type	Spectral bandwidth as a function of the supply voltage frequency
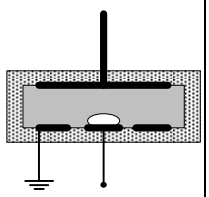 Earth electrode bounded cavity	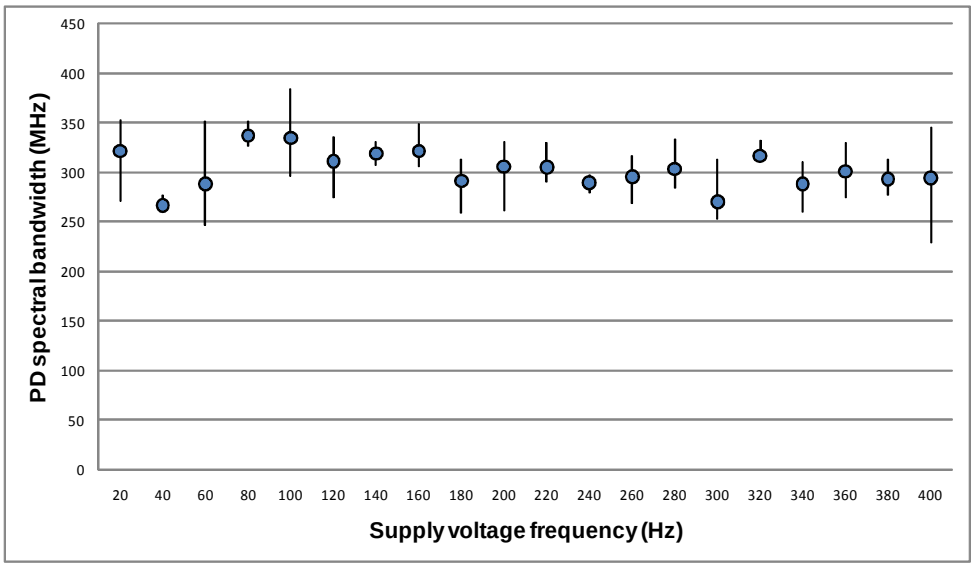
	Typical spectra at lowest and highest frequency of the supply voltage
	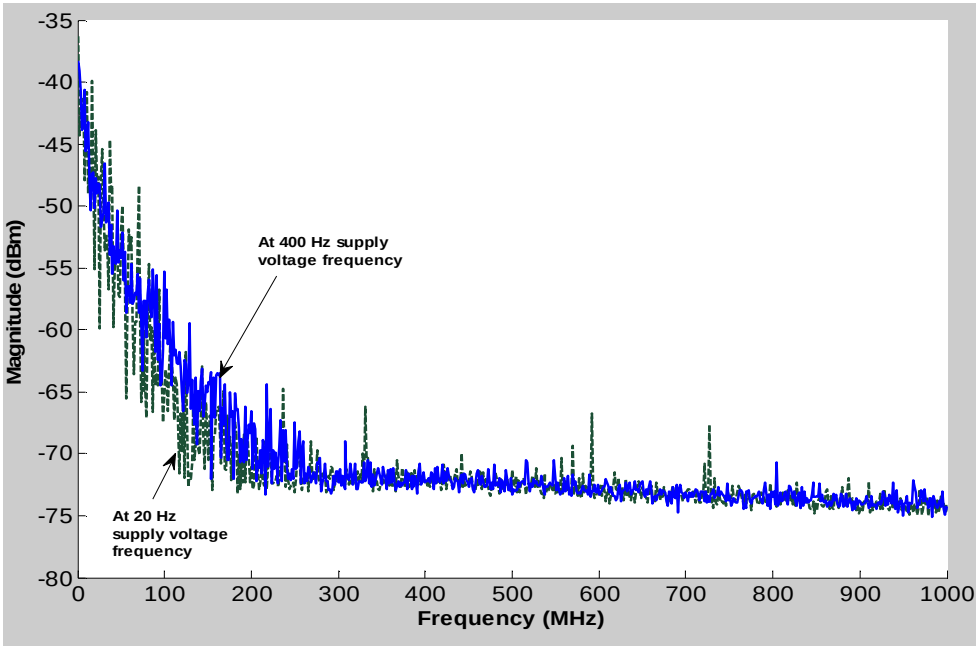

Figure 5-6: PD spectral bandwidth variation as a function of SVF for earth electrode bounded cavities in polymer insulation.

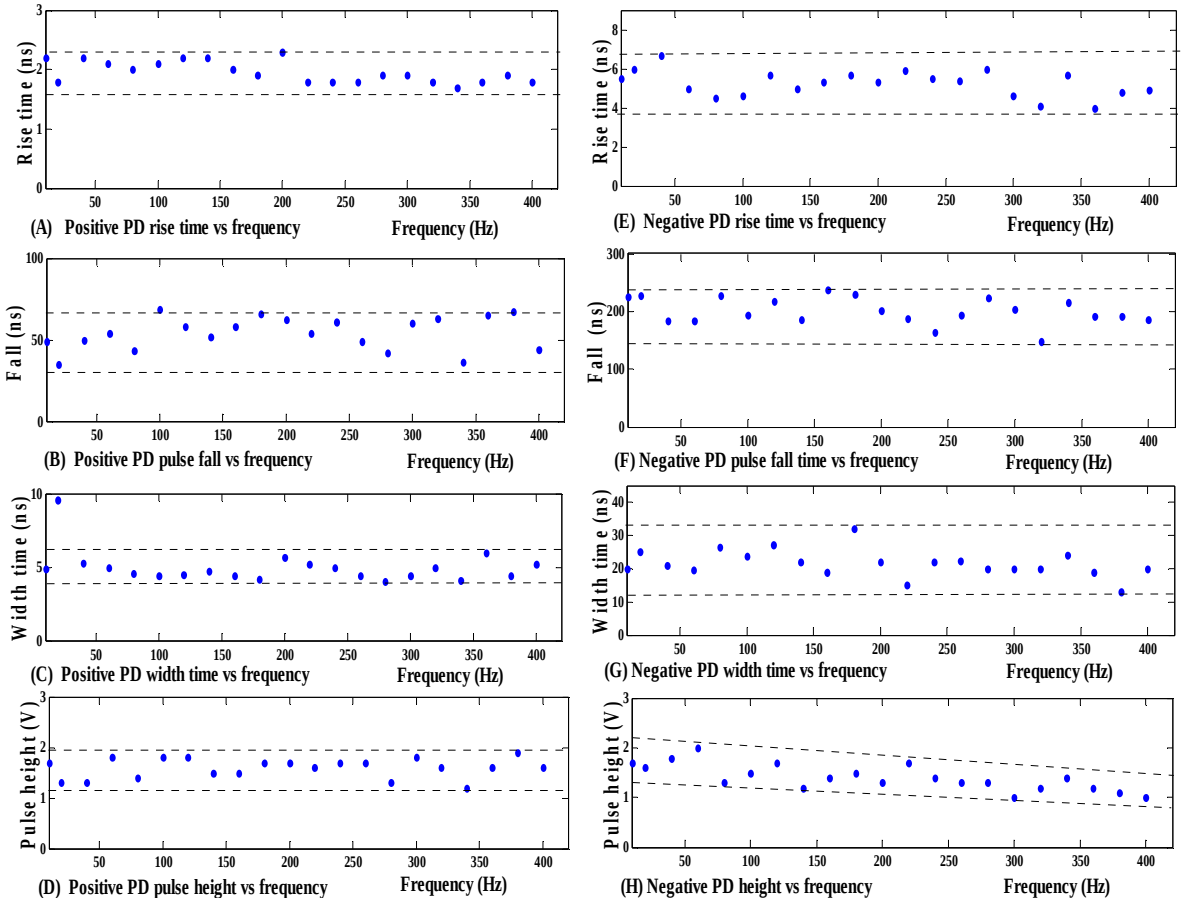

Figure 5-7: ***Scatter plots of cavity PD pulse parameters as a function of the supply voltage frequency (Nyamupangedengu & Jandrell, 2008).***

5.4.2 Cavity PD tests results analysis and discussion

It is evident from the discharge model outlined earlier in Section 5.2.1 that the residual space charge in the cavity plays a critical role in determining the phase angle at which discharge occurs on the test voltage cycle. This in turn affects the nature of the discharge avalanches and manifest as distinct discharge current pulse shape or frequency spectra. Assuming the residual charge decay parameters remain constant, λ_{cond} (due to cavity surface conductivity) and λ_{tr} (due to charge migration to deeper insulation traps), the amount of residual charge generated at each discharge event depends on the length of the time (Δt_{PD}) between consecutive pulses. With reference to ***Figure 5-1***, Δt_{PD} is proportional to the rate of increase of the resultant field $E_i(t)$ which in turn is a function of the rate of change of the supply

voltage. If the rate of change of $E_i(t)$ is much slower relative to λ_{cond} and λ_{tr} then the discharge characteristics are not influenced by the SVF. *This is considered as a possible explanation of the observation in this experimental work where the positive PD pulse parameters were not influenced by the variations of the SVF in the range 20 to 400 Hz. An increase in the SVF causes reduction of the time slot (ΔT_{PD}) that is available for the occurrence of PD pulses in the first quadrant of the voltage cycle. The number of PD pulses therefore reduces with increase in SVF*. This relationship was noted by some researchers as they investigated the influence of SVF on PD characteristics (Cavallini & Montanari, 2006; Radu et al., 2003).

In the zero crossing regions, particularly on polarity reversal from positive to negative, different conditions exist. The amount of residual charge remaining after the 'quiet' time interval $\Delta t^1{}_{PD}$ (and assuming no significant changes in λ_{cond} and λ_{tr}) is proportional to the number of PD pulses that would have occurred in the period preceding this time interval. Since the latter is a function of the SVF, the residual charge in the zero crossing region can be considered to depend on the SVF. It follows that PDs occurring after this quiet interval are in turn dependent on changes in the SVF. In the zero crossing region, the $E_i(t)$ and E_{res} are in phase. Furthermore where polarity changes from positive to negative, it is more difficult to extract seed electrons from negatively charged surfaces. Discharges therefore occur at bigger gap overvoltages. These factors mean that maximal magnitudes occur in this region in addition to being influenced by the SVF. *This was confirmed by observations in the time domain measurements in this work where the negative PD pulse magnitude decreased with increase in SVF as shown in pulse parameter scatter plots of* ***Figure 5-7***. Other researchers have attributed the appearance of 'rabbit ear' like portion of PRPD patterns to these type of PDs. These 'ears' were observed to disappear with increase in SVF (Cavallini & Montanari, 2006) thus further confirming the model.

When observed in the frequency domain in this work, the cavity frequency spectral characteristics were generally not responsive to changes in the SVF as shown in ***Figure 5-4***, ***Figure 5-5*** *and* ***Figure 5-6***. *This is explained as follows: The frequency spectra were recorded using a spectrum analyser in the maximum hold mode. It implies that the frequency components of both positive and negative PDs were overlayed. Since the negative PDs decreased in magnitude with increase in SVF, the resultant overall spectra were dominated*

by the positive PDs and therefore did not change with changes in the SVF even though the negative PD changed.

5.4.3 Some remarks on practical challenges in cavity PD measurements

When investigating the influence of SVF on cavity discharge characteristics, all the other parameters that influence PD characteristics had to be held constant. One parameter however that was difficult to control was the ageing related changes of the discharge environment. It is known that once a discharge process is initiated in a cavity encapsulated in solid organic insulation, the nature of the subsequent discharges depend on the changes to the discharge environment caused by the previous discharge.

PDs in un-aged cavities are known to be more unstable within the first hour of initial inception and that is why most researchers such as Forssen & Edin (2008) and Morshuis (1995b) preconditioned samples for about an hour before taking measurements. Similarly in this thesis work, samples were preconditioned by continuously stressing at about 120% of the inception voltage for an hour before taking measurements. Furthermore the test duration of each sample was limited to 3 hours during which 5 measurements were taken at each frequency from 20 to 400 Hz in steps of 20 Hz. Despite these precautions however, some degree of ageing could still have occurred and manifested as the observed relatively big variance of data at each measuring point (***Figure 5-4***, ***Figure 5-5*** and ***Figure 5-6***). The unstable behaviour of cavity PDs was also experienced by Miller & Black (1977) who noted that it was more pronounced in polyethylene than epoxy insulation. It is for the same reason that Forssen & Edin (2008) used polycarbonate insulation in their studies as the PDs were relatively more stable.

5.4.4 Key findings on cavity discharges

In small cavities the PD spectral content is immune to variations in the supply voltage frequency. The life span of residual space charge in the cavity (after each PD event) relative to the rate of change of the supply voltage, determines how the discharge characteristics respond to the supply voltage frequency.

5.5 Results: Surface discharges dependency on supply voltage frequency variation

The experimental observations and results discussion of tests on surface discharge samples are presented in this section. The observations and measurement results are analysed and interpreted using the widely accepted theory of surface discharge mechanisms.

5.5.1 Measurements and observations

Surface discharge spectral bandwidth increased with increase in the supply voltage frequency from 20 to 400 Hz as shown in the scatter plots in ***Figure 5-8*** and ***Figure 5-9***. The same trend was observed for the two cases of surface discharges: those on the earth electrode interface with the insulation and those on the HV electrode interface with insulation. As the supply voltage frequency was increased from 20 Hz to 400 Hz the average spectral bandwidths increased by aproximately 170% for HV electrode surface discharges and by approximately 40% in the case of the earth electrode surface discharges. Other forms of energy such as optical and audio increased in intensity as the SVF increased. Photographic images of the discharges at 20 Hz and at 400 Hz supply voltage frequencies are shown in ***Figure 5-10***. The difference in light intensities in the two cases is apparent.

Related measurements conducted in the time domain showed that negative surface discharge PD pulse shapes changed in response to changes in the supply voltage frequency in the range 20 to 400 Hz as shown in ***Figure 5-11***. Examples of the recorded PD pulses are shown in Appendix B.

PD defect type	Spectral bandwidth as a function of the supply voltage frequency
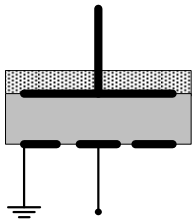 Surface discharges on earth electrode & insulation interface	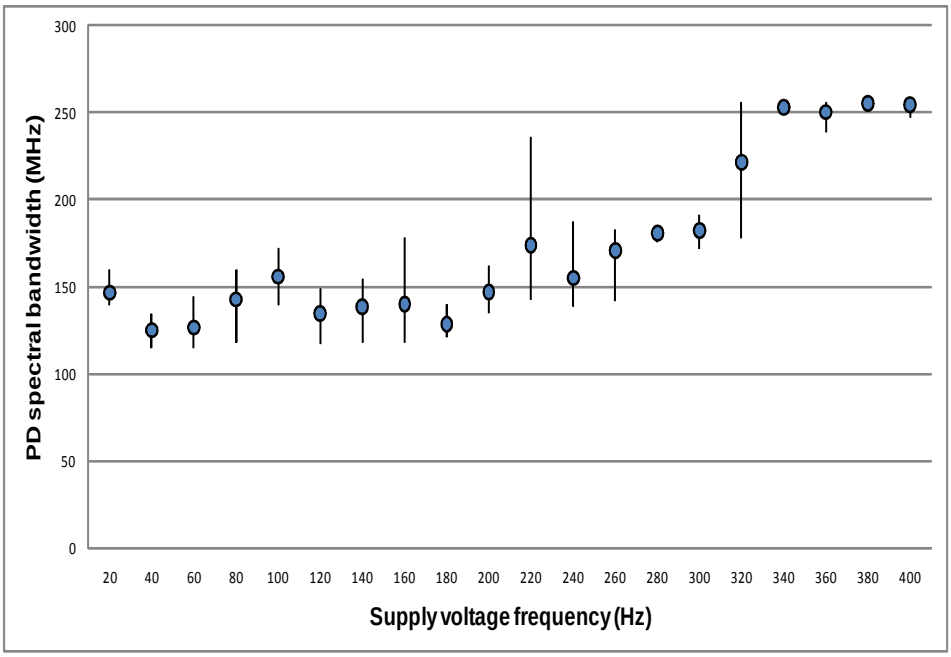
	Typical spectra at lowest and highest frequency of the supply voltage
	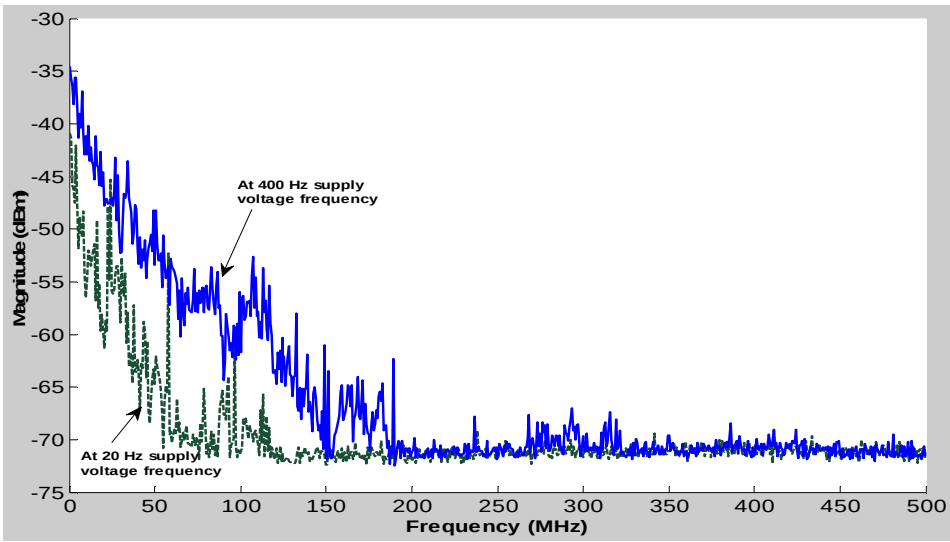

Figure 5-8: ***PD spectral bandwidth variation as a function of SVF for surface discharges occurring along the interface of earth electrode and polymer insulation. An example of the PD spectra (plotted on the same axis) but obtained at two extreme values of the SVF is shown.***

PD defect type	Spectral bandwidth as a function of the supply voltage frequency
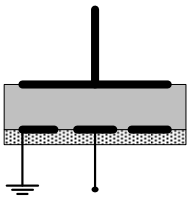 Surface discharges on HV electrode & insulation interface	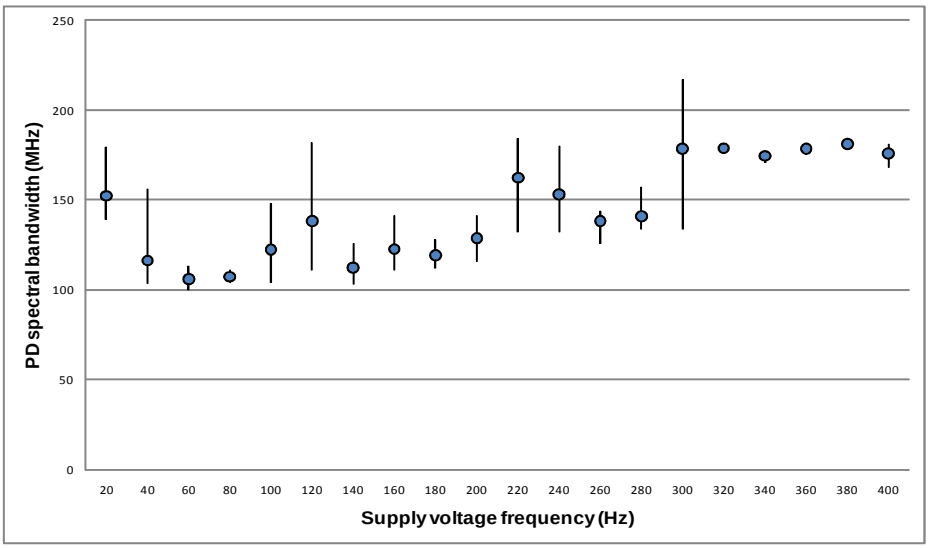
	Typical spectra at lowest and highest frequency of the supply voltage
	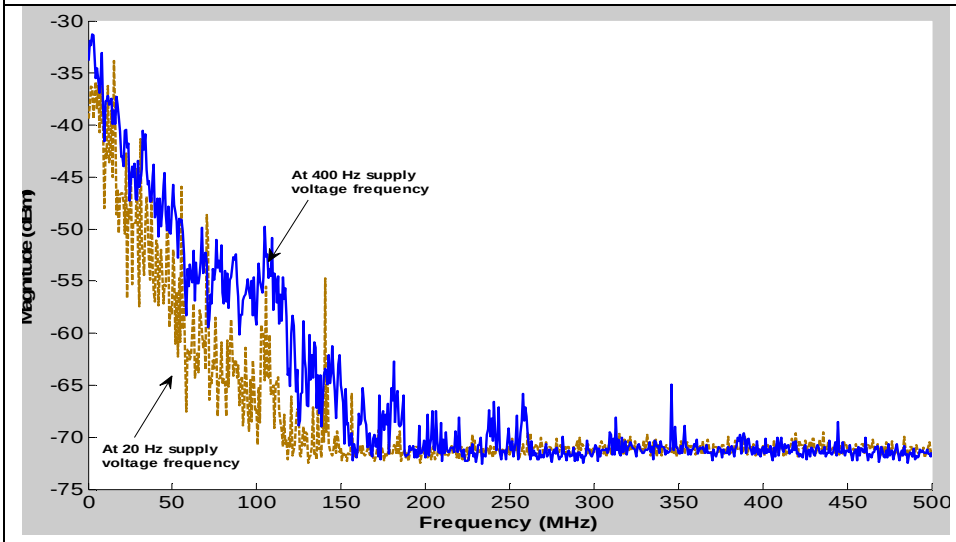

Figure 5-9: *PD spectral bandwidth variation as a function of SVF for surface discharges occurring along the interface of HV electrode and polymer insulation. An example of the PD spectra (plotted on the same axis) obtained at two extreme values of the SVF is shown.*

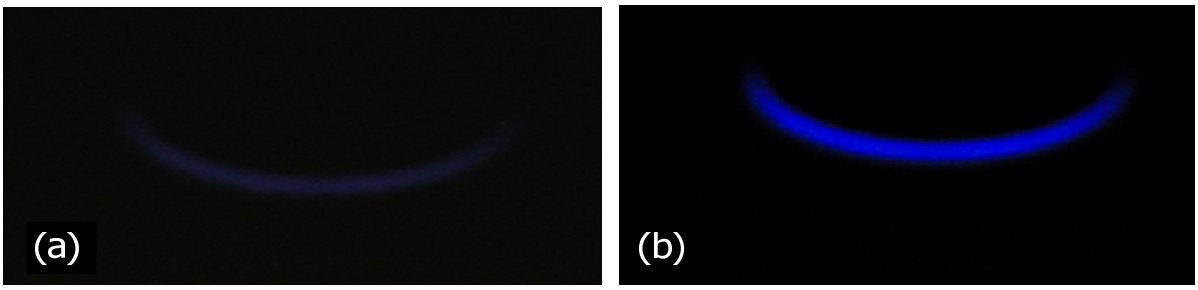

Figure 5-10: *Photographs of surface discharges taken at same camera exposure settings: at supply voltage frequency of a) 20 Hz and b) 400 Hz*

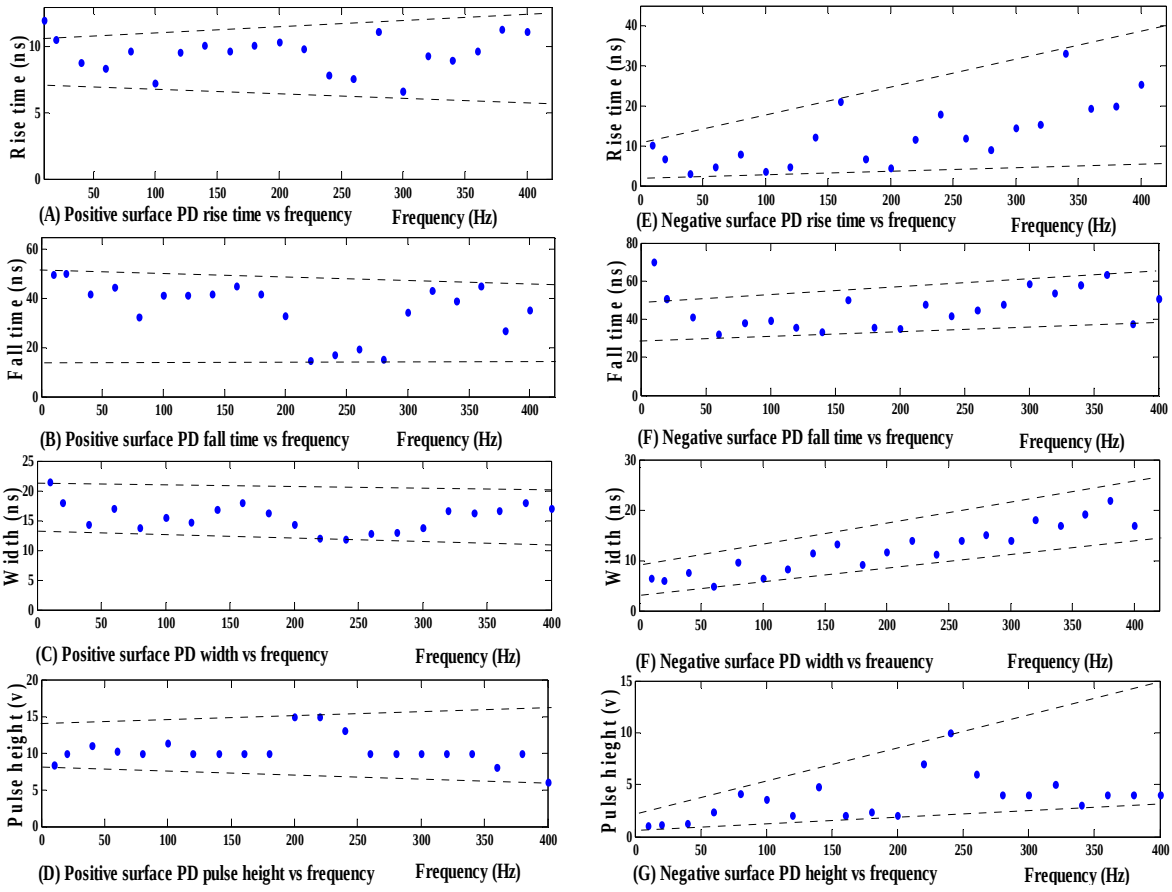

Figure 5-11: ***Scatter plots of surface discharge pulse parameters as a function of the supply voltage frequency (Nyamupangedengu & Jandrell, 2008).***

5.5.2 Surface discharge mechanism analysis

The surface discharge response to variations in the supply voltage frequency can be explained in terms of space charge dynamics in the discharge region along the insulation interface with the metallic electrode. Researchers such as Murooka et al (2001) studied surface discharge mechanisms using techniques such as the dust and photographic figure methods. The surface discharge mechanisms are illustrated as depicted in ***Figure 5-12***.

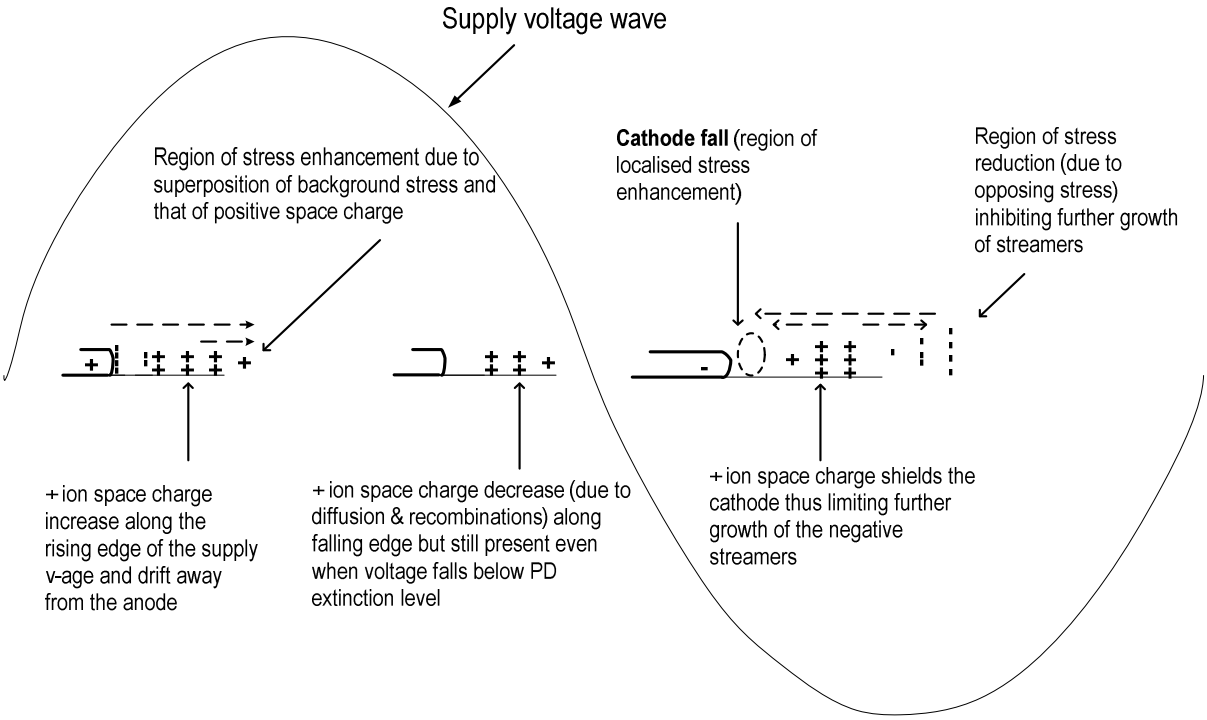

Figure 5-12: ***An illustration of surface discharge mechanisms showing the influence of the slower positive ion cloud.***

The space charge dynamics' response to increase in SVF can be deduced from the illustration of the surface PD mechanisms in ***Figure 5-12***. In the positive half cycle at the tip of the positive ion cloud the stress due to the space charge cloud superimposes on the background stress. The maximum electric field therefore occurs at the advancing plasma tip (Murooka et al., 2001; Fouracre et al., 1999). Assuming constant space charge decay, an increase in the supply voltage frequency gives less time for the positive ion space charge to disperse during the full cycle of the supply voltage. With increasing SVF, the amount of positive ion space charge available in each discharge event increases. An increase in the amount of the positive ion space charge results in more stress enhancement at the tip of the positive ion space cloud causing faster avalanches and further extension of the discharge streamer. *This manifests as increased discharge frequency bandwidth, optical and audible emissions as observed in the experimental tests.*

In the negative half cycle the positive ion cloud near the cathode causes enhanced stress region between the ion cloud and the cathode. This region is known as the cathode fall (Murooka et al., 2001). More avalanches are consequently initiated producing more positive ions as electrons (being much lighter) are quickly swept away to the opposite electrode. Since

increased SVF results in increased positive ion space charge, it follows that the size of the cathode fall region increases with increase in the SVF. *The shielding effect of the positive ion cloud increases resulting in further limitation of the negative discharge streamer growth. This could be the reason why in this work in the negative half cycle the discharge pulse magnitudes were observed to decrease with increase in the SVF. However in the frequency domain, where both positive and negative discharges were detected simultaneously using a spectrum analyser in a maximum hold mode, the frequency components of the positive discharges prevailed over those of the negative discharges. The overall surface discharge spectral bandwidth therefore increased as the SVF increased although that of the negative discharges would have decreased due to the increased cathode fall.*

Although the positive surface discharge pulse rise-time increased with increase in SVF, the pulse width decreased with increase in SVF as shown in ***Figure 5-13(c)***. Since the spectral content bandwidth is not only related to rise-time as the pulse width decreases, the spectral bandwidth increases as observed in this work. The possible effect of pulse superposition is also noted as a phenomenon that makes it difficult to correlate spectral bandwidth with the corresponding pulse parameters. Incidences of pulse superposition have a high probability of occurrence in surface discharges particularly with the type of samples used in this work where a disc electrode was pressed against a layer of dielectric insulation. The concept of pulse superposition phenomenon resulting in the distortion of the measured pulse parameters was also experimentally and analytically explored by Reid et al (2006) as well as Brosche et al (1999). They reported that current pulses could occur in bursts of up to ten individual pulses in as short time as 1.0 ns. Such pulses are difficult to resolve using ordinary signal measuring instruments.

5.5.3 Key findings on surface discharges' dependency on SVF

Surface discharge spectral bandwidth increase with increase in supply voltage frequency. Positive ion clouds effectively determine how surface discharges respond to variations in the SVF through either influencing streamer mechanisms in the positive half cycle or the cathode fall magnitude in the negative half cycle.

5.6 Results: Point-plane corona PD dependency on supply voltage frequency variation

The experimental tests results as well as observations for point to plane corona in air are presented and discussed in this section. The measurement results are interpreted using the commonly agreed theory of corona discharges.

5.6.1 Measurements and observations

The relationships between spectral bandwidth of point to plane corona in air with variations in the SVF (in the range 20 to 400 Hz) are shown as scatter plots in ***Figure 5-14*** and ***Figure 5-15***. Adjacent to the scatter plots are examples of the corona spectral signatures recorded at the lowest (20 Hz) and at highest (400 Hz) SVF frequencies. The spectral bandwidth of corona discharges decreased with increase in the SVF. The trends for both HV electrode and earth electrode corona however had a step-wise trend. Equivalent measurements conducted in the time domain gave scatter plots of pulse parameters as a function of SVF presented in ***Figure 5-17***. The changes in the pulse shapes were visually distinct as shown in some examples of the pulses in Appendix B. As in the frequency domain the pulse rise-time and height decreased and in distinct steps in response to increase in the SVF. The corresponding audio and optical energy emitted from the corona PDs also decreased with increase in SVF. Examples of the optical images of the corona at the lowest and highest supply voltage frequencies are shown in ***Figure 5-16***. On the photographic images, the differences in intensities can be discerned.

PD defect type	Spectral bandwidth as a function of the supply voltage frequency
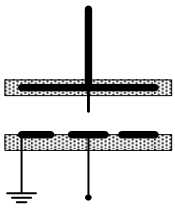 Point-to plane corona in air on HV electrode	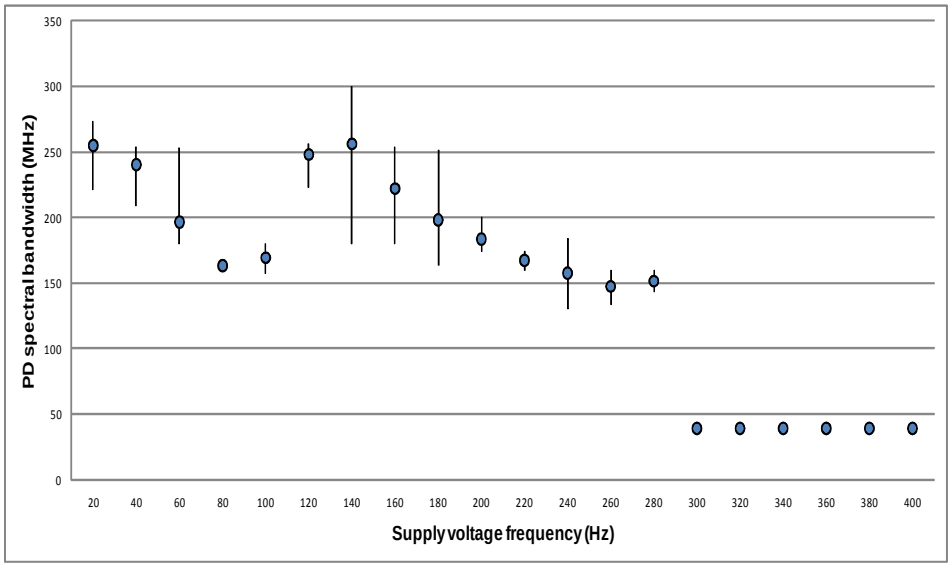
	Typical spectra at lowest and highest frequency of the supply voltage
	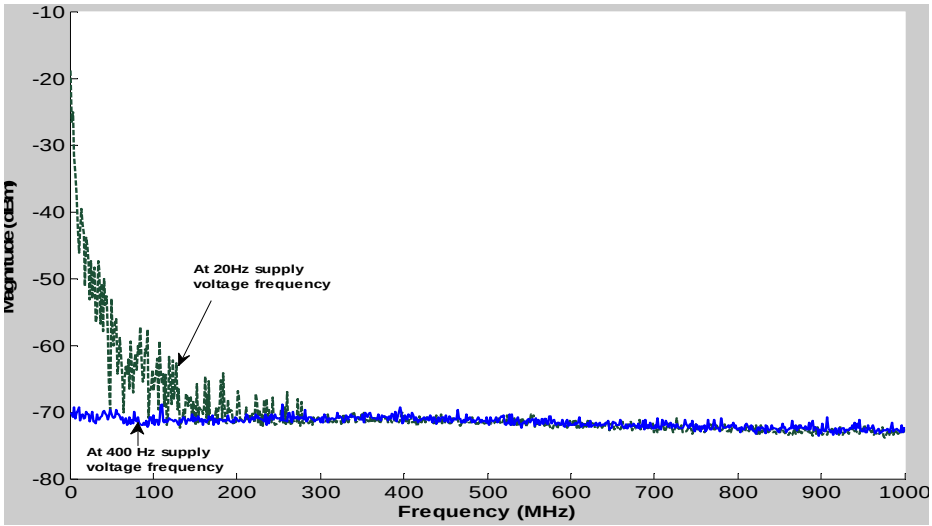

Figure 5-14: ***PD spectral bandwidth variation as a function of SVF for point-plane corona discharges in air on HV electrode. An example of the PD spectra (plotted on the same axis) obtained at two extreme values of the SVF is shown.***

PD defect type	Spectral bandwidth as a function of the supply voltage frequency
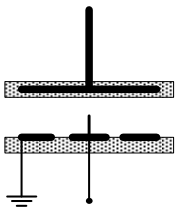 Point-to-plane corona in air on earth electrode	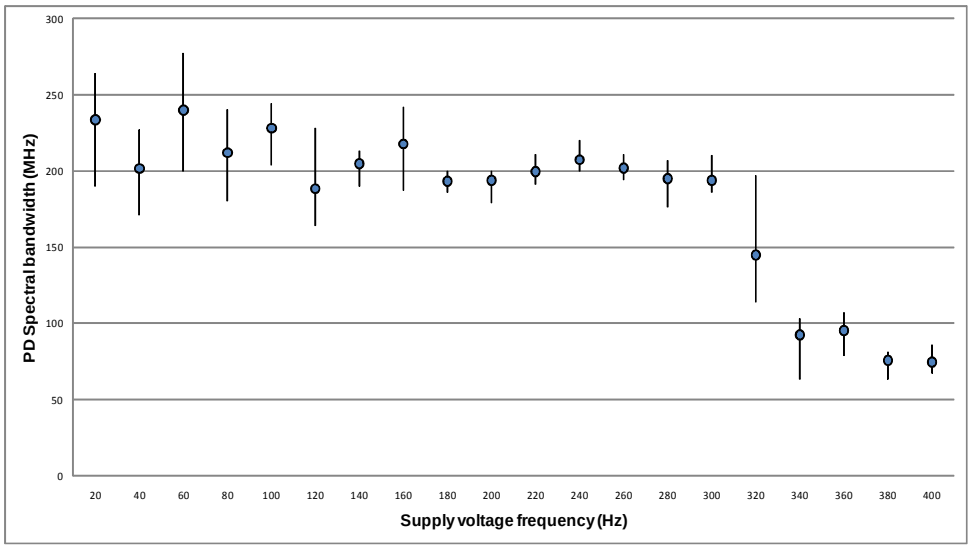
	Typical spectra at lowest and highest frequency of the supply voltage
	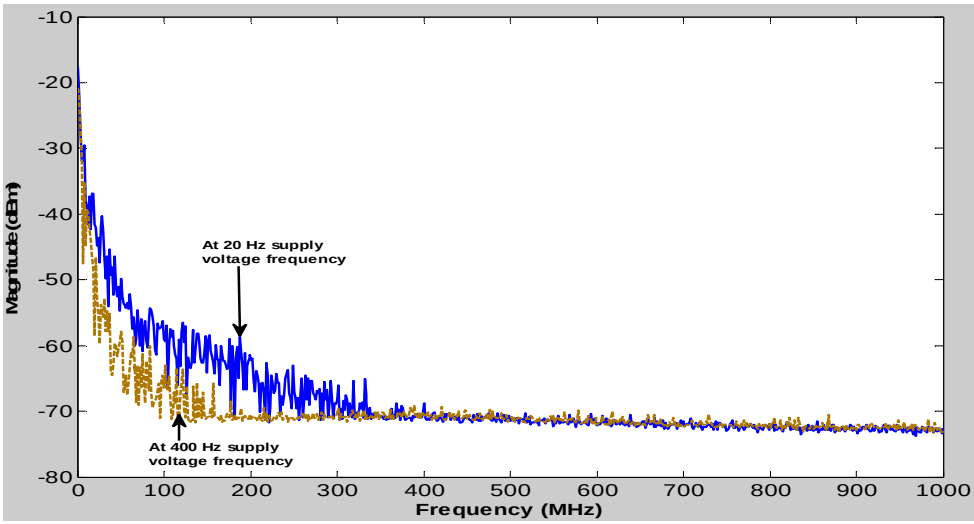

Figure 5-15: ***PD spectral bandwidth variation as a function of SVF for point-plane corona discharges in air on earth electrode. An example of the PD spectra (plotted on the same axis) obtained at two extreme values of the SVF is shown.***

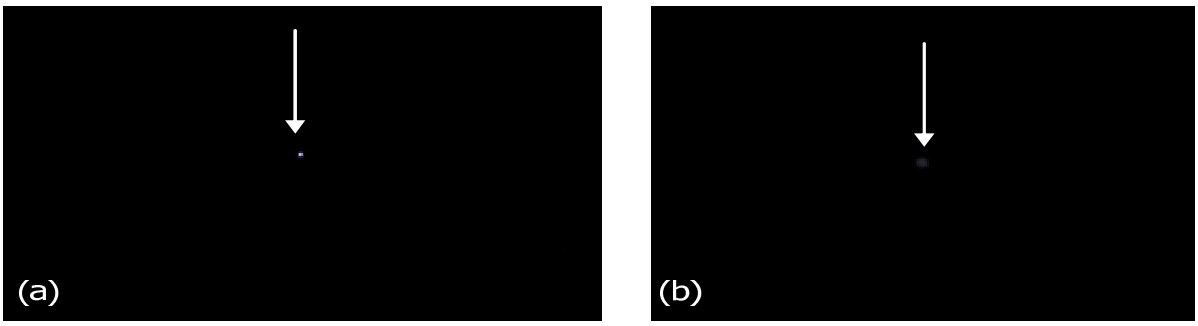

Figure 5-16: ***Images of HV electrode corona discharges taken with same camera settings: at supply voltage frequency of a) 20 Hz and at b) 400 Hz.***

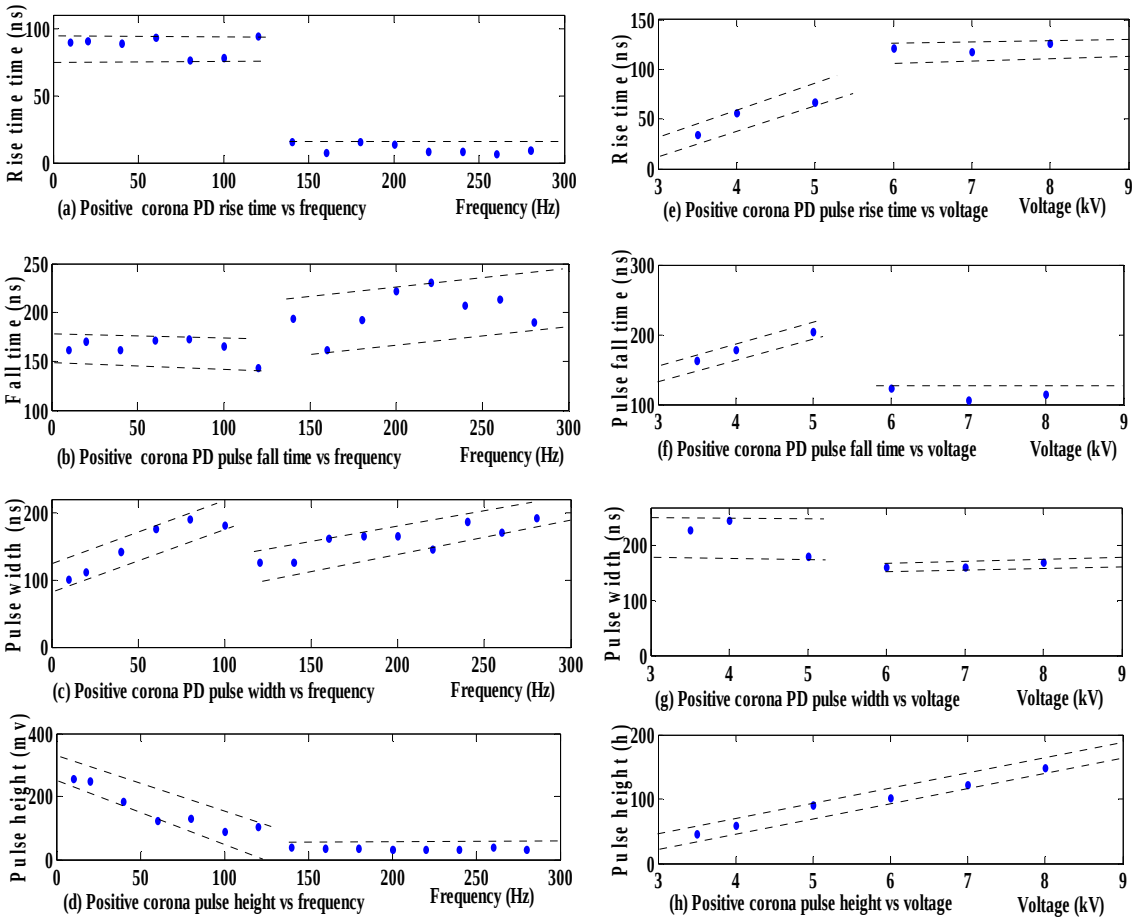

Figure 5-17: ***Point to plane corona in air pulse parameters as a function of supply voltage frequency and magnitude.***

5.6.2 Corona mechanism analysis and test results discussion

The behaviour of corona discharges under varying SVF is remarkable as it contrasts that of surface and cavity discharges. With reference to schematic illustrations of corona discharge mechanisms derived from literature (Maruvada, 2000; Kreuger, 1989; Comber et al., 1987; Lama & Gallo, 1974), the tests results and observations are discussed.

The phase-resolved patterns of point-to-plane corona in air have typical distinct features shown in ***Figure 5-18 (a)*** & ***(b)***. Discharge pulses that occur on the needle tip at negative potential are typically very small and of uniform distribution and are called negative corona. With the needle tip at positive potential, much bigger and irregular pulses magnitude occur on the voltage cycle crest (positive corona). When an oscilloscope was used to detect the corona pulses for pulse shape analysis as a function of frequency, the negative corona also

known as Trichel pulses could not be detected as they were below the sensitivity level of the system at the given test voltage level. Only positive corona pulses could be detected. Similarly in the frequency domain when both negative and positive corona (under ac voltage) were detected simultaneously using a spectrum analyser in the maximum hold mode, the resultant spectrum was dominated by positive corona. Analysis and discussion of the experimental findings in this work are therefore about positive corona as they were the only corona type detected under the given experimental conditions. The corona discharge models in literature (Maruvada, 2000; Kreuger, 1989; Comber et al., 1987; Lama & Gallo, 1974) were used to analyse and discuss the experimental results obtained in this work where the behaviour of corona under varying SVF was investigated.

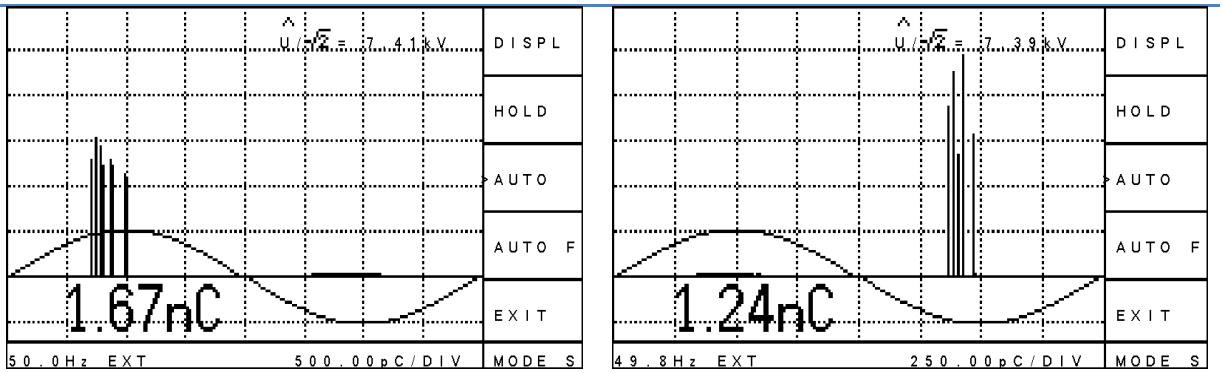

(a) (b)

Figure 5-18: ***Examples of phase-resolved pattern snap shots of point-plane corona recoded using a Power Diagnostics ICMCompact® PD detection system; (a) needle electrode at high voltage (b) needle electrode at earth potential.***

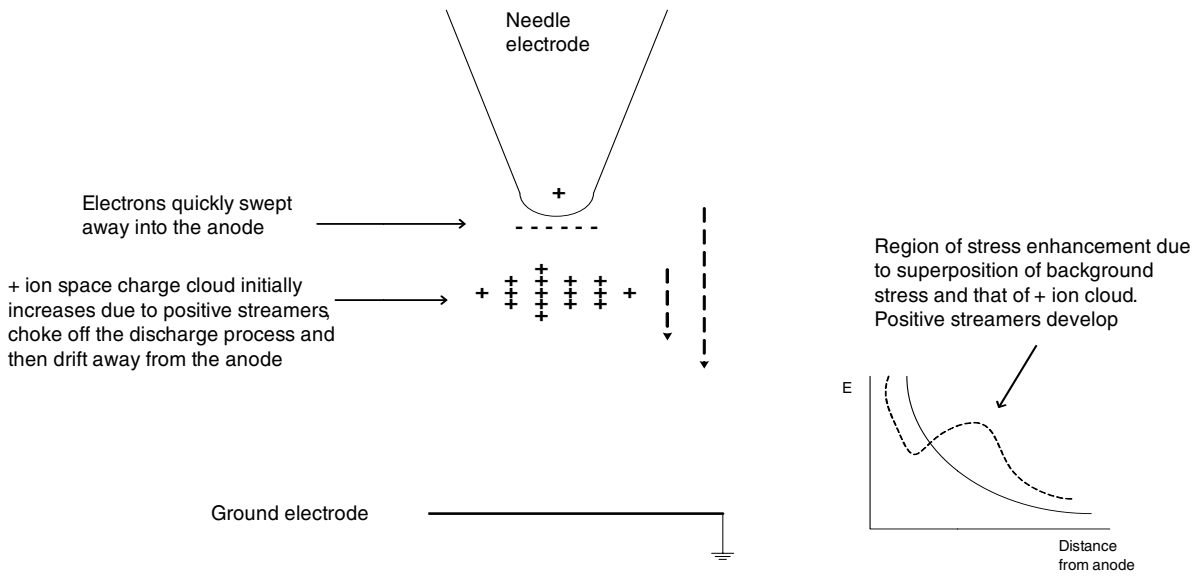

Figure 5-19: ***An illustration of positive corona mechanism (Maruvada, 2000).***

Distinctly different modes of corona discharges occur depending on the stress conditions at the anode. At an electric stress that is significantly above the discharge inception level, the discharges are dominated by the onset corona streamer type (Maruvada, 2000; Comber et al., 1987).

As illustrated in ***Figure 5-19***, after initial avalanches, a space charge cloud enhances the field in the gap and this initiates secondary avalanches that extend radially into the lower field regions of the gap. Unlike in the negative corona discharge process, where negative ions influence the process (Lama & Gallo, 1974), in positive corona, electrons are always under the influence of strong electric field and are quickly swept away by the anode without a chance to form negative ion molecules. An increased size of the positive ion space charge forms around the anode thereby effectively shielding the anode from the opposite electrode. The local electric field at the anode drops and the discharge extinguishes. The positive ion cloud then drifts away at a speed of about $1.5x10^4$ (m^2/Vs) (Maruvada, 2000; Ryzko, 1965) under the influence of the electric field thus clearing up the shielding effect. The re-establishment of the high stress conditions at the anode initiates another discharge event. The process then repeats.

Under sinusoidal stress conditions the stress in the gap changes in magnitude and polarity as a function of time. After the peak, the stress decreases until it gets to zero and then increases again in the opposite direction. The effect on the positive ion cloud, still present in the gap after the last positive corona discharge, is a reduction in the rate of drift. On stress polarity reversal the remnant space charge cloud drifts in reverse. An increase in the rate of change in polarity of the stress results in increased retention of the residual positive ion cloud and that causes more effect on the nature of the subsequent discharges. *This explains the observed decrease in bandwidth and magnitude of corona spectra as the SVF increased from 20 to 400 Hz as shown in scatter plots in* ***Figure 5-14*** and ***Figure 5-15***.

5.6.3 Key findings on corona discharges dependency on SVF

Point to plane corona spectral bandwidth in air decreased with increase in the supply voltage frequency. Positive corona discharge mechanisms depend on the dynamics of the positive ion cloud in the discharge gap. Factors such as increase in the SVF, that cause prolonged

presence of the space charge cloud in the discharge gap, inherently alter the positive corona discharge characteristics as observed.

5.7 Summary and pointers to the next chapter

The experimental work on investigating influence of SVF on PD spectra has been presented. It is revealed that the PD frequency content responds distinctly to variations in the SVF from 20 to 400 Hz for each defect type. The behaviour is explained in terms of the discharge mechanism theory of each PD type. It is interesting to note that the relationship between the SVF and PD spectral content can be narrowed down to the nature of the positive ion space charge dynamics' response to changes in the SVF. Each PD type responds uniquely. This is incremental academic knowledge on PD phenomena. Possible diagnostic applications of this knowledge are discussed later in Chapter 8. In the next chapter the experimental exploration of the other key aspect of PD spectral behaviour, the spectral content evolution with time of voltage application, is presented.

6 Experimental Work Part II: Investigation into the time-dependent evolution of PD spectral content

In the previous chapter the PD spectral bandwidth dependency on SVF was explored and it was concluded that PD spectral content is a function of SVF for each defect type. In the present chapter the exploration of PD spectral behaviour was extended to the dependency on the time of continuous ageing. The chapter begins with additional background notes to this part of the work. The accelerated ageing experimental procedure is then presented followed by test results and discussion.

6.1 Introduction

The second of the two key variables whose influence on PD frequency spectra was investigated in this thesis is the time of ageing under continuous PD activity. The reason why this variable is of interest, just like the supply voltage frequency, is that researchers have shown similar interest but focusing on other aspects of PD characteristics. The ageing related effects on the PD phenomena have been studied mainly using non-frequency domain PD characteristics such as phase-resolved patterns and pulse shape. The related literature was reviewed earlier in Section 3.2.

PD ageing phenomena studied through PD frequency spectral analyses have mainly been through firstly detection of the PD pulses in the time domain and then transformation into the equivalent frequency spectra using techniques such as Fourier transforms (Thayoob et al., 2003; Kim et al., 2002; Hudon et al., 1994; Morshuis, 1993). There has not been extensive and conclusive work on how PD frequency content depends on the time of ageing for various defect types. Furthermore the techniques of studying PD ageing phenomena using spectrum analyser instruments are generally scarce in literature. Moreover most PD frequency spectral studies have been on cavity discharges with no similar attention given to other types such as surface and corona discharges.

The growing popularity of UWB PD detection techniques in which PD spectral analysis techniques are employed, makes it imperative to understand the time-dependent PD spectral characteristics for a wide range of common PD defects. Experiments were performed, as presented in the next section, in which the time evolution behaviour of different PD spectra was studied.

6.2 The experimental test setup

The laboratory experiment to investigate time variation of broadband PD frequency spectra of different defects was set up as depicted schematically in ***Figure 6-1***. A photograph of the setup is shown in ***Figure 6-2***.

The setup was an accelerated ageing test rig comprising an array of test cells exposed to long term PD activity. Each test cell had a defect that was artificially made to simulate the common defects that are found in high voltage solid polymer insulation such as XLPE shielded medium voltage power cables. ***Table 6-1*** shows the information about the test cells and the corresponding defects.

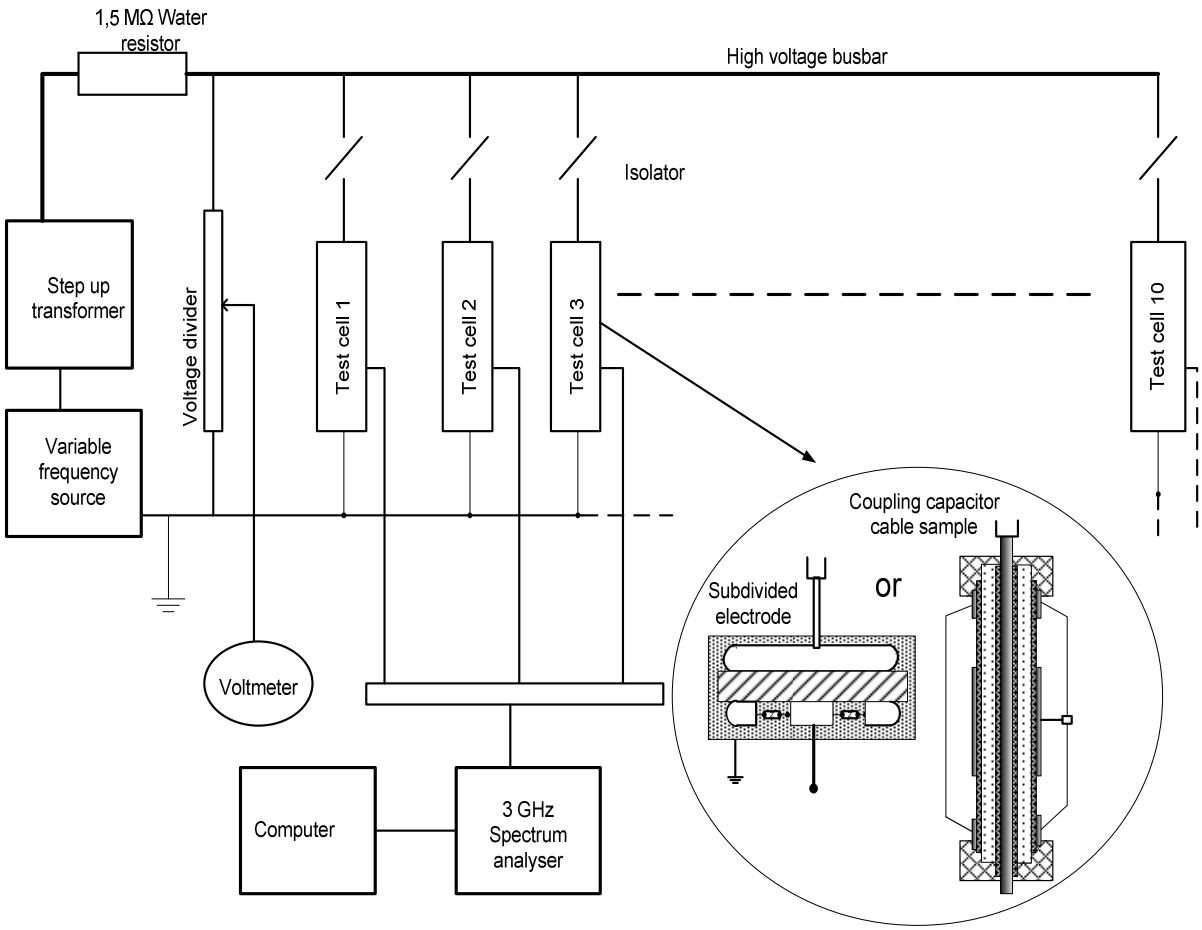

Figure 6-1: ***The accelerated ageing test rig for the PD defects. The inset shows some details of the two test cell types used.***

Figure 6-2: ***A picture showing one of the accelerated ageing tests.***

Table 6-1: Information about the test cells used in the accelerated ageing tests of the PD defects.

Test cell schematic	Test cell specifications	Comments
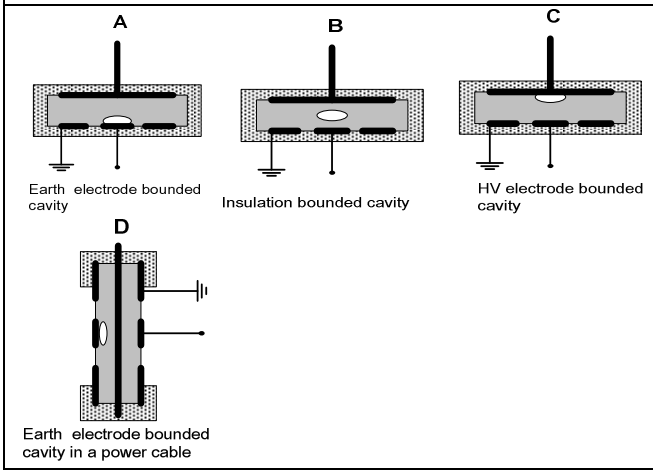	Disc shaped air cavities of 1 mm deep and 2 mm diameter. Insulation thickness was 3 mm so as to create stress conditions comparable to those in medium (MV) distribution cables.	Defects A, B & C were unvented and D was partially vented. Cavity defects simulated air bubbles trapped in insulation during manufacturing or assemble of cable accessories.
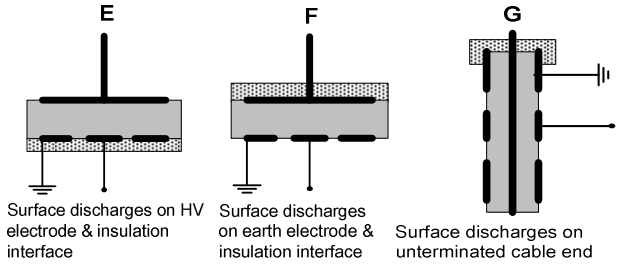	The distance between the edge of insulation and nearest point of contact with the metallic electrode was 30 mm in all the cases.	Surface discharge defects E, F & G simulated construction flaws that create conditions of high tangential electric field in cable accessories.
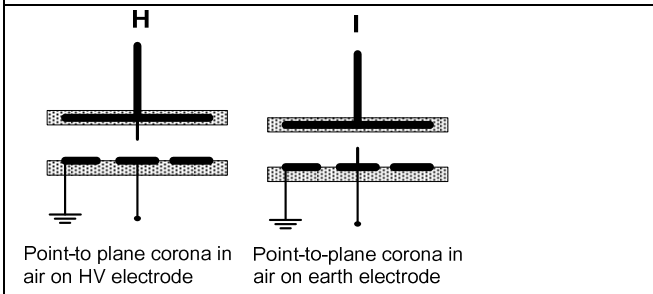	The distance between the flat sections of the electrodes was 27 mm. The needle was of copper, 10 mm long and of 50 μm tip radius.	Point to plane corona in air discharges simulated defects that occur in insulation systems where construction errors create sharp metallic points that that stick out in air.

In order to compare the PD activities from different defects in different test samples, all the test cells were dimensioned (as explained in detail in Chapter 4) such that PDs initiated almost at the same voltage of about 6 kV. This voltage was chosen as it created stress conditions similar to those in medium voltage (MV) power cables under normal operational voltage conditions.

6.3 The testing procedure

The test cells were simultaneously stressed continuously with a sinusoidal voltage at twice the PD inception level. The supply voltage frequency was elevated to 400 Hz in order to accelerate the PD induced degradation. PD measurements were made at 50 Hz (at the same electric stress as that in equipment under normal service conditions), and at suitable time intervals. Though during the accelerated ageing episodes all the cells were connected in parallel and to the test voltage source, in order to avoid 'cross-talk' during measurements, each cell was tested in isolation.

The PD signal data logging process (as illustrated in ***Figure 6-3***) comprised of a sequence of cyclic steps namely: switching off the supply, physical isolation of the test cells, connection of the cell to be tested, reduction of the supply voltage frequency to 50 Hz and then re-energisation of the voltage busbar. Each set of measurements took a total of approximately 30 minutes to record the PDs from all the 10 test cells in sequence after which the cells were reconnected in parallel and the 400 Hz supply voltage applied until the next set of measurements. The cycle was then repeated until the defects failed. The shortest time to failure of a test cell was 400 hours. The 1.5 MΩ water resistor in series with the test cells (as shown in ***Figure 6-3***) successfully prevented flow of excessive short circuit currents whenever a complete failure occurred.

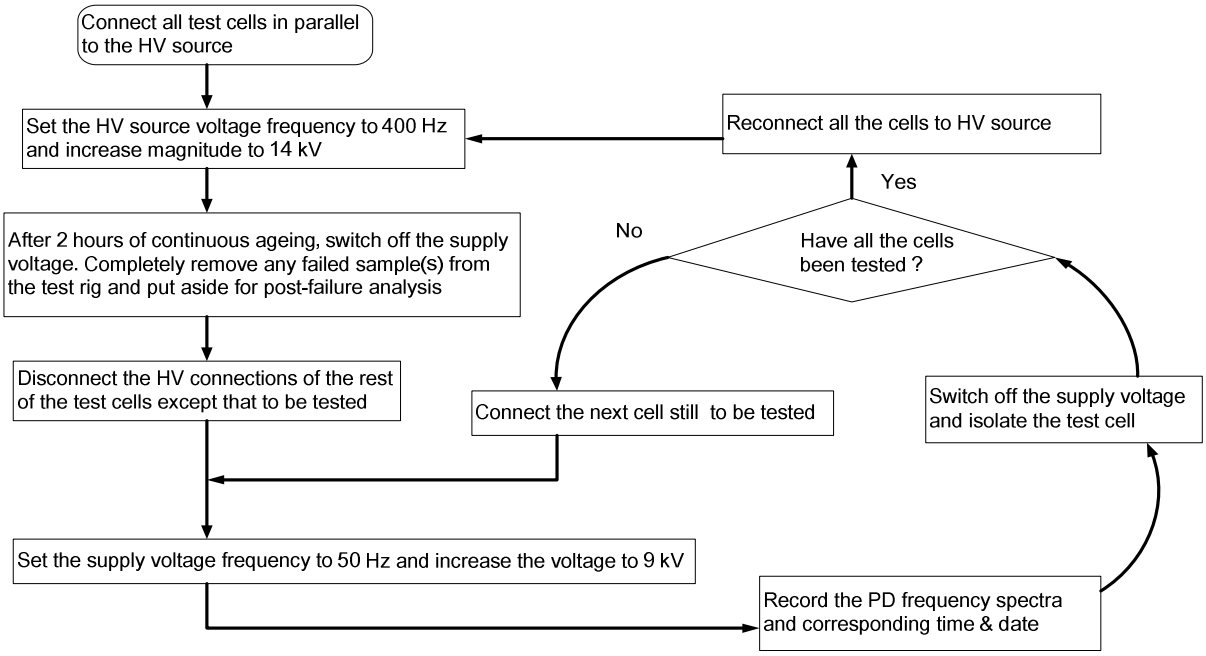

Figure 6-3: ***Flowchart illustration of the test procedure.***

The PD signals were detected as power frequency spectra using a 3.5 GHz sweep-tuned spectrum analyser. The spectrum analyser was connected and controlled through a computer as shown in the test rig schematic in ***Figure 6-1***. The spectra were recorded as maximum hold trace giving a profile that comprised of maximum amplitude registered at each frequency component for repeated sweeps in a 2-minute measurement period. The sweep time was set at a maximum possible value of 250 ms for the 1 GHz span. The resolution and video bandwidths were also set at maximum possible values of 1 MHz each. Such spectrum analyser settings gave the optimal sensitivity for PD detection as explained earlier in Section 4.5.

For each test cell the PD frequency spectra and the corresponding time and date of measurement were recorded and stored for further analysis. All tests were conducted in a screened high voltage laboratory. Prior to commencement of the tests, the background noise spectrum was noted and recorded with the test rig energised but voltage held below the PD inception level. The atmospheric conditions in the laboratory, though not deliberately controlled, were monitored. The temperature and humidity were on average 20°C and 50% respectively and varied within ±10% throughout the duration of the tests.

6.4 Cavity discharge PD spectral evolution test results

The test results on the evolution of cavity PD spectral features are presented. The results are interpreted and discussed by firstly analysing the theory of cavity PD mechanisms and then relating the theory with the observed spectral behaviour.

6.4.1 Measurements and observations

The time distribution of PD frequency spectra descriptors (bandwidth and variance) exhibited two distinct clusters as shown in the cluster plots of ***Figure 6-4***. In ***Table 6-2*** examples of the spectra at various stages of evolution are shown.

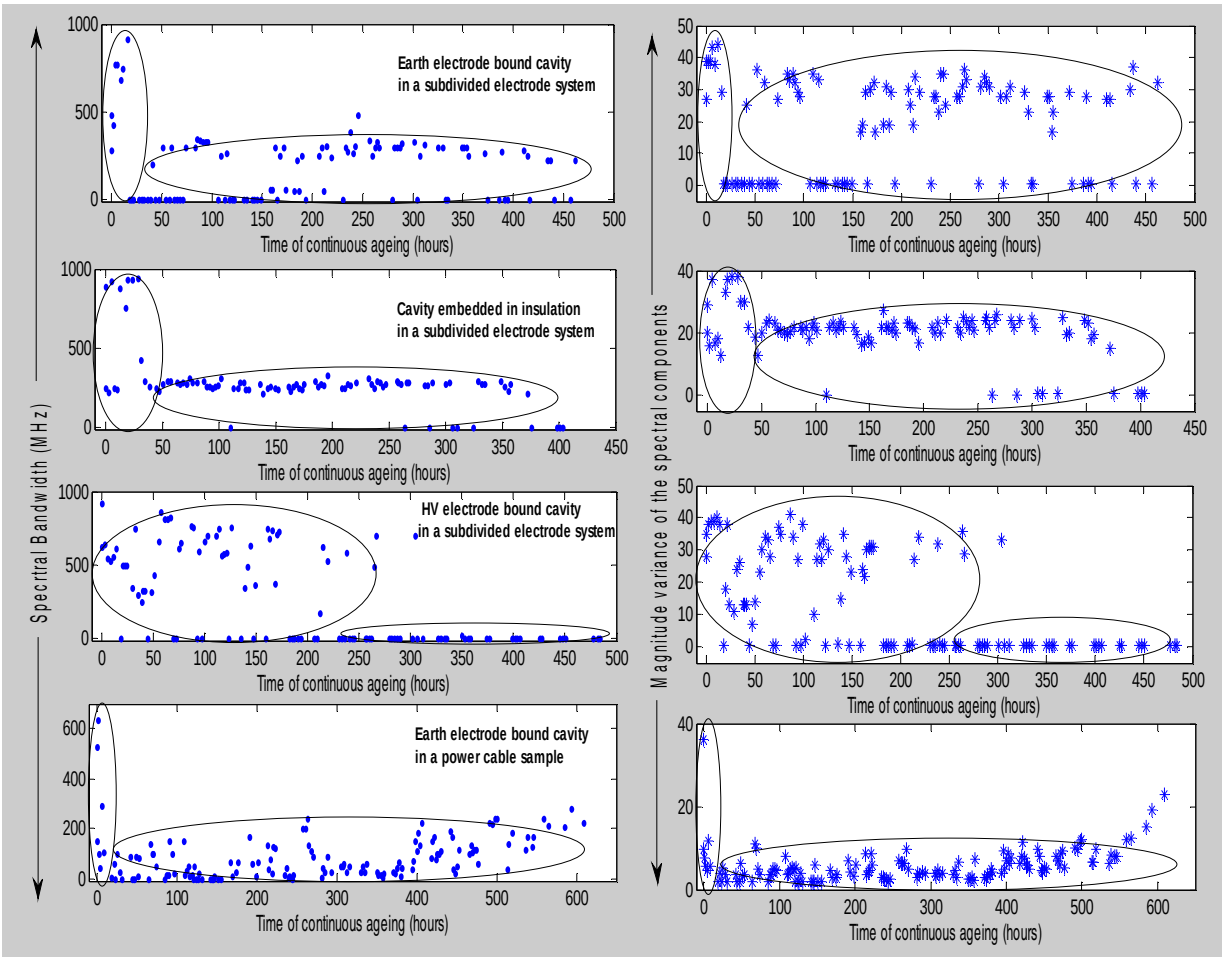

Figure 6-4: ***Cluster plots of void PD frequency evolution as a function of ageing to total failure.***

Table 6-2: Characterisation of the time evolution of PD frequency spectra for the void defects

Defect type	Ageing phase	Typical spectral signal	Average spectral bandwidth (*excluding instances of null signal*)	Std deviation of non-zero parameters
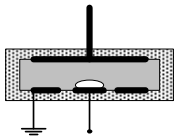 Earth electrode bounded cavity	Initial phase	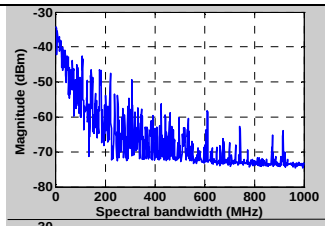	635 MHz	**12** times more than that of mature aged spectral bandwidth distribution
	Mature phase	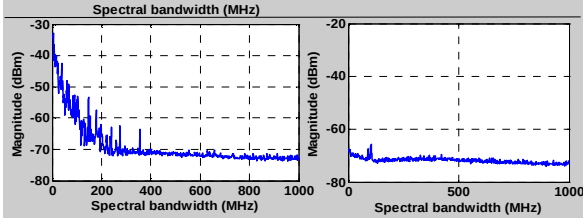	267 MHz	
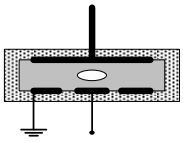 Insulation bounded cavity	Initial phase	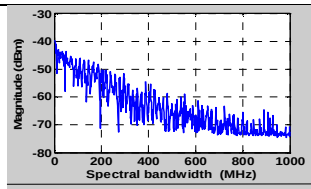	638 MHz	**3** times more than that of mature aged spectral bandwidth distribution
	Mature phase	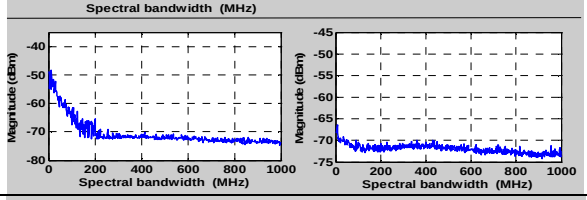	273 MHz	
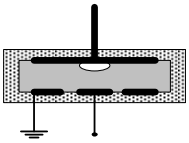 HV electrode bounded cavity	Initial phase	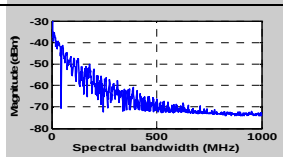	717 MHz	**3** times more than that of mature aged spectral bandwidth distribution
	Mature phase	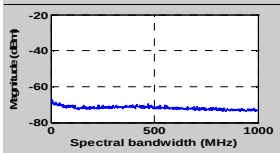	461 MHz	
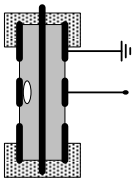 Earth electrode bounded cavity in a power cable	Initial phase	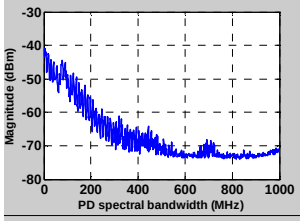	213 MHz	**3** times more than that of mature aged spectral bandwidth distribution
	Mature phase	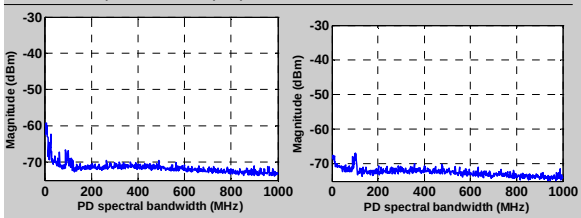	89 MHz	

Void PD evolution Cluster 1 occupied a period of about 25 hours of PD activity from the moment of initial inception. In this initial ageing phase the PD spectral characteristics were distinctly stochastic; characterised by a wide dispersion of frequency spectra bandwidth and magnitude variance. On average, in all the cavity PD cases, the standard deviation of spectral bandwidth was at least 3 times greater than those of cluster 2. The highest possible frequency content and magnitude of the PD signal were recorded in this initial period of the defect life.

Void PD evolution Cluster 2 was the period that followed the initial 25 hours of continuous ageing (cluster 1). It was the bigger of the two clusters and extended up to the moment of total failure which occurred anytime after 400 hours. In this period of the defect life the following were noted: both the PD frequency spectra descriptors (bandwidth and variance) had relatively narrow variations as the standard deviations were at least 3 times less than those in cluster 1. Compared to signals in cluster 1, the maximum frequency was much smaller: an average of about 250 MHz, compared to 665 MHz of cluster 1. Another interesting characteristic of cluster 2 PD activity is that there were incidences of complete evanescence of PD signals and in some cases for prolonged periods of up to tens of hours.

6.4.2 Cavity PD mechanisms analysed for interpretation of PD spectra evolution

In this section the observed evolution of cavity discharge frequency spectra is discussed and interpreted in the context of the commonly agreed cavity PD mechanisms theory.

In un-aged defects, conditions in the discharge environment cause delayed availability of seed electrons. Discharges therefore initiate at bigger gap overvoltages. The latter is defined as the difference between the theoretical discharge inception voltage and the actual higher PD inception voltage due to delayed availability of the seed electron (Devins, 1984; Tanaka, 1986).

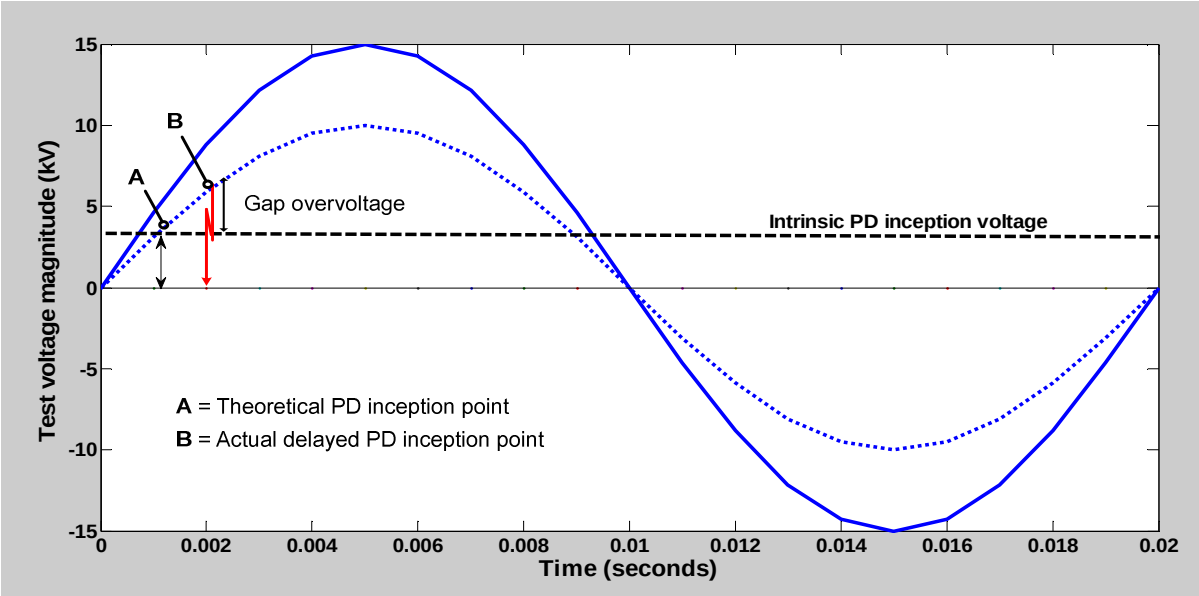

Figure 6-5: ***An illustration of the overvoltage that develops in a discharge gap due to the statistical delay of seed electron availability***

Figure 6-5 is an illustration of how gap overvoltage develops in a discharge cavity. When the electric stress reaches the minimum intrinsic PD inception value, the discharge does not initiate until a seed electron is available. If the seed electron does not appear at the moment of the minimum inception voltage, the stress in the gap continues to increase such that when the electron eventually arrives, the discharge initiates under the influence of higher stress.

The free electron accelerates towards the anode and gains energy under the influence of the electric field. As the electron accelerates towards the anode it collides with gas molecules and causes ionisation that produces more electrons and positive ions. Notwithstanding loss of electrons through recombination and diffusion, an avalanche occurs. Electrons, being light, are quickly swept away by the anode leaving behind the heavier and slower positive ions that drift towards the cathode. As the cloud of the positive ions approaches the cathode it creates a space charge field in the region near the cathode. The electric field established by the space charge superimposes on the background field resulting in stress enhancement as illustrated in ***Figure 6-6***. Under such high stress conditions the positive ions emit photons that bombard the cathode and make it release more electrons. Secondary avalanches follow and increase rapidly until the total breakdown of the gap. The phenomenon is referred to as the cathode effect (Bartnikas, 2004).

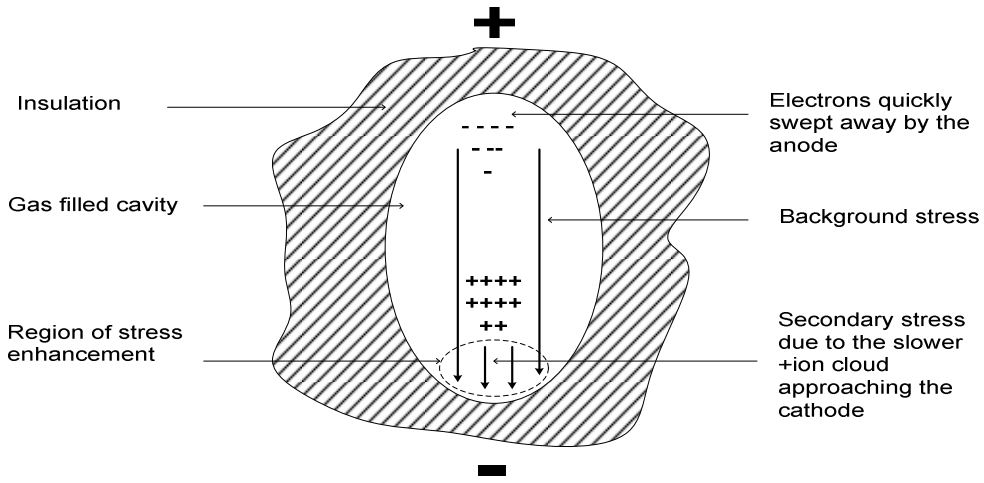

Figure 6-6: ***A sketch of simplified space charge distribution with a cathode emission condition in a gas-filled insulation cavity during a discharge event initiation process.***

The size of the positive ion cloud that is responsible for the initial cathode emission effect is proportional to the gap overvoltage at the instant of initial avalanche inception. A big gap overvoltage (in un-aged defects where seed electrons are scarce) causes more positive space charges that result in a stronger cathode effect which in turn produces more and faster avalanches. In such a discharge the strong stress in the cavity causes faster motion of the electrons and positive ions resulting in a PD with sharp rise time (electronic part of the pulse) and fall time (positive ionic part of the pulse) and bigger heights. Such discharges have been termed spark type or fast or streamer-like. The pulses are of relatively big and widely varying magnitudes as they depend on the random availability of initiatory electrons. The short pulse rise-time and short pulse width translates into a wide spectral bandwidth in the frequency domain.

Developments that create conditions for increased chances of seed electron availability in the discharge area indirectly cause the production of slower rise-time pulses. Such conditions may include depletion of electronegative gases such as oxygen in unvented cavities in solid dielectrics (Hikita et al., 1994; Tanaka, 1986) and electrons trapped in liquid by-products of PDs. These conditions may be symptoms of an ageing insulation defect (Kim et al., 2004; Morshuis & Kreuger, 1990). As the discharge physical environment changes from being un-aged to aged as illustrated ***Figure 6-7*** in the corresponding gap-overvoltage becomes smaller as point B shifts towards point A in ***Figure 6-5***.

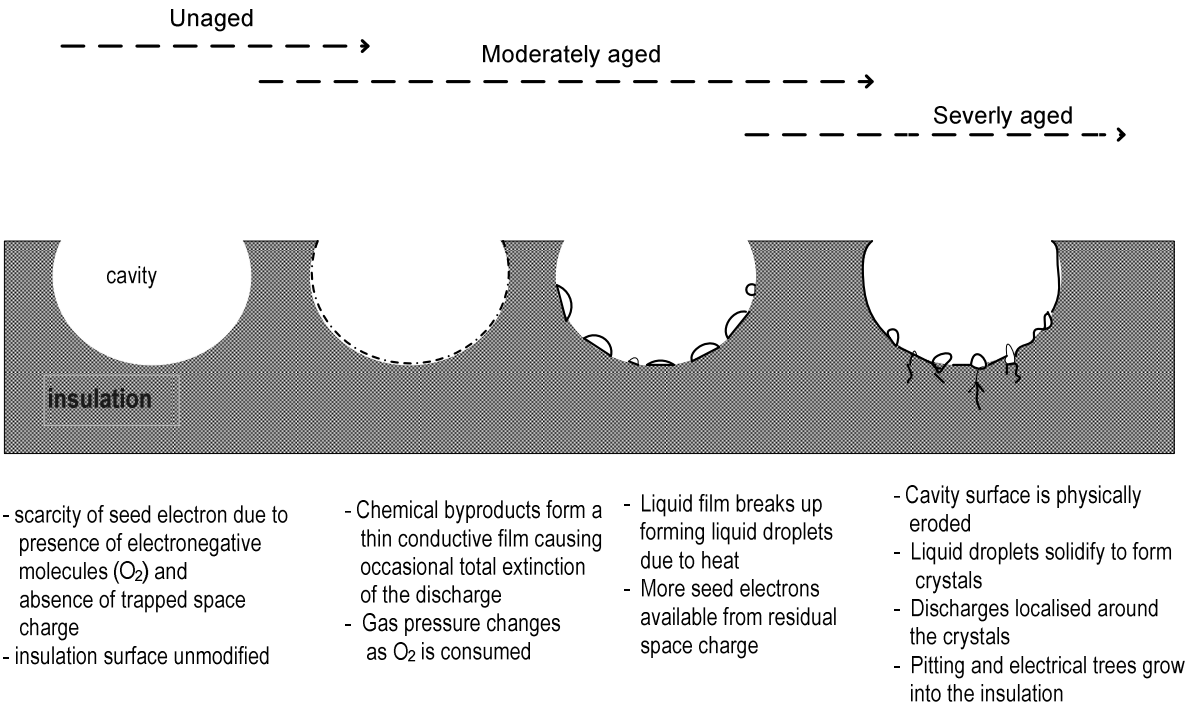

Figure 6-7: ***An illustration of the physiochemical changes occurring in a cavity under continuous PD exposure up to total failure (Morshuis, 2005; Temmen, 2000).***

6.4.3 Cavity PD spectral evolution results discussion

In this work the discharges were detected as broadband frequency spectra. The discharge signals under un-aged conditions were characterised by *spectral bandwidths that significantly varied in the range 1 GHz to 200 MHz during the initial 25 to 50 hours of continuous exposure as presented in* ***Figure 6-4****. Such behaviour is consistent with the aforementioned PD mechanism model where the random availability and scarcity of seed electron causes inception to initiate at larger gap overvoltage; this produces high frequency spectral components.*

Impingement of the PD energy on cavity gas as well as the insulation surface causes physical and chemical reactions that produce active species comprising of electrons, positive and negative ions, photons, excited atoms, free and reactive molecules such as CO, CO_2, H_2, ozone, various nitrogen oxides, polymer radicals and other species. Space charges are deposited on the insulation surface. The gaseous by-products dissolve in H_2O vapour (present in the original cavity gas or diffused into the cavity gas from the insulation body) to form conductive liquid droplets deposited on the cavity insulation walls. The discharge

environment is consequently modified by the physically eroded insulation surface, conductive liquid droplets on the cavity walls, residual space charge trapped on the insulation surface, the pressure variations and other changes such as temperature. These physiochemical changes directly alter the discharge process (Devins, 1984; Morshuis & Kreuger, 1990; Bartnikas & Novak, 1992; Laurent & Mayoux, 1992; Morshuis 1993; Hudon et al., 1993; Gulski & Krivda, 1995; Mason, 1995; Hudon et al., 1995; Mayoux & Laurent, 1995; Mayoux, 1997; Temmen, 2000; Wu et al., 2005; Kim et al., 2004; Bartnikas, 2008).

The resultant abundance of seed electrons in the cavity emanating from cavity wall modifications and liquid PD by-products deposits (that 'store' and act as sources of free electrons) cause discharges to occur at smaller gap overvoltages. The reduced gap overvoltage produces smaller positive ion clouds in the primary avalanche that cause less cathode emission effect resulting in PD pulses with slower rise and fall times, wider widths and smaller heights. Such PD regimes have been given names such as pseudo-glow, Townsend-like or slow discharges (Devins, 1984; Morshuis, 1995b; Bartnikas & Novak, 1995). The minimal cathode effect and weaker field conditions in the discharging cavity create conditions that favour 'unrushed' transit of positive ions across the cavity. This manifests as slower fall time and wider width where the latter directly corresponds to the cavity depth (Bartnikas & Novak, 1995; Morshuis & Kreuger, 1990). *In the frequency domain the signals exhibited smaller and fairly consistent bandwidth and magnitude. The standard deviations of the values were on average 3 to 12 times less than those of the unaged phase as shown in* ***Table 6-2.*** *These type of discharges prevailed in the longer and last period of the PD ageing life. The ageing phase was characterised by relatively small variations in spectral features compared to those of the initial ageing phase and could be termed the mature aged phase.*

As the cavity wall becomes extensively polluted many free electrons act as seed electrons and cause several independent discharge avalanches initiating concurrently on several sites on the cathode. In severely aged cavities, the cavity surfaces are littered with solid crystals having been formed from liquid PD by-products. The crystals cause localised stress enhancement regions that become PD sources. Such discharges in the history of PD research, eluded scrutiny by researchers for some time until improved optical PD detection technology was effectively used in conjunction with the UWB techniques. This resulted in identification of

discharges now termed glow, pitting, swarm or pulseless (Bartnikas & Novak, 1992; Morshuis, 1993).

Further localised insulation erosion occurs due to localised PD as the crystals cause stress enhancement in the regions of interface with the insulation. Electrical trees initiate on these sites and quickly bridge the insulation resulting in total insulation failure (Morshuis, 1993; Mason, 1995; Mayoux, 1997; Hudon et al., 1995; Mayoux & Laurent, 1995).

It was noted that the position of the cavity had no influence on how the PD spectra evolved. This could be attributed to the PD by-products deposited on the metallic electrode surface being part of the cavity boundaries. The liquid coating eventually turns into solid. Consequently for the aged cavities, the PDs behave almost the same irrespective of whether adjacent to metallic electrode or completely embedded in the insulation (Reynders, 1978). A picture of an HV electrode (***Figure 6-8***) that was adjacent to a void which eventually failed shows clear evidence of deposits on the area that made one boundary of the cavity. Since the picture was taken after opening up the failed electrode bounded cavity, it could be argued that the deposits could not be entirely attributed to the ageing as there was a possibility of the deposits being splashed onto the metallic surface area during the short circuit failure process.

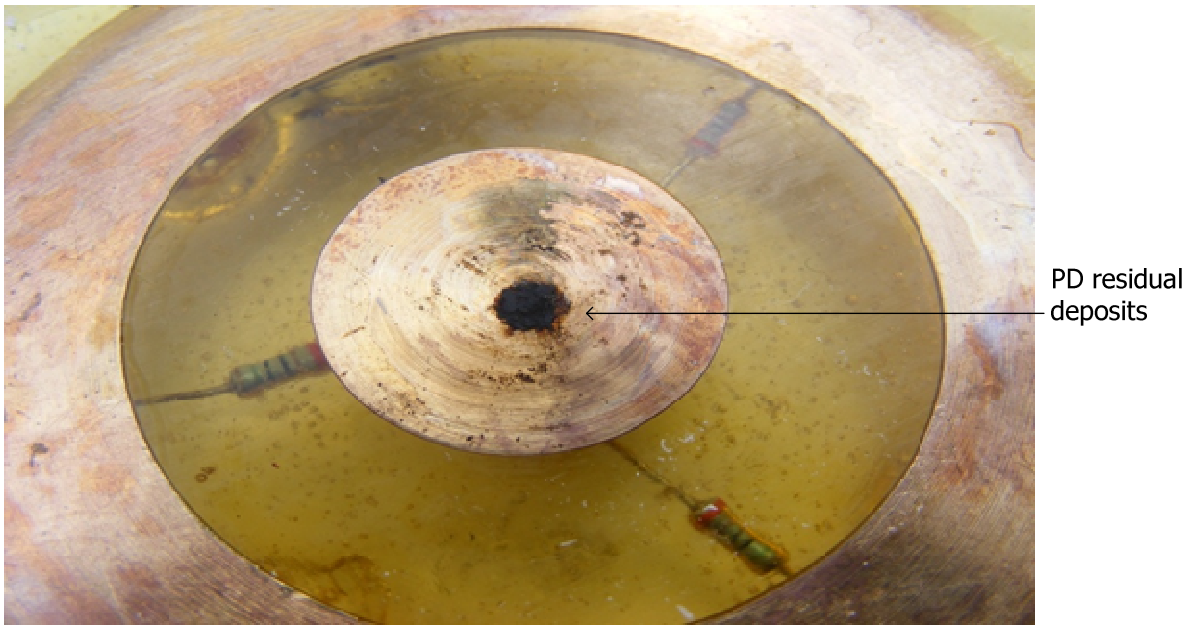

Figure 6-8: ***An image of an electrode showing carbonised remnants of solid PD by-products deposited by an earth electrode bounded cavity that failed after about 450 hours.***

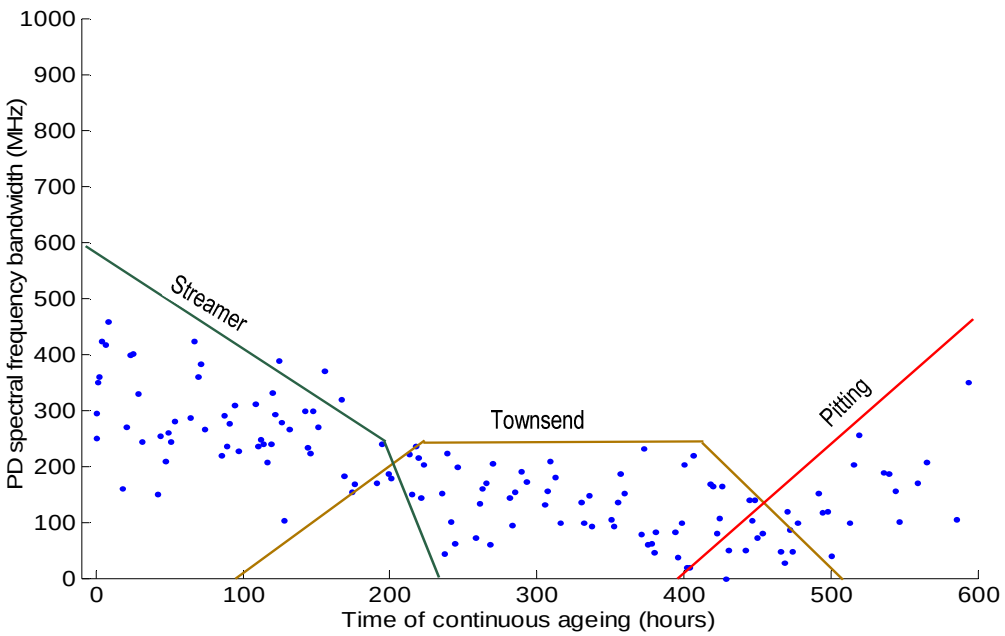

Figure 6-9: ***Prevalence of different PD regimes during the course of defect progression towards total failure.***

Under long term ageing conditions (from virgin state to total failure) different PD regimes (but not necessary all) can occur simultaneously in the cavity. At any time however one regime prevails over the others. ***Figure 6-9*** shows the three regime classification of frequency domain PD features of surface discharges on unterminated cable-end obtained in this work. The tendency for the spectral bandwidth to increase in the pitting discharges is remarkable. This however should not be confused with the decrease in magnitude as observed by Morshuis (1993). Similar classification, but in the time domain, was performed by Morshuis (1995c). It is noted that in most of the test samples, the streamer and Townsend regimes could be easily identified using the spectral features. The pitting discharges however were not always apparent in some cases. This could be attributed to co-existence of both the Townsend and pitting discharges that when detected using a spectrum analyser were superimposed. Similarly during the transition period, specific PD regimes could not be easily identified through the spectrum analyser acquired spectral features. Precise demarcations of the transition points were difficult.

6.5 Surface discharges PD spectral evolution

6.5.1 Experimental measurement results and observations

Like void discharges, the surface discharge spectral features exhibited distinct clusters as shown in ***Figure 6-10***.

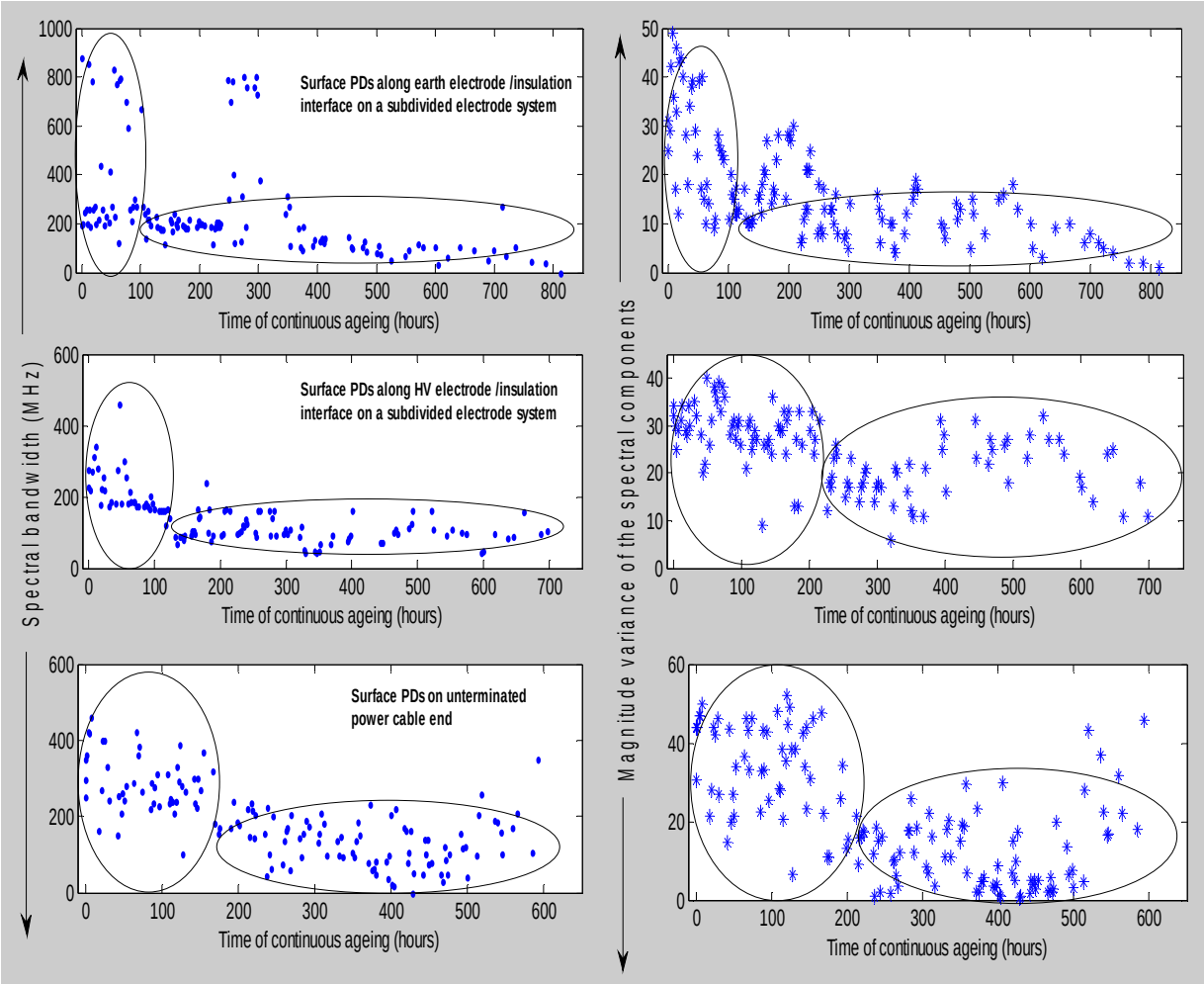

Figure 6-10: ***Cluster plots of surface discharges frequency evolution as a function of ageing to total failure.***

Surface discharges evolution Cluster 1 occupied the first 50 to 150 hours of continuous accelerated ageing where the frequency spectra bandwidth and magnitude variance exhibited wide ranging variations. This trend was observed in most of the surface discharge test cells

irrespective of whether they were subdivided electrode configuration or actual cable samples, and whether the insulation was low density polyethylene, Mylar® or XLPE. Furthermore the behaviour was independent of whether the discharges were near the earth electrode or HV electrode.

Surface discharges evolution Cluster 2 occupied the time period subsequent to the first 150 hours of continuous ageing up to the moment of total failure. Discharges in this cluster were characterised by significantly reduced bandwidth (compared to that in cluster 1). Moreover the random variations of the bandwidth from one measurement to another were significantly smaller such that the standard deviation of the values was approximately twice less than that of cluster 1. ***Table 6-3*** gives examples of the frequency spectra of different regimes for the artificial defects used in the tests. Another notable characteristic of cluster 2 surface discharges is that unlike in the case of void discharges, there were no instances of complete discharge evanescence.

6.5.2 Results analysis and discussion: surface discharge spectral evolution

The evolution of surface discharge spectral signals observed in this work is discussed using the theory of surface discharge mechanisms drawn from similar work done by other researchers such as Murooka et al (2001), Fouracre et al (1999), Handala & Lamrous (2008).

Table 6-3: Characterisation of the 'time evolution' of the surface discharges.

Defect type	Ageing phase	Typical spectral signal	Average spectral bandwidth	Std deviation of non-zero parameters
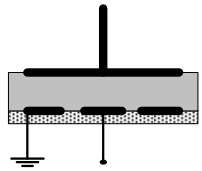 Surface discharges on HV electrode & insulation interface	Initial phase	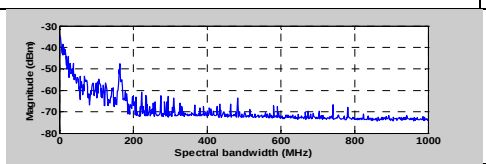	211 MHz	**2** times more than that of aged spectral bandwidth distribution
	Mature phase	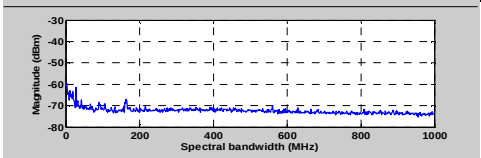	106 MHz	
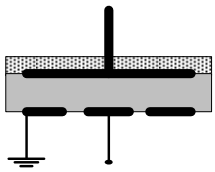 Surface discharges on earth electrode & insulation interface	Initial phase	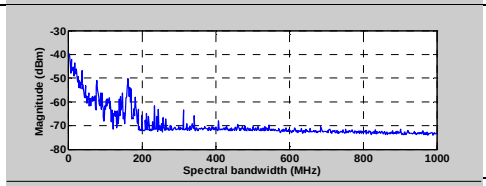	409 MHz	**1.5** times more than that of aged spectral bandwidth distribution
	Mature phase	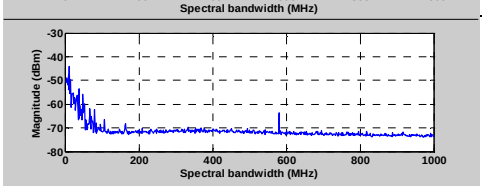	223 MHz	
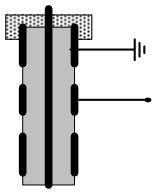 Surface discharges on unterminated cable end	Initial phase	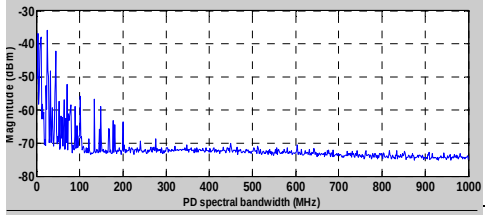	237 MHz	**1.5** times more than that of aged spectral bandwidth distribution
	Mature phase	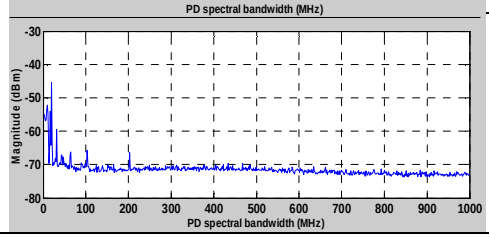	76 MHz	

As explained for cavity discharges in the previous sections, in the initial stages of the PD activities, the availability of PD seed electrons is dependent on the ionisation of air from cosmic radiation. There is therefore relative scarcity of the seed electrons and this causes discharges to occur at relatively higher discharge gap overvoltages. Furthermore the discharge initiation delay period varies randomly with a significant scatter. Cases of prolonged delay in discharge initiation results in bigger spectral bandwidth and magnitude. *In this work this surface discharge phenomenon manifested as a cluster of randomly varying frequency spectral features with a wide ranging scatter as shown in Cluster 1 of* ***Figure 6-10****.*

As the defect aged, visible whitish material developed as a coating on the insulation surface and splatter on the adjacent metallic electrode surfaces. The corresponding PD signal at this stage had smaller and less varying bandwidths and magnitude variance. The amount of deposits increased with time of ageing and the corresponding signal bandwidth and magnitude variance decreased until the defects completely failed. On the cluster plots, this period of evolution is indicated as Cluster 2 and termed mature aged phase.

A closer examination of the areas exposed to surface discharge on the polyethylene insulation sheets shows visible signs (cracks and craters) of erosion as shown in ***Figure 6-11.***

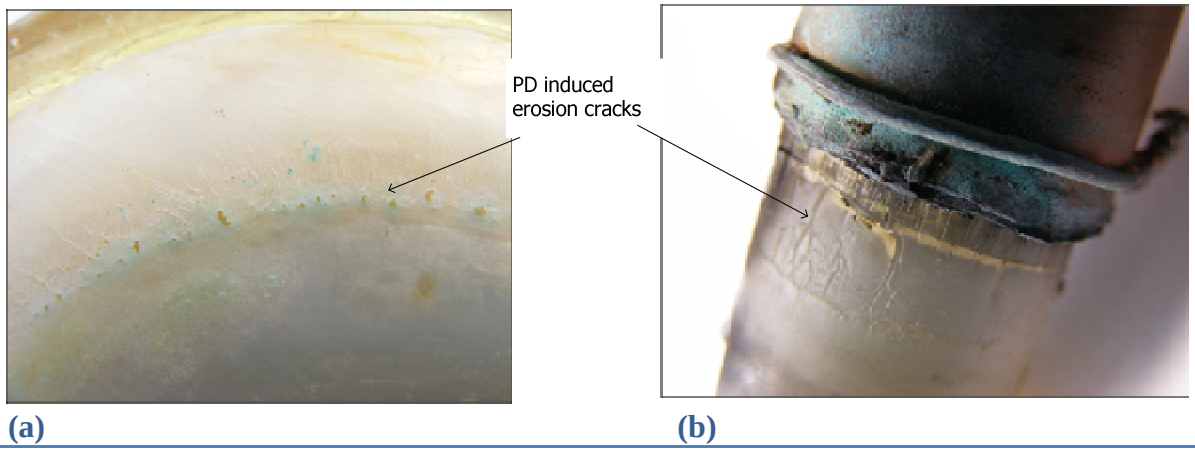

Figure 6-11: ***Portion of some of the surface discharge samples showing visible signs of cracks and microvoids after long term (400 hours) ageing under PD activity.***

The coated metallic electrode surface together with the morphological changes of the adjacent insulation reduced the electric field intensity. Consequently the corresponding PDs became slower and smaller. *In this work, measurements that were conducted in the frequency domain showed PDs with narrower spectral bandwidth and smaller magnitudes.* The microcavities seen as craters in the insulation were sources of localised intense discharges that eventually created electrical trees to completely bridge the insulation with a short circuit. ***Figure 6-12*** shows examples of samples that eventually failed due to long term exposure to surface discharges.

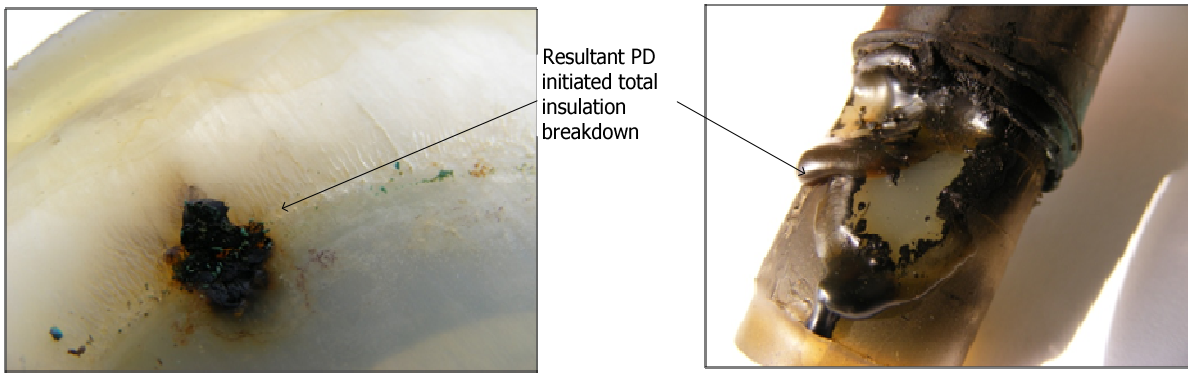

(a) **(b)**

Figure 6-12: ***Examples of completely failed surface discharge test samples: a) is a subdivided electrode sample where discharges were along the interface between the HV electrode and insulation, b) is a cable sample which failed due to surface discharge on the unterminated end.***

6.6 Point-plane corona in air discharge 'evolution'

6.6.1 Experimental results and discussion

As intuitively anticipated, corona discharges in air did not show any significant evolutionary changes during the entire period of observation. This was because the discharge environment had no polymer dielectric boundaries that would undergo physiochemical changes and influence the progression of the discharge process. The corona discharge frequency bandwidth however exhibited variations but these were narrow and consistent as shown in the corona cluster plots in ***Figure 6-13*** and ***Table 6-4***. The variations are attributed to the natural random nature of electrical discharges and possible minor surface erosions of the metallic electrodes.

In both cases of the discharging point location (HV electrode and earth electrode) there were no distinct changes in the spectral features except for natural statistical variations.

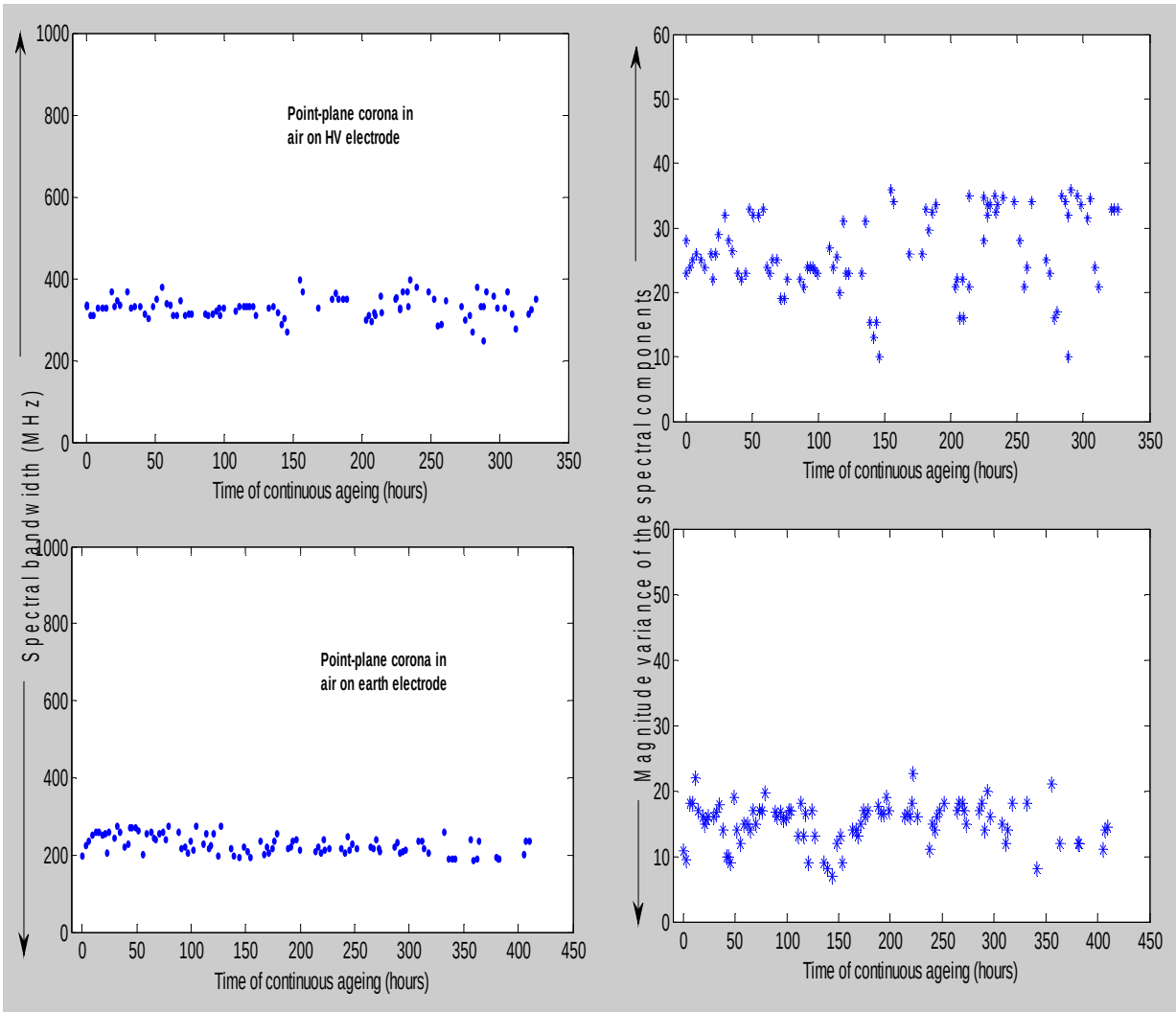

Figure 6-13: ***Cluster plots of point-plane in air corona PD spectral bandwidth and magnitude variance over long time ageing. The time-invariant behaviour is evident.***

Table 6-4: Characterisation of the 'time evolution' of the point-plane corona in air defects.

Defect type	Ageing phase	Typical spectra signal	Average bandwidth
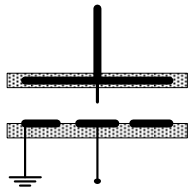 Point-to plane corona in air on HV electrode	Initial ageing phase Mature ageing phase	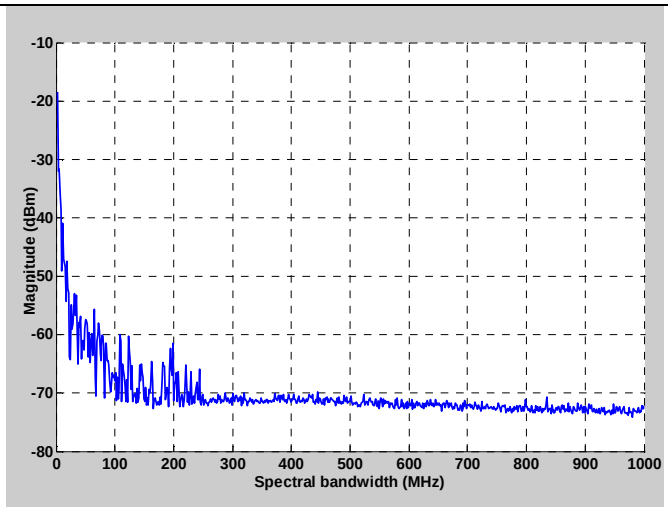	250 MHz
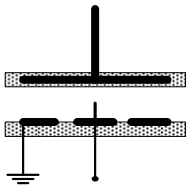 Point-to-plane corona in air on earth electrode	Initial ageing phase Mature ageing phase	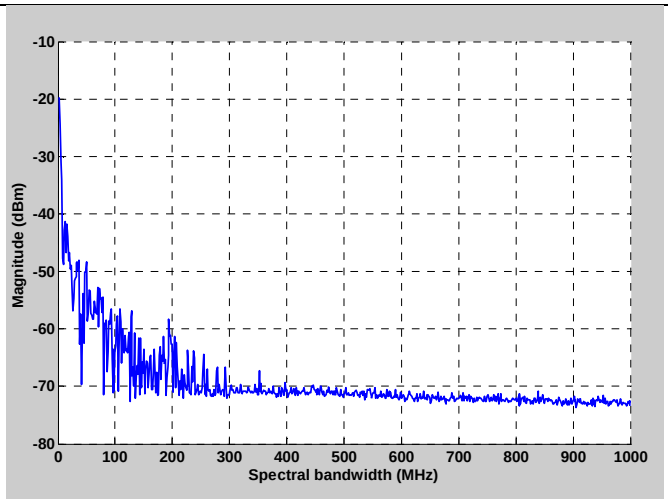	300 MHz

6.7 Summary and pointers to the next chapter

The spectral frequency content of PDs of different defects in polymer insulation were monitored from initial inception to total breakdown under accelerated ageing conditions. For defects that progressed to failure, the spectral features such as bandwidth were found to change with time of voltage application. It is concluded that each defect type gives PDs with spectral features that evolve uniquely. PD frequency long term evolutionary behaviour is a PD type dependent spectral characteristic. In the next chapter the implications of the research findings of this work are discussed.

7 Discussion of prospective diagnostic application of the research findings

The findings of this work are that PD frequency spectral bandwidth is influenced by the supply voltage frequency as well as the time of ageing under continuous PD activity, and this behaviour is defect-type dependent. The findings are incremental academic knowledge on fundamental PD mechanisms. Furthermore there are prospects for immediate transfer of this knowledge to technology applications. This chapter discusses the prospective applications.

7.1 Prospective diagnostic applications of the knowledge on the supply voltage dependency of frequency spectra

The manner in which the PD frequency spectra respond to variations in the supply voltage frequency depends on the type of defect. PDs from small cavities are immune to changes in frequency of the supply voltage. Surface discharges spectral bandwidth and magnitude variance increase with increase in supply voltage frequency. The opposite is true for corona discharges where frequency components diminish as the frequency supply voltage frequency increases.

The revealed supply frequency dependent behaviour of PDs suggests the following possible diagnostic applications:

i) Unknown insulation defects can be recognised through checking how the frequency spectra respond to variations in the supply voltage frequency. By sweeping the test voltage frequency through a range such as 10 Hz to 400 Hz, the nature of an unknown PD can be deduced from the frequency spectral changes during the sweep. This technique can be used as a quick PD defect pre-classification or elimination of corona interference by elevating the frequency of the test voltage.

ii) If different tests of the same equipment are conducted at different supply voltage frequency, comparison of results must take into account the findings of this work. In the commercial PD diagnosis practice, tests can be done at various frequencies such as 0.1 Hz, damped and power frequency voltage.

iii) There are PD recognition techniques that use frequency spectra as characteristic PD signatures (Ahmed & Srinivas, 1998; Cheng et al., 2000; Balkon et al., 2009; Thayoob et al., 2003; Thayoob et al., 2009). In such cases the influence of the SVF can poses a challenge in the reliability of the diagnostic results. As an example, spectral patterns of surface discharges in a power cable termination that is energised at 0.01 Hz test voltage can be remarkably different from that obtained at 50 Hz test voltage. It is imperative that in classifying PD types using spectral characteristics, the influence of SVF on the spectral features has to be appropriately taken into account.

iv) Accelerated ageing results obtained through elevated SVF may not be linearly extrapolated to normal ageing for all types of defects.

7.2 Prospective diagnostic applications of the knowledge on the time evolutionary characteristics of the PD frequency spectra

The manner in which the PD frequency spectra evolve with time from initial inception to total failure depends on the type of defect causing the PD. While corona PD, as intuitively expected, exhibits no time dependency characteristics, void and surface discharges change as a function of ageing. In the first few days of initial inception, under continuous PD exposure, the frequency bandwidth of unaged void and surface discharges are significantly higher than that of aged defects. Moreover the values of the bandwidths vary randomly and significantly over a wide range compared to those of the aged. After the initial period of PD activity, void discharges extinguish (in some cases for many hours or days) at random intervals until the moment of total failure.

The way in which different PD frequency spectra evolve over time suggests the following concerning PD diagnosis tests:

i) PD tests of new equipment such as in factory tests, or commissioning or after laying cable tests are the most sensitive and reliable because PDs in un-aged defects (at least for few days after initial inception) have the highest possible frequency content and magnitude.

ii) PD tests, whether online or offline after the system has been in operation for longer than a couple of days have a high risk of giving misleading results. This is because these tests assess the PD condition in the evolution phase where the discharge activity, particularly in void defects, has a high probability of being in a state of prolonged extinction or low magnitude and low repetition rate. At the instant of measurement, the absence or low magnitude may be erroneously regarded as an indication of good equipment condition. In literature there have been cases reported where power cables failed later and yet had been judged 'healthy'. Large PDs had been identified in the first of periodical measurements but in the subsequent measurements (after a couple of months) the PDs had diminished (Kyprianou et al., 2006; Orton, 2003). It can therefore be argued that PD diagnostic measurements that are conducted for purposes of maintenance decisions should be interpreted in the context of previous continuous PD trending records of the equipment under test. A trend of diminishing PD signal strength or intermittent presence and absence of the signal may indeed be a sign of impending failure! Similar conclusions were drawn by Victoria et al (2006) and also Renforth et al (2008).

iii) The spectral patterns viewed through fixed frequency slots 'windows' in the HF and UHF techniques can shift away from the window or diminish with time. Where PD frequency spectra are used as defect signatures, the evolutionary phenomena of the PDs pose a challenge in the efficacy of such PD recognition techniques. It is imperative that when classifying PD defects using spectral characteristics, the influence of ageing on the PD spectral features is appropriately taken into account.

iv) Based on the defect-type-dependent evolutionary behaviour of PDs, general diagnostic guidelines for frequency domain online continuous monitoring of PDs in polymer dielectrics can be suggested.

When continuously monitoring PD frequency spectral signals under online conditions and taking regular periodical measurements, the following general guidelines are suggested:

Guideline no.1

If an unknown defect gives spectral bandwidth and magnitude variance that significantly change with time *but with no incidences of complete extinction*, then it is likely to be a surface discharge defect that is progressing to total failure.

Guideline no. 2

If an unknown defect gives a PD signal with spectral bandwidth and magnitude variance that significantly change with time *and have incidences of complete extinction*, then it is most likely to be a cavity defect that is progressing towards total failure.

Guideline no. 3

If an unknown defect gives a PD signal with spectral features bandwidth and magnitude variance that are *consistent and time invariant*, then it is likely to be corona in air and may not be a major cause for concern.

7.3 Summary and pointers to the next chapter

The knowledge generated in this work adds value to the usefulness of PD frequency spectra-based insulation diagnosis methods. Taking cognisance of the influence of supply voltage and ageing on PD spectra enables more informed interpretation of frequency domain PD measurements. Furthermore the uniqueness in response to supply voltage frequency and ageing of each PD type can be a basis for developing defect classification criteria in the frequency domain. In the next chapter the thesis is concluded by summarising the key findings of the research work. Possible related future work is then suggested.

8 The thesis conclusion and suggestions for future study

8.1 Conclusions on the key findings

This thesis work revealed that there are defect-type-dependent PD spectral characteristics that should be taken into cognisance in interpretations of frequency domain PD tests. The work identified two defect-type-dependent PD spectral characteristics namely: dependency on supply voltage frequency (SVF) and dependency on continuous exposure to PD activity.

The bandwidth and magnitude variance of surface discharges increase with increase in SVF. On the contrary corona discharges spectra bandwidth and magnitude decrease with increase in the SVF. For small cavities however, the bandwidth and magnitude are immune to variations in the SVF.

The time dependent evolution is such that PD spectra evolve with time of continuous voltage application. The manner in which the spectra evolve from initiation to total failure is a function of source type. Surface discharge spectral bandwidth and magnitude after initial significant randomness and wide variations, decrease in magnitude and with narrower randomness. Corona spectral bandwidth and magnitude variance are time invariant. Cavity PD spectral bandwidth and magnitude variance, like surface discharges, decrease with time but differ from surface discharges in that they are characterised by instances of prolonged extinction.

These findings imply that correct interpretation of PD frequency spectra diagnostic information requires that the influence of SVF and time of ageing on the spectra be taken into account.

8.2 Suggestions for future further studies

The findings of this work reveal some research areas that merit further study. These topics have potential in further extending knowledge in PD diagnosis.

8.2.1 Studying evolution of positive and negative PDs separately

In this thesis the evolution of partial discharges was studied without separating the positive from the negative PD spectra. It could be interesting to find out whether more knowledge can be revealed through studying separately the positive and negative discharges but still using a spectrum analyser. Studying PD spectral content at different parts of the supply voltage waveform might produce more useful knowledge about PD phenomena. Such work however may need to deal with challenges of sensitivity and the feasibility of gating the spectrum analyser input.

8.2.2 Could insulation defects farthest from the high voltage electrode be more harmful than those closest?

An interesting observation noted during the long term ageing tests is that there was a tendency of samples with defects closer to the earth electrode failing first than those closer to the HV electrode. This applied to both surface and cavity discharges. It can be suggested that such behaviour is contrary to intuition.

Hypothetically the trend can be explained in terms of the influence of the electric field distribution between the electrodes on the rate of defect progression to total failure. Progression of a PD defect in the final phases towards total failure involves development of electrical tree channels that extend from the defect into the opposite electrode to completely bridge the insulation and cause a short circuit (Morshuis, 1993). It can be suggested that the rate of electrical tree progression depends on whether the electric stress in the insulation increases or decreases in the direction of the tree progression. Since defects nearest the earthed electrode create electrical trees that progress into the insulation towards the higher electric stress regions near the HV electrode, the rate of progression increases with time and causes failure faster than the opposite case. More extensive studies of this phenomenon can yield valuable knowledge leading to the much desired ability to rank insulation defects according to the degree of harmfulness.

Appendix A: Sizing cavity PD defects for accelerated ageing tests

Since PD behaviour also depends on defect dimensions, the latter had to be deliberately predetermined. This appendix presents the methodology followed in determining the dimensions of the disc shaped cavities used in this work.

A.1 Introduction

Accelerated ageing tests have been widely used in studying power cable insulation behaviour under multi-stress conditions (Sarma et al., 2002). The concept has also been applied where partial discharge (PD) phenomenon is the main insulation ageing agent (Candela et al., 2000; Morshuis, 1995a; Hudon et al., 1995). The time-dependent PD behaviour that is manifested in phase-resolve patterns and other PD characteristics have been studied by other researchers using accelerated ageing techniques (Gulski & Krivda, 1995). The work conducted in this thesis was to investigate PD behaviour in the frequency domain and this entailed creating artificial defects in insulation for use in the various tests that included accelerated ageing under continuous PD activity. Air-filled cavities were among the artificial insulation defects studied. A question that had to be answered was: how big would the cavity defect be?

The cavity dimensions were to be such that they gave discharges of suitable magnitudes and inception voltage under given experimental conditions. The test conditions included test voltage magnitude, PD detection system sensitivity, minimum required ageing time, defect position and anticipated reduction in PD magnitude with ageing. In this appendix the procedure followed in optimising the cavity dimensions for the tests is presented.

A.2 Determination of cavity dimensions

Air cavities in insulation can appear in different positions such as those illustrated in ***Figure A1(a).*** Disc cavity dimensions are indicated in ***Figure A1(b)***.

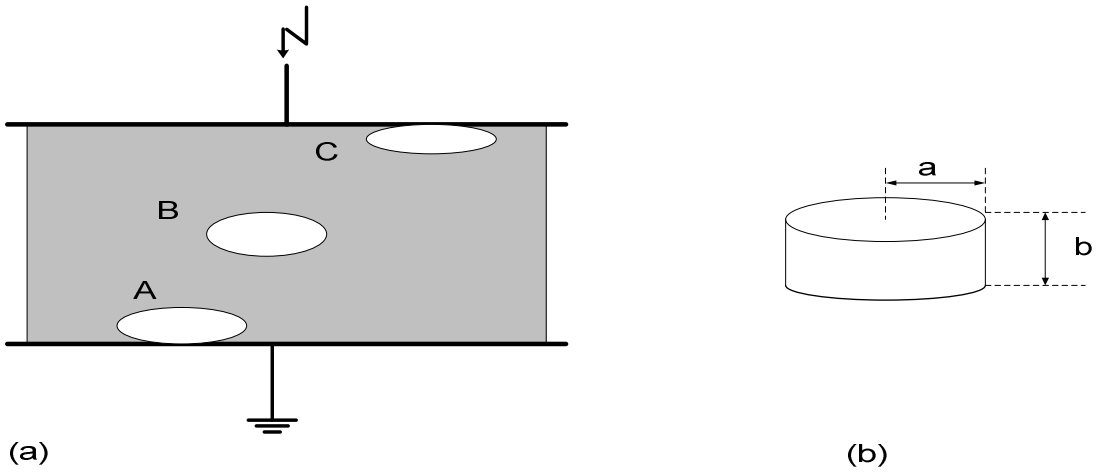

Figure A1: ***An air filled cavity in a solid dielectric at different possible positions between the two electrodes.***

Step 1: Determination of the optimum defect radius

In this work it had to be ensured that the cavity aged uniformly. In order to achieve this, the entire cavity should be exposed to partial discharges. The cavity area that is involved in a discharge process is known as the effective discharge area and according to Wetzer et al., (1991) this area can be expressed analytically as given in Equation A1.

$$a_{eff} = A\{1 - e^{(-a/A)}\} \tag{A1}$$

Where:

a_{eff} = the effective cavity radius [m]

a = the actual cavity radius [m]

A = is a constant = 2.147

A plot of the effective radius as a function of the actual cavity radius shows that the cavity area is fully exposed to discharges in small radii cavities. As the cavity radius increases beyond a certain value, part of the cavity area becomes redundant. A cavity radius of 1.5 mm would give marginal redundant area.

Consequently in this work all the artificial cavities were made with diameter **of 2 mm.**

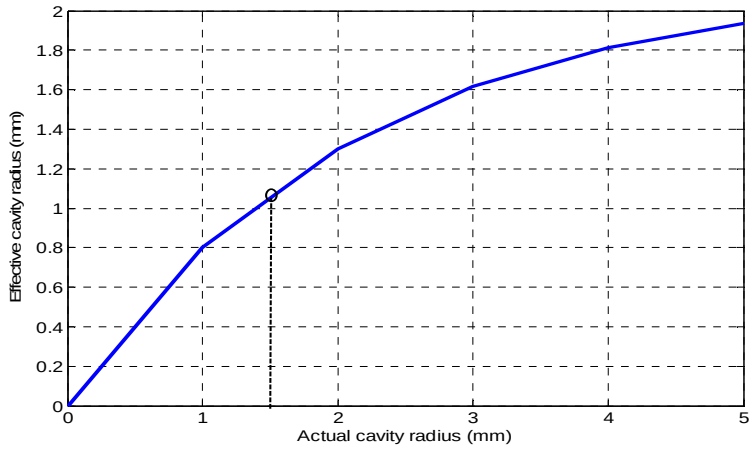

Figure A2: ***A plot of the effective radius (a_{eff}) of cavity exposed to PDs as a function of the actual cavity radius (a).***

Step 2: Determination of the optimum cavity height

The cavity height should be such that with the given radius (as determined in step 1) the resultant cavity volume gives PDs that initiate at the desired inception voltage. In this work the inception voltage was chosen to be 6 kV which emulated PDs in 11 KV rated power cables under normal operating conditions. Moreover the cavity height should also be as small as possible in order to avoid overstressing the remaining portion of insulation in series with the cavity between the electrodes. Such condition could result in undesired non-PD induced failure. According to the streamer criterion, the minimum field (E_i) required for discharge initiation within a spheroidal cavity with a non-attaching gas is expressed as in Equation A2;

$$\frac{E_i}{p} = \left(1 + \frac{B}{\sqrt{(a+b)p}}\right)\frac{E_l}{p} \qquad \text{(A2)}$$

Where:

E_l	=	the minimum field necessary to sustain a discharge or the field in the cavity after a discharge [V/m]
B	=	a characteristic constant dependent on the type of gas and for air is = 8.6 [Pa.m]
E_l/p	=	24.2 for air [V/Pa.m]
a and b	=	the cavity radius and height respectively [m]

Simplifying Equation A2 by substituting known values gives Equation A3;

$$E_i = 24.2p\left\{1 + \frac{8.6}{\sqrt{(a+b)p}}\right\} \quad \text{(A3)}$$

If the electric field in the insulation is E_0, that in the cavity is enhanced by a factor (f) which is a function of the cavity dimensions (Gutfleisch & Niemeyer, 1995; Chang et al., 1986). For a spherical cavity $f = \frac{3\varepsilon_r}{2\varepsilon_r+1}$, where ε_r is the relative permitivity of the dielectric thus $E_i = fE_0$.

In order to express the electric field at the cavity position in terms of the voltage across the electrodes, for a coaxial electrode configuration and parameters as shown in ***Figure A3(a)***, $E_0 = \frac{V_i}{rln\frac{R_0}{R_i}}$ and $E_0 = \frac{V_i}{x}$ for parallel plane electrodes separated by distance x as shown in ***Figure A3(b).*** Expressing E_i in terms of E_0 and then finally in terms of V_i gives the two expressions; Equation A4 for coaxial and Equation A5 for parallel plate electrode configurations (Chan et al., 1991).

$$V_i(rms) = 24.2p\left(rln\left(\frac{R_0}{R_i}\right)\right).\left(\frac{2\varepsilon_r+1}{3\varepsilon_r}\right).\left(\frac{8.6}{\sqrt{(a+b)p}} + 1\right).\frac{1}{\sqrt{2}} \quad \text{(A4)}$$

or

$$V_i(rms) = 24.2p(x).\left(\frac{2\varepsilon_r+1}{3\varepsilon_r}\right).\left(\frac{8.6}{\sqrt{(a+b)p}} + 1\right).\frac{1}{\sqrt{2}} \quad \text{(A5)}$$

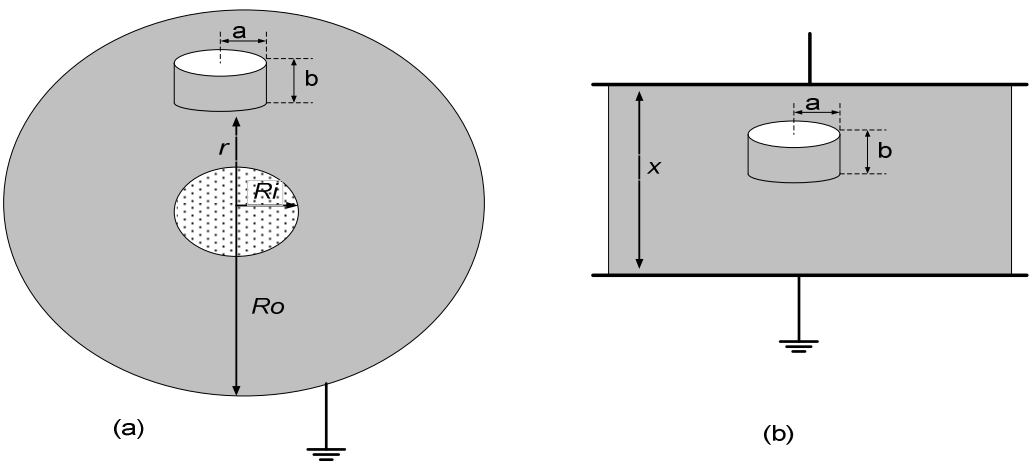

Figure A3: ***Illustration of air filled cavity in insulation between (a) coaxial and (b) parallel plate electrodes configurations.***

By substituting in (A4) the cable dimensions, the cavity radius, the parallel electrode separation and all the other known parameters, the cavity height (b) that gives rms inception voltage of 6 kV is calculated as **1 mm**. It should be noted however that the calculated values only apply in un-aged insulation defect conditions only. When aged due to continuous exposure to PD activity, both the spatial distribution of the PDs in the cavity and the inception voltage behave in a manner that cannot be modelled using the aforementioned analytical expressions.

A3. Conclusion

Suitable cavity dimensions were analytically determined that gave partial discharges of required inception voltage and also ensure that the discharge activity occurred in the whole cavity. The theoretical predictions were verified through practical tests. There was close correlation between the results as explained in detail in (Nyamupangedengu & Jandrell, 2007). The obtained cavity dimensions were then used in the thesis experimental work.

Appendix B: Examples of time domain PD pulse shapes responding to changes in the supply voltage characteristics

The investigations in this work were largely performed in the frequency domain. Corresponding time domain measurements were also conducted to independently verify the frequency domain measurements. In this appendix, examples of pulses recorded in the time domain at various supply frequency voltages are presented. These are appropriately referred to in various sections in the main document.

Samples of the void, surface and corona PD pulses at various frequencies and supply voltage magnitudes are shown in Figures B1, B2 and B3 respectively. The corona pulses in Figure B3 are clearly different from both the void and surface discharges.

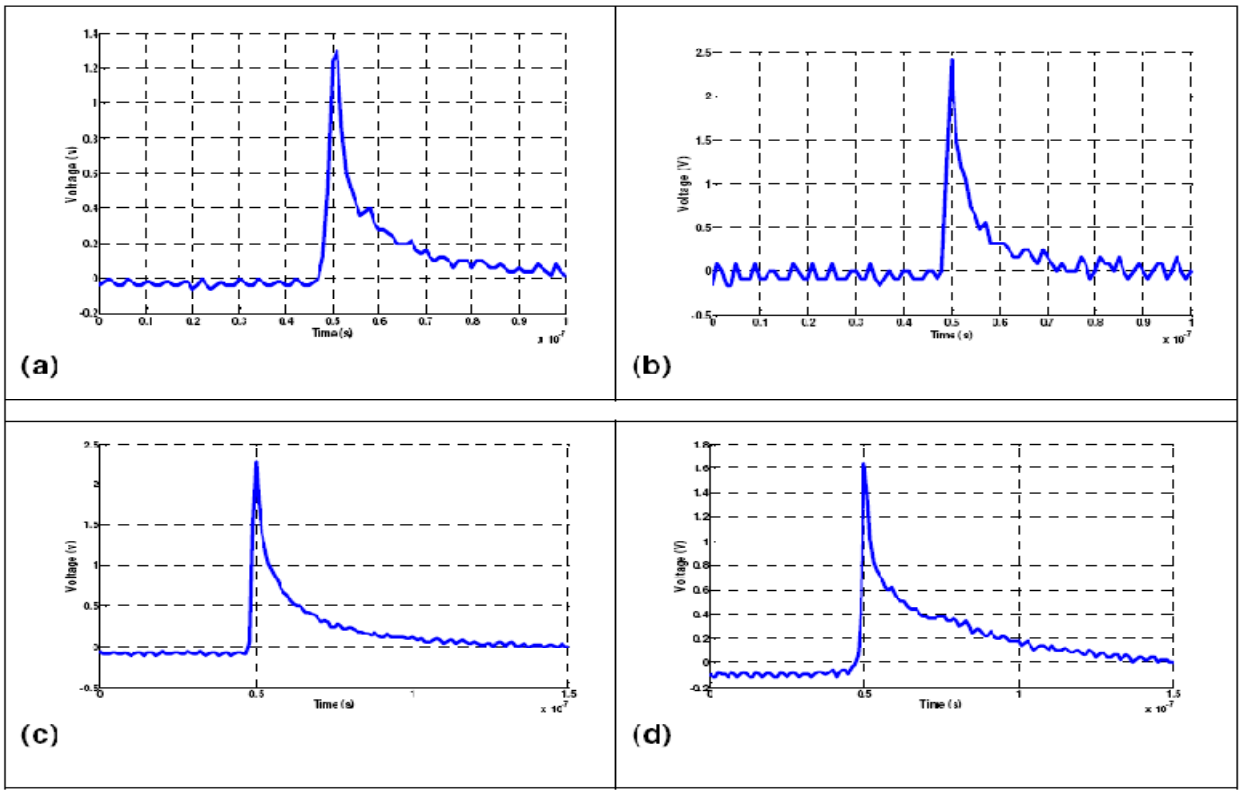

Figure B1: ***Samples of void defect partial discharge pulses where Figures B1a and B1b are pulses at 2 kV and 11 kV respectively with supply frequency maintained at 50 Hz. Figures B1c and B1d are the void defect pulses at supply frequencies of 10 Hz and 400 Hz respectively with test voltage magnitude maintained at 7 kV.***

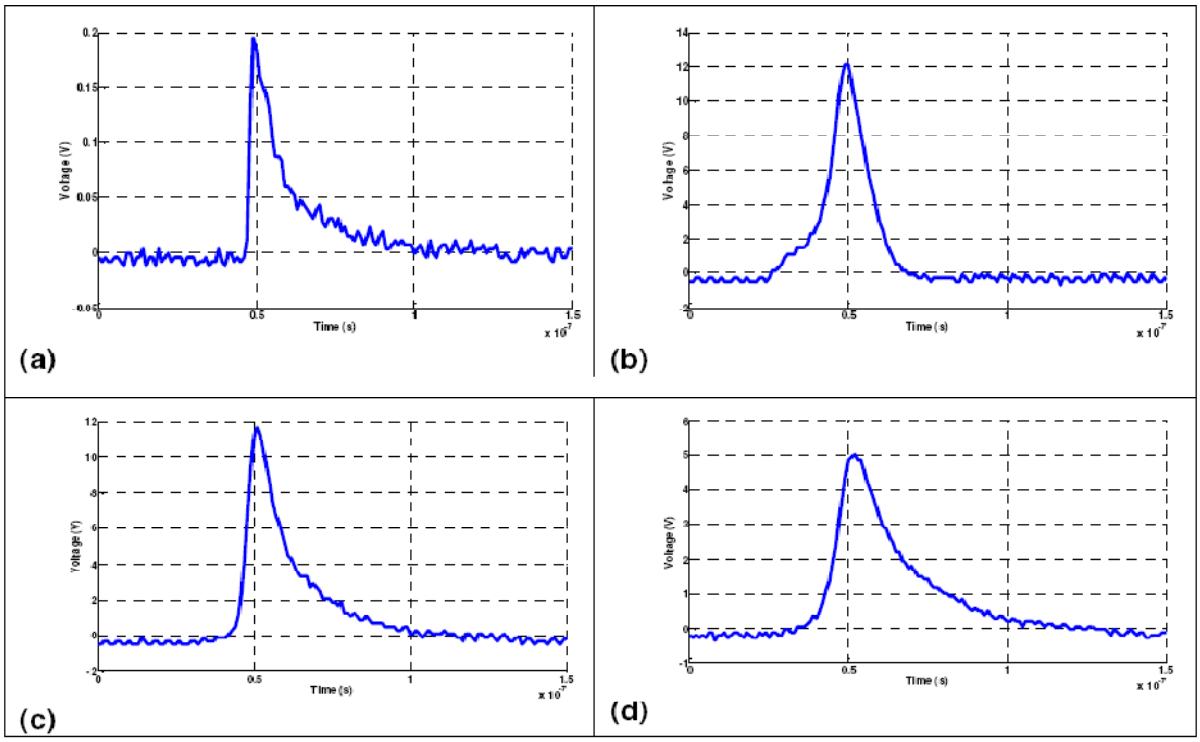

Figure B2: ***Samples of surface partial discharge pulses where Figures B2a and B2b are pulses at 2 kV and 11kV respectively with supply frequency maintained at 50 Hz. Figures A2c and A2d are the surface discharge pulses at supply frequencies of 10 Hz and 400 Hz respectively with test voltage magnitude maintained at 7 kV.***

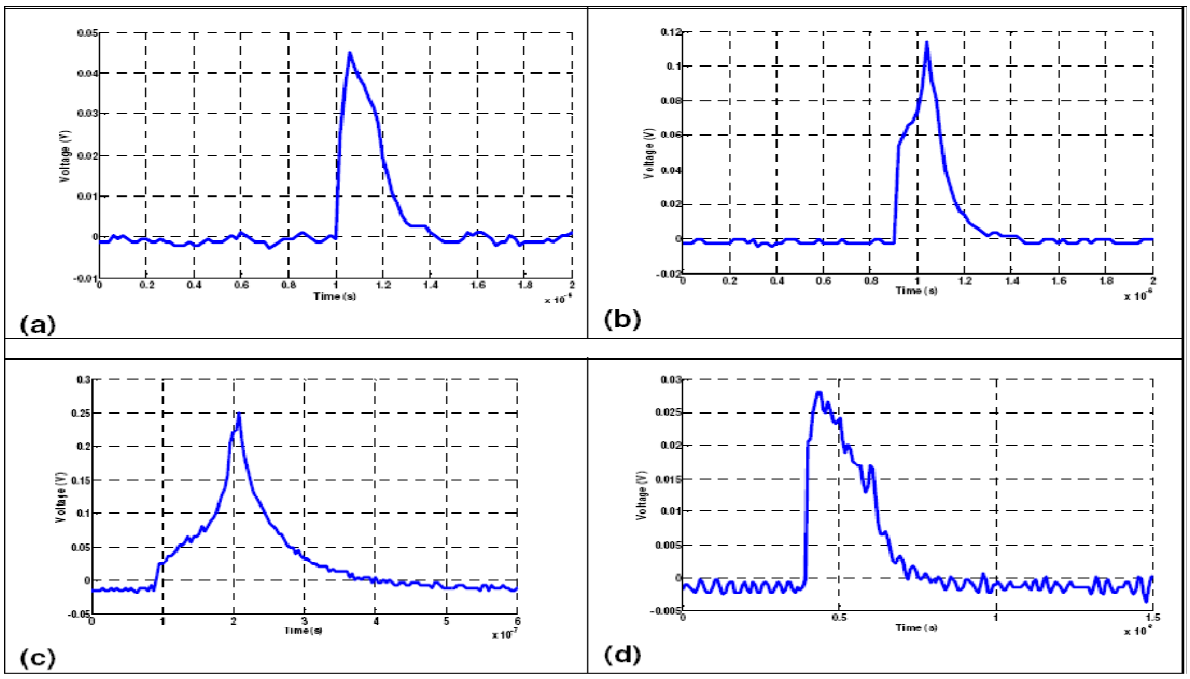

Figure B3: ***Samples of point-to-plane corona in air discharge pulses where Figures B3a and B3b are pulses at 3 kV and 9 kV respectively with supply frequency maintained at 50 Hz. Figures B3c and B3d are the corona pulses at supply frequencies of 10 Hz and 280 Hz respectively with test voltage magnitude maintained at 7 kV.***

References

Ahmed, N. H., & Srinivas, N. N. (1998). On-line partial discharge detection in cables. *IEEE Transactions on Dielectrics and Electrical Insulation , 5* (No.2), 181-188.

Alshelkhly, A., & Kranz, H. G. (1991). A new approach for a basic understanding of PD-phenomena. *7th International Symposium on High Voltage Enegineering*, (pp. 21-24). Dresden.

Balkon, C., Kalkner, W., Obralic, A., Plath, R., & Rethmeier, K. (2009). Potential of multispectral PD measurement for differentiation of interfering impulses and multiple PD sources. *Proceedings of the 16th International Symposium on High Voltage Engineering (ISH)*, (pp. paper D-30). Cape Town, South Africa.

Bartnikas, R. (2004). A comment concerning the rise times of partial discharge pulses. *IEEE Transactions on Dielectrics and Electriacal Insulation , Vol.12* (No.2), 197-202.

Bartnikas, R. (1987). A Commentary on Partial Discharge Measurement and Detection. *IEEE Transactions on Electrical Insulation , EI-22* (No. 5), 629-653.

Bartnikas, R. (2002). Partial Discharges: Their mechanism, detection and measurement. *IEEE Transactions on Dielectrics and Electrical Insulation, Vol. 9, , Vol. 9* (No.5), 763-808.

Bartnikas, R. (2008). Some observations concerning the influence of dielectric surfaces upon the PD behaviour. *IEEE Transactions on Dielectrics and Electrical Insulation , Vol. 15* (No. 6), 1488-1493.

Bartnikas, R., & Levi, J. H. (1969). A simple pulse-height analyzer for partial-discharge rate measurements. *IEEE Transactions on Instrumentation and Measurement , Vol. IM-18* (No.4), 341-345.

Bartnikas, R., & Novak, J. P. (1995). Effect of overvoltage on risetime and amplitude of PD pulses. *IEEE Transactions on Dielectrics and Electrica Insulation , Vol. 2* (No. 4), 557-565.

Bartnikas, R., & Novak, J. P. (1992). On the spark to pseudoglow and glow discharge transition mechanism and discharge detectability. *IEEE Transactions on Dielectrics and Electrical Insulation , Vol. 27* (No. 4), 3-14.

Bodega, R., Cavallin, A., Morshuis, P. H., & Wester, F. J. (2002). The Effect of Voltage Frequency on Partial Duscharge Activity. *2002 Annual Report Conference on Electrical Insulation and Dielectric Phenomena*, (pp. 685-689).

Bodega, R., Morshuis, H. F., Lazzaroni, M., & Wester, F. J. (2004). PD Recurrence in Cavities at Different Energising Methods. *IEEE Transactions on Instrumentation and Measurement , Vol. 53* (No. 2), 251-258.

Boggs, S. A. (2001, July/August). 500Ω-m - Low enough resistivity for cable ground shield semicon? *IEEE Electrical Insulation Magazine , Vol. 17* (No. 4), pp. 26-32.

Boggs, S. A. (1990, July/August). Partial Discharge: Overview and Signal Generation. *IEEE Electrical Insulation Magazine , Vol. 6* (No. 4), pp. 33-39.

Boggs, S. A., & Stone, G. C. (1982). Fundamental Limitations in the Measurement of Corona and Partial Discharge. *IEEE Transactions on Electrical Insulation , Vol. EI-17* (No. 2), 143-150.

Boggs, S. (2003). The case of frequency domain PD testing in the context of distribution cables. *IEEE Electrical Insulation Magazine , Vol. 19* (No. 4), pp. 13-19.

Bolliger, A., & Lemke, E. (2001, December 3 & 4). PD Diagnostics - Its History and Future. *PD Workshop* . Virginia, USA: Accessed on 20/06/2010 from - http://hvtestanddiagnostics.com/images/pulications/.

Brengtsson, T., Dijkhuizen, F., Ming, L., Sahlen, F., Liljestrand, L., Bormann, D., et al. (2009, July/August). Repetitive Fast Voltge Stress - Causes and Effects. *IEEE Electrical Insulation Magazine , Vol. 25* (No. 4), pp. 26-39.

Brosche, T., Hiller, W., & Fauser, E. (1999). Novel characteristion of PD signals by real-time measurement of pulse parameters. *IEEE Transactions on Dielectrics and Electrical Insulation , Vol. 6* (No. 1), 51-59.

Candela, R., Romano, P., & Schifani, R. (2000). A novel HV system for multi specimens ageing tests under partial discharges and temeperature. *IEEE Conference on Electrical Insulation and Dielectric Phenomena.* Victoria, Canada.

Cavallini, A., & Montanari, G. C. (2006). Effect of Supply Voltage Frequency on Testing of Insulation System. *IEEE Transactions on Dielectrics and Electrical Insulation , Vol. 13* (No. 1), 111-121.

Chan, C., Duffy, P., Hiivala, L. J., & Wasik, J. (1991, September/October). Partial Discharge - Part VIII: PD Testing of Solid Dielectric Cable. *IEEE Electrical Insulation Magazine , Vol. 7* (No. 5), pp. 9-20.

Chang, D. D., Sudarshan, T. S., & Thompson, J. E. (1986). Analysis of electric stress distribution in cavities embedded within dielectric structures. *IEEE Transactions on Electrical Insulation , Vol. EI-21* (No. 2), 213-219.

Cheng, Y., Xie, H., & Li, W. (1998). Study on characteristics of ultra-wideband partial discharge of typical insulation samples. *IEEE Dielectrics and Electrical Insulation and the 30th Symposium on Electrical Insulating Materials,* (pp. 697-700). Toyohashi, Japan.

Cheng, Y., Xie, H., Song, J., Jiang, Y., Zheng, & T. (2000). The characteristics of ultra-wideband partial discharge of insulation in aging process. *Proceedings of the 6th International Conference on Properties and Applications of Dielectric Materials,* (pp. 194-197). Xi'an, China.

Cigre WG 15.06, (2002). *Development of a partial discharge analysis method to assess the dielectric quality of GIS.* Cigre session 2002.

Cigre WG 21.16. (2001). *Partial Dsicharge Detection in Installed HV Extruded Cable Systems.* Cigre report 182.

Cigre, WG 21.03. (1969). *Recognition of Discharges.* Paris: Cigre.

Comber, M. G., Deno, D. W., & Zaffanella, L. E. (1987). Corona Phenomena on AC Transamission Lines. In *EPRI Transamission Refence Book, 345 kV and Above* (pp. 169-186). EPRI.

Crichton, G. C., Karlsson, P., & Pedersen, A. (1989). Partial Discharges in Ellipsoidal and Spheroidal Voids. *IEEE Transactions on Electrical Insulation , Vol. 24* (No.2), 335-342.

Denissov, D., Kohler, W., Hoek, S. M., Tenbohlen, S., & Klein, T. (2007a). On-line partial discharge diagnostics for cable terminations. *15th International Symposium on High Voltage Engineering (ISH),* (pp. Paper no. T7-70). Ljubljana.

Dennisov, D., Pfisterer, R. G., Pfisterer, T. K., & Tenbohlen, S. (2007b). UHF partial discharge diagnosis of plug-in cable terminations. *Jicable'07.*

Devins, J. (1984). The physics of partial discharges in solid dielectrics. *IEEE Transactions on Dielectrics and Electrical Insulation , Vol. EI-19* (No. 5), 475-495.

Forssen, C., & Edin, E. (2008). Partial Discharges in a Cavity at Variable Applied Frequency Part 1: Measurements. *IEEE Transactions on Dielectrics and Electrical Insulation , Vol. 15* (No. 6), 1601-1609.

Fouracre, R. A., MacGregor, S. J., & Tuema, F. A. (1999). An Investigation into the Mechanisms of Surface Discharges. *12th IEEE International Conference on Pulsed Power, Vol. 2,* pp. 1380-1383.

Fruth, B., & Niemeyer, L. (1992). The Importance of Statistical Characteristics of Partial Discharge Data. *IEEE Transactions on Electrical Insulation , Vol. 27* (No. 1), 60-69.

Gockenbach, E., & Hauschild, W. (2000, November/December). The selection of frequency range for high-voltage on-site testing of extruded insulation cable systems. *IEEE Electrical Insulation Magazine , Vol. 16* (No.6), pp. 11-16.

Golubev, A., Blokhintsev, I., Paoletti, G., & Modrowski, J. (2001). On-line partial discharge applications to MV electrical switchgear. *Proceedings of Electrical Insulation Conference and & Electrical Manufacturing & Coil Winding Conference,* (pp. 225-232).

Gulski, E. (1993). Computer-aided measurement of partial discharges in HV equipment. *IEEE Transactions on Electrical Insulation , Vol. 28* (No.6), 969-983.

Gulski, E. (1995). Digital analysis of partial discharges. *IEEE Transactions on Dielectrics and Electrical Insulation , Vol. 2* (No. 5), 822-837.

Gulski, E., & Krivda, A. (1995). Influence of ageing on classification of PD in HV components. *IEEE Transactions on Dielectrics and Electrical Insulation , Vol. 2* (No. 4), 676-684.

Gulski, E., Hamerling, B. R., Wester, F. J., Smit, J. J., Groot, E., & Schikarski, P. (2005). On-line and off-line partial discharge diagnostics for medium voltage power cables. *14th International Symposium on High Voltage Engineering (ISH).* Beijing.

Gulski, E; Kreuger, F H. (1992). Computer aided recognition of discharge sources. *IEEE Transactions on Electrical Insulation , Vol. 27* (No.1), 82-92.

Gutfleisch, F., & Niemeyer, L. (1995). Measurement and Simulation of PD in Epoxy Voids. *IEEE Transactions on Dielectrics and Electrical Insulation , Vol. 2* (No.5), 729-743.

Handala, M. A., & Lamrous, O. (2008). Surface degradation of styrene acrylonitrile exposed to corona discharge. *European Transactions on Electrical Power , Vol. 18*, 494-505.

Harrold, R. T. (1971). The spectrum analyser applied to the measurement of EHV power line radio noise. *IEEE Transactions on Power Apparatus and Systems , Vol. PAS-90* (No. 4), 1837-1841.

Hauschild, W. (2006). Discussion: Effect of Supply Voltage Frequency on Testing of Insulation System. *IEEE Transactions on Dielectrics and Electrical Insulation , Vol. 13* (No. 5), 1189-1191.

Heitz, C. (1999). A Generalised Model for Partial Dicsharge Processes Based on a Stochastic Process Approach. *Journal of Applied Physics, D: Appl. Phys. , Vol. 32*, 1012-1023.

Hikita, M, Yamada, M, Nakamura, A; Mizutani,T; Oohasi, A ; Ieda, M. (1990). Measurement of partial discharges by computer and analysis of partial discharge distribution by the Monte Carlo Method. *IEEE Transactions on Electrical Insulation , Vol. 25* (No. 3), 453-468.

Hikita,M; Komori, F; Nishiguchi, N; Mizutani, T. (1994). Phase-resolved and time-sequential partial discharge pulse measurements in a metal-void-insulator system using a personal computer. *J. Pys. D: Appl. Phys. , 27*, 1220-1228.

Holboll, J. T., & Stone, G. C. (1995). Partial discharges in flat, dielectric/metallic bounded cavities. *IEE Pro. -Scie. Meas. Technol , Vol. 142* (No. 6), 490-494.

Hudon, C., Bartnikas, R., & Wertheimer, M. R. (1995). Effect of physio-chemical degradation of epoxy resin on partial discharge behaviour. *IEEE Transactions on Dielectrics and Electrical Insulation , Vol. 2* (No. 6).

Hudon, C., Bartnikas, R., & Wertheimer, M. R. (1993). Spark-to-glow discharge transition due to increased surface conductivity on epoxy resin specimens. *IEEE Transactions on Electrical Insulation , Vol. 28* (No. 1), 1-8.

Hudon, C., Reed, C. W., & Tmperley, J. E. (1994). Use of spectral analysis and phase resolved partial discharge measurements for generator testing. *IEEE Conference on Electrical Insulation and Dielectric Phenomena, Annual Report 1994*, (pp. 103-111).

IEC-60270, (2000). High voltage test techniques - Partial discharge measurements.

IEEE std 400.3, (2007). *IEEE Guid for Partial Discharge Testing of Shielded Power Cable Systems in a Field Environment.* New York: IEEE Power Engineering Society.

IEEE C57.113, 1. (1991). Guide for Partial Discharge Measurement in Liquid Filled Power Transformers and Shunt Reactors.

Jager, K., & Lindbom, L. (2005, January/February). The continuing evolution of semiconductive materials for power cable applications. *IEEE Electrical Insulation Magazine , Vol. 21* (No. 1), pp. 20-34.

Jiang, Z., Li, F., Qiao, F., Sun, H., Wan, H., Wang, J., et al. (2009). A vision of smart transmission grids. *IEEE Power & Energy Society General Meeting, 2009 PES 09*, (pp. 1-10). Calgary AB.

Kelen, A. (1995). Trends in PD Diagnosis: When new options proliferate, so do old and new problems. *IEEE Transactions on Dielectrics and Electrical Insulation , Vol. 2* (No. 4), 529-534.

Kelen, A., & Danikas, M. G. (1995). Evidence and Presumption in PD Diagnosis. *IEEE Transactions on Dielectrics and Electrical Insulation , Vol.2* (No. 5), 780-794.

Kemp, I. J. (1995). Partial discharge plant-monitoring technology: Present and future developments. *IEE Proc. - Sci. Meas. Technol. , Vol. 142* (No.1), 4-10.

Kim, C S; Kondo, T; Mizutani, T. (2004). Change in PD pattern with ageing. *IEEE Transactions on Dielectrics and Electrical Insulation , Vol. 11* (No. 1), 13-18.

Kim, C. S., Hirase, T., & Mizutani, T. (2002). PD frequency characteristics for a void bounded with LDPE. *IEEE 2002 Annual Report Conference on Electrical Insulation and Dielectric Phenomena*, (pp. 712-715).

Kreuger, F. H., Gulski, E., & Krivda, A. (1993). Classification of partial discharges. *IEEE Transactions on Electrical Insulation , Vol. 28* (No.6), 917-931.

Kreuger, F. (1989). *Partial discharge detection in high-voltage equipemnt.* London: Butterworths.

Krivda, A. (1995). *Recognition of partial discharges: Discrimination and classification* (PhD Thesis ed.). Delft: Delft University.

Kuffel, E., Zaengl, W. S., & Kuffel, J. (1984). *High Voltage Engineering.* Butterworth-Heinemann.

Kulla, A. (2003). Learning to Detect Critical Changes in Partial Discharges. *13th Symposium in High Voltage Engineering (ISH).* Delft, Netherlands.

Kurrat, M., & Peier, D. (1991). Wideband measurement of partial discharges for fundamental diagnosis. *7th International Symposium on High Voltage Engineering (ISH), Paper no. 72.02*, pp. 47-50. Dresden.

Kyprianou, A., Lewin, P. L., Efthimiou, V., Stavrou, A., & Georghiou, G. E. (2006). Wavelet packet denoising for online partial discharge detection in cables and its application to experimental field results. *Measurement Science Technology , Vol. 17*, 2367-2379.

Ladde, R. C., Meijer, S., Smit, J. J., & Hermans, T. J. (2007). Developments concerning HF/VHF/UHF measurements for on-line PD detection in power cable accessories. *15th International Symposium on High Voltage Engineering (ISH)*, (pp. Paper no. T7-736). Ljubljana.

Lama, W. L., & Gallo, C. F. (1974). Systematic Study of the Electrical Characteristics of the "Trichel" Current Pulses from Negative Needle-to-plane Coronas. *Journal of Applied Physics , Vol. 45* (Issue 1), 103-113.

Lapp, A & Kranz, H G. (2000). The use of the CIGRE data format for PD diagnosis applications. *IEEE Transactions on Dielectrics and Electrical Insulation , Vol. 7* (No. 1), 102-111.

Laurent, C., & Mayoux, C. (1992, March/April). Partial Discharge - Part XI: Limitations to PD as a diagnostic for deterioration and remaining life. *IEEE Electrical Insulation Magazine , Vol. 8* (No. 2), pp. 14-17.

Lemke, E., & Schmiegel, P. (1991). Progress in PD-probe Measuring Technique. *7th International Symposium on High Voltage Engineering*, (pp. 43-46). Dresden.

Lemke, E., Berlinjn, S., Gulski, E., Muhr, M., Pultrum, E., Strehl, T., et al. (2008a). *Guide for Partial Discharge Measurements in Compliance to IEC 60270.* Cigre, WG D1.33.

Lemke, E., Elze, H., & Weissenberg, W. (2003). Experience in PD diagnosis tests of HV cable terminations in service using the ultra-wide band PD probing. *XIIIth International Symposium on High Voltage Engineering* (pp. 1-4). Delft, Netherlands: Millpress, Rotterdam.

Lemke, E., Strehl, T., & Markalous, S. (2008b). Ultra-wide-band PD Diagnostics of Power Cable Terminations in Service. *IEEE Transactions on Dielctrics and Electrical Insulation , Vol. 15* (No. 6), 1570-1575.

Lundgaard, L. E. (1992, July/August). Partial Discharge - Part XIII: Acoustic Partial Discharge Detection - Fundamental Considerations. *IEEE Electrical Insulation Magazine , Vol. 8* (No. 4), pp. 25-31.

Markalous, S., Tenbohlen, S., & Feser, K. (2008). Detection and location of partial discharges in power transformers using acoustic and electromagnetic signals. *IEEE Transactions on Dielectric and Electrical Insulation , Vol. 15* (No. 6), 1576-1518.

Maruvada, S. P. (2000). Corona and Gap Discharges. In S. P. Maruvada, *Corona Performance of High Voltage Transmission Lines.* Research Studies Press Ltd.

Mason, J. H. (1992). Effects of frequency on the electric strength of polymers. *IEEE Transactions on Electrical Insulation , Vol.21* (No.6), 1213-1216.

Mason, J. H. (1995). Enhancing the signficance of PD measurements. *IEEE Transactions on Dielectrics and Electrical Insulation , Vol. 2* (No. 5), 876-888.

Mayoux, C. (1997). Aging of polymeric insulating materials in power cables. *IEEE Transactions on Dielectrics and Electrical Insulation , Vol. 4* (No. 6), 665-673.

Mayoux, C., & Laurent, C. (1995). Contribution of partial discharges to electrical breakdown of solid insulating materials. *IEEE Transactions on Dielectrics and Electrical Insulation , Vol. 2* (No.4), 641-652.

Meijer, S., Gulski, E., Smit, J. J., Wester, F. J., Grun, T., & Turner, M. (1999). Interpretation of PD in GIS Using Spectral Analysis. *11th International Symposium on High Volatge Engineering (ISH)* (pp. 124-127). London: IEE.

Meijer, S., Pantelis, D., Gulski, E., Seitz, P. P., & Hermans, T. J. (2006). Condition assessment of power cable accessories using advanced VHF/UHF PD detection. *Conference Record of the 2006 IEEE International Symposium on Electrical Insulation*, (pp. 482-485).

Meijer, S., Rutgers, W. R., & Smit, J. J. (1996). Acquisition of Partial Discharges in SF6 Insulation. *1996 IEEE Annual Report - Conference on Electrical Insulation and Dielectric Phenomena. Vol. 2*, pp. 581-584. San Francisco: IEEE.

Miller, R., & Black, I. A. (1977). Partial Discharge Measurements Over The Frequency Range 0.1 Hz to 50 Hz. *IEEE Transactions on Electrical Insulation , Vol. EI-12* (No.3), 224-233.

Montanari, G. C. (2006). Partial discharge measurements: becoming a fundamental tool for quality control and risk assessment of electrical equipment? *Conference Record of the 2006 IEEE International Symposium on Electrical Insulation*, (pp. 281-284).

Montanari, G. C., Contin, A., & Cavallini, A. (2000). Random Sampling and data processing PD-pulse height and shape analysis. *IEEE Transactions on Dielectrics and Electrical Insulation , Vol.7* (No. 1), 30-39.

Montanari, G. (2008, Nov/Dec). Envisaging links between fundamental research in electrical insulation and electrical assest management. *IEEE Electrical Insulation Magazine , Vol. 24* (No.4), pp. 7-21.

Morshuis, P. (1995a). Ageing of polymers studied by spectral analysis of UWB partial discharge signals. *IEEE Annual Report of the Conference on Electrical Insulation and Dielectric Phenomena*, (pp. 226-229).

Morshuis, P. (1995b). Assessement of dielectric degradation by ultrwaide-band PD detection. *IEEE Transactions on Dielectrics and Electrical Insulation , Vol. 2* (No. 5).

Morshuis, P. H. (1995c). Partial discharge mechanisms in voids related to dielectric degradation. *IEE Proceedings in Science Measurements Technology , Vol. 142* (No.1), 62-68.

Morshuis, P. H. (2005). Degradation of Solid Dielectrics due to Internal Partial Discharge: Some thoughts on progress made and where to go now. *IEEE Transactions on Dielectrics and Electrical Insulation , Vol. 12* (No. 5), 905-912.

Morshuis, P. H. (1993). *Partial discharge mechanisms: Mechanisms leading to breakdown, analysed by fast electrical and optical measurements.* PhD thesis, Delft University.

Morshuis, P. H., & Kreuger, F. H. (1990). Transition from streamer to Townsend mechanisms in dielectric voids. *J. Phys. D; Appl. Phys. , Vol. 23*, 1562-1568.

Murooka, Y., Takada, T., & Hidaka, K. (2001, March/April). Nanosecond Surface Discharge and Charge Density Evaluation Part 1: Review and Experiments. *IEEE Electrical Insulation Magazine , Vol. 17* (No.2), pp. 6-16.

Nattrass, D. A. (1993, July/August). Partial Discharge XVII: The Early History of Partial Discharge Research. *IEEE Electrical Insulation Magazine , Vol. 9* (No. 4), pp. 27-31.

Niemeyer, L. (1995). A generalised approach to partial discharge modeling. *IEEE Transactions on Dielectrics and Electrical Insulation , Vol. 2* (No.4), 510-519.

Niemeyer, L., Fruth, B., & Gutfleisch, F. (1991). Simulation of Partial Discharges in Insulation Systems. *7th International Symposium on High Voltage Engineering*, (pp. 25-28). Dresden.

Nyamupangedengu, C., & Jandrell, I. R. (2008). Influence of Supply Voltage Frequency and Magnitude on PD Pulse Parameters. *IEEE Transactions on Dielectrics and Electrical Insulation , Vol. 15* (No. 6), 1590-1600.

Nyamupangedengu, C., & Jandrell, I. R. (2007). Sizing of artificial PD defects for an accelerated ageing test of power cable solid dielectric insulation. *Southern Africa Universities Power Engineering Conference.* Cape Town.

Nyamupangedengu, C., Jandrell, I. R., & Reynders, J. P. (2007). Optimisation of the sensitivity and bandwidth of a capacitive coupler for wideband PD detection in solid dielectric power cables. *15th International Symposium on High Voltage Engineering (ISH).* Ljubljana, Slovenia.

Okamoto, T & Tanaka, T. (1986). Novel partial discharge measurement computer-aided measurement systems. *IEEE Transactions on Electrical Insulation , Vol. EI-21* (No. 6), 1015-1019.

Okubo, H., Hayakawa, N., & Matsushita, A. (2002, May/June). The relationship between partial discharge current pulse waveforms and physical mechanisms. *IEEE Electrical Insulation Magazine , Vol. 18* (No. 3), pp. 38-45.

Orton, H. E. (2003). Diagnostic Testing of In-situ Power Cables - an Overview. *13th International Symposium on High Voltage Engineering.* Delft, Netherlands.

Pearson, J. S., & Harrison, J. A. (1969). A uniform field electrode for use in a discharge chamber of restricted size: design and performance. *British Journal of Applied Physics (J. Phys. D) , Vol. 2* (Ser. 2), 77-84.

Pearson, J. S., Farish, O., Hampton, B. F., Judd, M. D., Templeton, D., Pryor, B. M., et al. (1995). Partial Discharge Diagnosis for Gas Insulated Substations. *IEEE Transactions on Dielectrics and Electrical Insulation , Vol. 2* (No. 5), 893-905.

Petzold, F., Schlapp, H., Gulski, E., Seitz, P. P., & Quak, B. (2008). Advanced solution for on-site diagnosis of distribution power cables. *IEEE Transactions on Dielectrics and Electrical Insulation , Vol. 15* (No. 6), 1584-1589.

Radu, I., Bartnikas, R., & Wertheimer, M. R. (2003). Frequency and voltage dependence of glow and pseudoglow discharges in Helium under atmospheric pressure. *IEEE Transactions on Plasma Science , Vol. 31* (No.6), 1363-1378.

Raja, K., & Floribert, T. (2002). Source Characteristion of Discharges in Transformers Using UHF PD Signatures. *Proceedings of the IEEE Power Engineering Society Winter Meeting. Vol. 2,* pp. 1383-1388. New York: IEEE.

Raja, K., Devaux, F., & Lelaidier, S. (2002, September/October). Recognition of Discharge Sources Using UHF PD Signatures. *IEEE Electrical Insulation Magazine , Vol.18* (No.5), pp. 8-14.

Reid, A. J., Judd, M. D., Stewart, B. G., & Fouracre, R. A. (2006). Partial discharge current pulses in SF6 and the effect of superposition of their radiometric measurement. *Journal of Physics: Applied Physics , Vol. 39,* 4167-4177.

Renforth, L., Mackinlay, R., Seltzer-Grant, M., & Shuttleworth, R. (2008). On-line partial discharge (PD) spot testing and monitoring of high voltage cable sealing ends. *Cigre Session 2008*, (pp. Paper B1-205).

Reynders, J. P. (1978). *Failure of polyethelene insulation as a result of partial discharge activity.* PhD Thesis, University of the Witwatersrand, Johannesburg.

Ryzko, H. (1965). Drift Velocity of Electrons and Ions in Dry and Humid Air and in Water Vapour. *Proceedings of the Physics Society (Proc. Phys. Soc.) , Vol. 85* (No. 6), 1283-1295.

Sahoo, N. C., & Salama, M. M. (2005). Trends in Partial Discharge Pattern Classification: A Survey. *IEEE Transactions on Dielectrics and Electrical Insulation , Vol. 12* (No. 2), 248-264.

Sarma, H., Cometa, E., & Densely, J. (2002). Accelerated ageing tests on polymeric cables using water-filled tanks - a critical review. *IEEE Electrical Insulation Magazine , Vol. 18* (No. 2), pp. 15-26.

Schwarz, R., Judendorfer, T., & Muhr, M. (2008). Review of Partial Discharge Monitoring Techniques Used in High Voltage Equipment. *IEEE Annual Report Conference on Electrical Insulation Dielectric Phenomena*, (pp. 400-403).

Shockley, W. (1938). Currents to conductors induced by a moving point charge. *Journal of Applied Physics , Vol. 9*, 635-636.

Srinivas, N., & Bernstein, B. S. (2007). Condition assessment of power cable systems in the energised state. *Jicable 2007*, (pp. 863-866). Versailles, France.

Stone, G. C. (2005). Partial Discharge Diagnostics and Electrical Equipment Insulation Condition Assessment. *IEEE Transactions on Dilectrics and Electrical Insulation , Vol. 12* (No. 5), 891-903.

Stone, G. C., Sedding, H. G., Fujimoto, N., & Braun, J. M. (1992). Practical Implementation of Ultrawideband Partial Discharge Detectors. *IEEE Transactions on Electrical Insulation , Vol. 27* (No. 1), 70-81.

Tanaka, T. (1986). Internal partial discharge and material degradation. *IEEE Transactions on Electrical Insulation*, Vol. EI-21 (No. 6), 899-905

Tanaka, T. (1995). Partial discharge pulse distribution analysis. *IEE Procedures of Science and Measurement Technologies , Vol. 142* (No. 1), 46-50.

Tanaka, T., & Ikeda, Y. (1971). Internal discharges in polyethylene with an artificial cavity. *IEEE Transactions on Power Applications & Systems (PAS) , PAS-90* (No. 6), 2692-2702.

Temmen, K. (2000). Evaluation of surface changes in flat cavities due to ageing by means of phase-angle resolved partial discharge measurement. *Journal of Applied Physics D: Appl. Phys , Vol. 33*, 603-608.

Thayoob, Y. H., Samsudin, M. R., Abd Ghani, A. B., & Ghosh, P. S. (2009). Analysis of partial discharge signal patterns in XLPE cable under various soil conditions using self organising

map. *Proceedings of the 16th International Symposium on High Voltage Engineering (ISH).* Cape Town, South Africa.

Thayoob, Y. M., Ghani, A. B., & Ghosh, P. S. (2003). Partial discharge pattern classification using frequency-domain statistical descriptors. *IEEE Proceedings of the 26th Electrical Insulation Conference and Electrical Manufacturing & Coil Winding Conference,* (pp. 171-175). Indianapolis.

Tian, Y., Lewin, P. I., Suttton, S. J., & Swingler, S. G. (2003). Partial Discharge Detection in Cables Using VHF Capacitive Couplers. *IEEE Transactions on Dielectrics and Electrical Insulation , Vol. 10* (No.2), 343-353.

Trinh, G. N. (1980). Electrode design for testing in uniform field gaps. *IEEE Transactions on Power Apparatus and Systems , PAS-99* (No. 3), 1235-1242.

Van Brunt, R. J. (1994). Physics and Chemistry of Partial Discharge and Corona. *IEEE Transactions on Dielectrics and Electrical Insulation , Vol. 1* (No. 5), 761-784.

Veen, J. (2005). *On-line signal analysis of partial discharges in medium-voltage power cables.* PhD Thesis, Technical University of Eindhoven.

Verhaart, H. F., & van der Laan, C. T. (1982). Fast current measurements for avalanche studies. *Journal of Applied Physics , Vol. 53* (No. 3), 1430-1436.

Victoria, R., Gockenbach, E., & Borsi, H. (2006). The influence of the stress time duration on the partial discharge behaviour in cast resin insulation. *Conference record of the 2006 IEEE International Symposium on Electrical Insulation,* (pp. 298-301).

Wang, P., Lewin, P. I., & Sutton, S. J. (2005, May/June). Calibration of Capacitive Couplers for Online Detection in HV Cables. *IEEE Electrical Insulation Magazine , Vol. 21* (No.3), pp. 28-39.

Wester, F. J., Gulski, E., & Smit, J. J. (2007, July/August). Detection of Partial Discharges at Different AC Voltage Stress in Power Cables. *IEEE Electrical Insulation Magazine , Vol. 23* (No. 4).

Wetzer, J. M., & van der Laan, P. C. (1989). Prebreakdown currents basic interpretation and time-resolved measurements. *IEEE Transactions on Electrical Insulation , Vol. 24*, 297-308.

Wetzer, J. M., Pemen, A. J., & Laan, v. d. (1991). Experimental study of the mechanism of partial discharges in voids in polyethylene. *Proceedings of the 7th International Symposium on High Voltage Engineeing,* (pp. 13-16). Dresden.

Wolter, K. D., Johnson, J. F., & Tanaka, J. (1978). REVIEW: Degradation Product Analysis for Polymeric Dielectric Materials Exposed to Partial Discharges. *IEEE Tarnsactions on Electrical Insulation , Vol. EI-13* (No. 5), 327-336.

Wong, K. L. (2004). Application of very-high-frequency (VHF) method to ceramic insulators. *IEEE Transactions on Dilectrics and Electrical Insulation , Vol. 11* (No. 6), 1057-1064.

Wu, K., Ijichi, T., Kato, T., Suzuoki, Y., Komori, F., & Okamoto, T. (2005). Contribution of surface conductivity to the current forms of partial discharges in voids. *IEEE Transactions on Dielectrics and Electrical Insulation , Vol. 12* (No. 6), 1116-1124.

Zhong, L., Chen, G., & Xu, Y. (2004). A Novel Calibration method for PD Measurements in Power Cables and Joints Using Capacitive Couplers. *Institute of Physics Publishing, Measurement and Science Technology , Vol.15*, 1892-1896.

Zoetmulder, R. G., Meijer, S., Smit, J. J., & Girodet, A. (2003). Influence of Spectrum Analyser Settings on Risk Assessment of GIS Containing Free Conducting Particles. *Proceedings of the 13th International Symposium on High Voltage Engineering*, (pp. 1-4). Delft, Nertherlands.